NASA TN D-50

TECHNICAL NOTE
D-50

WIND-TUNNEL INVESTIGATION OF THE AERODYNAMIC CHARACTERISTICS OF A MODEL REPRESENTATIVE OF A SUPERSONIC FIGHTER-CLASS AIRPLANE WITH AN EXTERNAL-FLOW JET-AUGMENTED FLAP IN LOW-SPEED FLIGHT

By William A. Newsom, Jr.

Langley Research Center
Langley Field, Va.

NATIONAL AERONAUTICS AND SPACE ADMINISTRATION

WASHINGTON September 1959

NATIONAL AERONAUTICS AND SPACE ADMINISTRATION

TECHNICAL NOTE D-50

WIND-TUNNEL INVESTIGATION OF THE AERODYNAMIC CHARACTERISTICS OF A MODEL REPRESENTATIVE OF A SUPERSONIC FIGHTER-CLASS AIRPLANE WITH AN EXTERNAL-FLOW JET-AUGMENTED FLAP IN LOW-SPEED FLIGHT

By William A. Newsom, Jr.

SUMMARY

A wind-tunnel investigation has been carried out to determine the aerodynamic characteristics of a supersonic fighter model with an aspect-ratio-3 unswept wing equipped with an external-flow jet-augmented double slotted flap in low-speed flight. Two engine nacelles were strut mounted beneath the wing with the jets diverted upward and outward toward the slots of the full-span double slotted flaps. Compressed air was used to represent the exhaust of these pod-mounted engines.

With the full-span, external-flow jet-augmented double slotted flap used on the model, lift coefficients as high as could be expected on the basis of the area and aspect ratio of the exposed (flapped) part of the wing were obtained. Interpretation of the experimental data in terms of the small supersonic fighter airplane indicated that a maximum usable lift coefficient of about 3.0 could be obtained by using the thrust normally available in an airplane of this class. Analysis indicated that, for the supersonic fighter, simple downward deflection of the jet exhaust to provide a large vertical component of thrust could result in total lift coefficients (aerodynamic lift plus jet lift) of approximately the same magnitude as those obtained with the jet-augmented flap because of the low circulation lift obtained with a low-aspect-ratio wing and the lift losses associated with the tail lift needed to trim the airplane pitching moments. Analysis indicated that, with a horizontal tail located on the chord plane of the wing and having an area of 40 to 45 percent of the wing area, stability and trim could be achieved for both the mid-wing and high-wing configurations.

INTRODUCTION

Recent investigations have shown the possibility of obtaining very high lift coefficients by means of a jet-augmented flap. These investigations have included large amounts of basic research on wings and have

also covered the application of the jet-augmented flap to a subsonic transport or bomber airplane (refs. 1 to 3). It seemed desirable to extend this work on the application of the jet-augmented flap to the case of a supersonic fighter since an airplane of this class has an entirely different type of wing and much larger quantities of exhaust gases in proportion to the airframe size than was the case with the subsonic transport or bomber. The objectives of the investigation were to determine how the jet-flap principle might be applied, to determine how high a lift could be obtained, and to study the longitudinal stability and trim problems.

The model used in the investigation had an unswept wing with an aspect ratio of 3 and a 37.5-percent-chord double slotted flap. It has two pylon-mounted nacelles from which the jet exhaust could be directed upward and outward toward the forward slots of the flap. The wing could be mounted in three vertical positions - high, mid, and low - and there were four possible horizontal-tail positions. The investigation consisted of measurement of the longitudinal and lateral aerodynamic characteristics for a range of angle of attack, sideslip angle, and mass flow for various combinations of the geometric variables. These systematic tests were made with the double slotted flap at 55° deflection (the first element being deflected 27.5° and the second element being deflected an additional 27.5°). Only a few exploratory tests were made at other flap deflections. In the tests an all-movable horizontal tail having an area equal to 25 percent of the wing area was used.

SYMBOLS

The basic data are referred to a center of gravity located at the reference line of the fuselage and at 0.40 mean aerodynamic chord.

b wing span, ft

C_D drag coefficient, Drag/qS

C_L lift coefficient, Lift/qS

$C_{L,t}$ lift coefficient of horizontal tail

C_l rolling-moment coefficient, Rolling moment/qSb

$C_{l_\beta} = \frac{\partial C_l}{\partial \beta}$

C_m pitching-moment coefficient, $M_Y/qS\bar{c}$

$C_{m,t}$ pitching-moment coefficient of horizontal tail

C_n yawing-moment coefficient, Yawing moment/qSb

$C_{n_\beta} = \frac{\partial C_n}{\partial \beta}$

C_Y side-force coefficient, Side force/qS

C_μ momentum coefficient based on thrust of two nacelles with conventional round nozzles, T/qS

$\bar{c}$ mean aerodynamic chord, ft

h height of horizontal tail above wing chord plane, ft

i_t angle of incidence of horizontal tail, positive when trailing edge is down, deg

M_Y pitching moment, ft-lb

q dynamic pressure, $\frac{1}{2}\rho V^2$, lb/sq ft

S wing area, sq ft

S_t horizontal-tail area, sq ft

T thrust, lb

V velocity, ft/sec

W weight, lb

α angle of attack, deg

β angle of sideslip, deg

δ_f deflection of rear element of double slotted flap with respect to wing chord line (measured parallel to plane of symmetry; deflection of forward element of flap is one-half that of rear element), deg

ρ air density, slugs/cu ft

PRELIMINARY ANALYSIS OF APPLICATION OF JET-AUGMENTED FLAP

There was no precedent on which to base the design of a model for an experimental study of the aerodynamic characteristics of a supersonic fighter class airplane with a jet-augmented flap. Therefore, before starting an experimental investigation, it was necessary to make a preliminary analysis of means of applying the jet-augmented-flap principle to this class of airplane and to lay out an airplane configuration on which to base a model that might give representative aerodynamic results.

In a supersonic fighter airplane which has relatively small thin wings it does not seem practical to route the large amount of exhaust gases available through the wing for an internal-flow application of the jet-augmented flap. Since the tests of reference 1 showed that it was possible to obtain almost as high a lift for an external-flow jet-augmented flap as for an internal-flow arrangement, it was decided to investigate the application of the external-flow jet-augmented-flap principle to the supersonic fighter. The use of an external-flow jet-augmented flap makes it desirable to use a relatively unswept wing since unpublished experimental data have shown that sweepback can cause losses in the lift induced by a jet flap. It is evident that a fighter with a jet flap should have as high an aspect ratio as is practical from high-speed considerations, because of the adverse effect of low aspect ratio on the lift that can be obtained with a jet-augmented flap (see ref. 4). It was decided therefore to use an unswept wing having an aspect ratio of 3 and a taper ratio of 0.5.

The external-flow jet-augmented-flap arrangement consists essentially of directing the exhaust of pod-mounted jet engines upward toward the slot of a slotted flap so that the exhaust gas is flattened out and directed downward as a jet sheet over the flap which induces a high circulation lift in the same manner as an internal-flow jet-augmented-flap arrangement. It seemed impractical to mount the engine far enough forward to deflect the exhaust from the tail pipe up to the slot in the flap. The main difficulties involved in mounting the engine so far forward were the structure needed and the acoustic-vibration and heat effects on the lower surface of the wing caused by afterburner operation at supersonic speed. The scheme that was devised to overcome these difficulties is illustrated in figure 1. It consists of a special section containing a butterfly diverting valve mounted between the engine and the afterburner. When the butterfly valve is deflected, the gas is diverted out through special ports in the top of the nacelle. The flap that uncovers the ports directs the gas upward and rearward toward the slot of the slotted flap. In preliminary static tests this arrangement was found to give good spreading and turning of the jet with reasonable

thrust losses. It was therefore decided to use this configuration in the model design.

With an external-flow jet-augmented-flap system of this type it was believed to be desirable to represent the size of the engine exhaust as well as its thrust because of the relatively large size of the exhaust stream in proportion to the size of the wing and flaps. It was therefore necessary to decide how much thrust would be applied to the flap and what the size of the exhaust stream would be. Preliminary analysis, in which the data from figure 4 of reference 4 for an aspect ratio of 3 was used, indicated that for a supersonic fighter airplane with afterburning engines, it would be possible to obtain higher lift coefficients with part of the engines exhausting through the jet-flap arrangement and part of them used solely for propulsion. This results from the fact that it does not seem logical to use the high-temperature reheated exhaust on a jet flap but it is very desirable to take advantage of the extra thrust available from afterburning for propulsion. If only part of the engines are used in conjunction with the jet flap, it is possible to use large flap deflections which result in a large net drag. The augmented thrust of the other engines with their afterburners operating could be used to overcome this high drag. This system would result in higher lift coefficients than those for a system in which all the engines were exhausted through the jet flap with a much lower flap deflection used to give a net thrust instead of a drag. The airplane configuration to be represented in the investigation was therefore assumed to be a 13,500-pound fighter with three engines, each having a static thrust of 2,500 pounds without afterburning and 3,600 pounds with afterburners operating. Two of the engines were pod mounted beneath the wing and one was mounted at the rear of the fuselage. A $\frac{1}{7}$-scale model was used in the investigation to represent this hypothetical airplane.

MODEL

A three-view drawing of the model used in the tests is shown in figure 2(a) and the geometric characteristics are given in table I. As mentioned previously, the model was intended to represent a supersonic fighter class of airplane. It had a thin unswept wing, a fuselage of circular cross section, and an all-movable horizontal tail. An engine nacelle was strut mounted beneath each wing with the jet diverted upward and outward toward the slot of the double slotted flap.

Cold compressed air used to simulate jet-engine exhaust was piped out through the wing and down through the pylons into the nacelles which were in effect large plenum chambers to which various diverter nozzles could be affixed. The sketch of figure 3 shows the internal arrangement

of the nacelle with the nozzle block which represented the case in which the engine butterfly valve was deflected to exhaust the gas out of the ports in the top of the nacelle. Actually, as shown in figure 4, the ports extended around approximately the upper one-fourth of the nacelle and the flow coming out the side of the ports was directed toward the wing root and tip to give a fairly even spread of the gases over the wing flap.

The wing of the model had 0° sweep of the 0.65-chord line, an aspect ratio of 3.00, a taper ratio of 0.5, and was equipped with a full-span 37.5-percent-chord double slotted flap of the type illustrated in figures 5(a) and 5(b). The noses of the flap elements did not have any special contour but were faired to approximately the shape shown in the sketches. Figure 5(b) shows the flaps in the extended position at a deflection of 55° which was the deflection used in most of the tests.

The airfoil section of the class of airplane represented by the model should be very thin but it was not possible to use a suitably thin airfoil on the model because of the size of the tubes supplying compressed air to the nacelles. The airfoil section used on the model was developed by thickening the NACA 65-003 airfoil section to accommodate the compressed air tubes as illustrated in figure 5(c). It was felt that this airfoil would represent the essential characteristics of the NACA 65-003 airfoil section insofar as the jet-augmented-flap operation is concerned since it had the same thin airfoil leading edge and flap nose section.

The wing of the model could be mounted at any of three positions - tangent with the top of the fuselage, tangent with the bottom of the fuselage, or on the fuselage center line as shown in figure 2(b). When the wing was in the high or mid position, the gap between the deflected flap and fuselage was sealed with a modeling-clay fillet. When the wing was in the low position, the flap was extended across beneath the fuselage, the section under the fuselage being a plain flap extending downward as far as the double slotted flap. The hinge brackets on the inboard end of the double slotted flap were rather large and served to seal the gap between the two types of flaps. The hinge bracket probably also served to prevent any flow from the nacelles from reaching the flap under the fuselage. The horizontal-tail position was also variable. Four tail positions were provided - one on the fuselage center line and three on the vertical tail. The position of the horizontal tail is always presented in terms of its height above the wing chord plane since this was considered the important parameter. The various combinations of wing and tail positions covered in the tests are shown in figure 2(b). The horizontal tail used in the tests had an area equal to 25 percent of the wing area, 25° sweep of the 25-percent chord, and an NACA 65-003 airfoil section.

TESTS

As pointed out previously, it was believed to be important to represent the size as well as the thrust of the engine exhaust. The following procedure was used to achieve this representation. The nacelles were fitted with ordinary round tail pipes of scaled diameter, and the pressures and flow quantities required to obtain various amounts of thrust were recorded. The mass flow was not actually measured but an indication of mass flow was obtained from the pressure drop in the given length of hose supplying compressed air to the nacelle. Then the nozzle blocks representing the exhaust diverters were installed and the size of the ports in the top of the nacelles was adjusted to give the same flow quantity - that is, the same pressure drop in the supply hose - for the same pressure inside the nacelle. The values of pressure required to produce a given thrust with the round nozzles were used as a calibration in setting the C_μ conditions in the tests since C_μ is defined (under the same flow conditions) as $\frac{\text{Thrust of round nozzles}}{qS}$.

Preliminary tests were made at zero airspeed to determine a suitable configuration for turning the jet. These tests showed that with the double slotted flap deflected 90° (deflection of 45° of each segment) the jet could be turned nearly 90° but that a 60-percent loss in thrust was incurred in turning the jet. With a flap deflection of 55° the jet was turned through an angle of about 55° with a thrust loss of only 25 percent; that is, the resultant force of the wing-nacelle combination was 75 percent of the thrust of the nacelles with standard round nozzles. This is about as low a loss as has ever been obtained in previous external-flow jet-augmented-flap tests. A flap deflection of 55° was therefore used throughout the test program. These tests included measurements of the lift, drag, and pitching moment for two tail positions and for the tail off for each of the three wing positions over a range of angle of attack from -10° to 25° and of momentum coefficient from 0 to 2.35. The tests also included measurements of the variation of rolling moment, yawing moment, and side force with angle of sideslip over a range of angle of attack from 0° to 20° with the vertical tail off and the vertical tail on for each of the three wing positions.

All the tests were made in the 12-foot octagonal test section of the Langley free-flight tunnel at a dynamic pressure of about 0.94 pound per square foot which corresponds to a velocity of about 25 feet per second and a Reynolds number of about 187,000 based on the mean aerodynamic chord of the wing tested. The model was mounted on a single vertical strut with a six-component strain-gage balance. Since the model was small relative to the size of the test section of the tunnel, no wind-tunnel corrections have been applied to the data.

RESULTS AND DISCUSSION

Presentation of Results

The aerodynamic characteristics of the model obtained in the wind-tunnel tests are presented in figures 6 to 11. A summary of the configurations investigated and of the figures that present the basic data is given in the following table:

Wing position	δ_f, deg	Horizontal tail		Vertical tail	Type of data	Figure
		$\frac{S_t}{S}$	$\frac{h}{\bar{c}}$			
High	55	0	-----	Off	Longitudinal	6(a)
		.25	0	On	-----do-----	6(b) to 6(e)
		.25	0.554	On	-----do-----	6(f) to 6(i)
		0	-----	Off	Lateral	7(a) to 7(e)
		.25	0	On	-----do-----	7(f) to 7(j)
Mid	55	0	-----	Off	Longitudinal	8(a)
		.25	0	On	-----do-----	8(b) to 8(e)
		.25	0.41	On	-----do-----	8(f) to 8(i)
		0	-----	Off	Lateral	9(a) to 9(e)
		.25	0	On	-----do-----	9(f) to 9(j)
Low	55	0	-----	Off	Longitudinal	10(a)
		.25	0.28	On	-----do-----	10(b) to 10(e)
		.25	.69	On	-----do-----	10(f) to 10(i)
		0	-----	Off	Lateral	11(a) to 11(e)
		.25	.28	On	-----do-----	11(f) to 11(j)

Lift

In figure 12 a comparison is presented of the lift coefficients obtained with the present model with those calculated by a semiempirical method. The lift was calculated from the data of reference 4 based on the area (310 sq in.) and aspect ratio (2.5) of the flapped part of the wing. The calculated data, however, were converted into coefficients C_L and C_μ based on the total wing area in order to make them directly comparable with the experimental data. The experimental data are for the high-wing–tail-off configuration at $\alpha = 0^\circ$. This comparison indicates that the jet-augmented-flap configuration used on the model was reasonably

efficient since it gave about as high lift coefficient as could be expected from an internal-flow system such as that used in reference 4.

The effect of wing position on the lift produced by the jet-augmented flap may be seen in figure 13. The data for this figure were obtained from figures 6(a), 8(a), and 10(a) since with the horizontal tail off the effect of the wing-fuselage interference is isolated. Figure 13 shows that there is not much difference in the lift for different wing positions but that the mid-wing configuration gave slightly higher values of lift over the whole C_μ range than either of the other two configurations. The mid-wing configuration had a somewhat smoother wing-fuselage juncture and it may be that, if the wing-fuselage junctures of the high-wing and low-wing configurations were improved, the lift for these configurations could be brought up to that of the mid-wing configuration.

Stability and Trim

Longitudinal.- The pitching-moment data of figures 6, 8, and 10 show that the longitudinal stability and trim characteristics were unsatisfactory for all of the configurations tested. An analysis has been made, therefore, to determine how large the horizontal tail has to be in order to trim the airplane pitching moment and to obtain a reasonable amount of static margin. Since a pitch-up (increasing static longitudinal instability with increasing angle of attack) is characteristic of configurations in which the horizontal tail is mounted above a low-aspect-ratio wing, the analysis has been made for the two lowest horizontal-tail configurations tested (mid wing, $h/\bar{c} = 0$ and high wing, $h/\bar{c} = 0$). The use of a tail position below the wing chord plane was not covered in the present investigation since it was not considered feasible to locate the tail in the exhaust of the pod-mounted engines which would have afterburners operating for supersonic flight.

The three stability and trim requirements that the horizontal tail must satisfy for purposes of analysis were that using a horizontal-tail lift coefficient of not more than 1.2 the airplane pitching moment at $C_\mu = 1.48$ should be trimmed and a static margin of about 5 percent $\bar{c}$ or greater should be attained at this and all lower values of C_μ. The results of the analysis are presented in figure 14. With the mid-wing configuration (fig. 14(a)), a horizontal tail having an area equal to 45 percent of the wing area in conjunction with a center of gravity at about 28 percent of the mean-aerodynamic-chord station would give a static margin of about 5 percent $\bar{c}$ at $C_\mu = 0$ and greater static margin at higher values of C_μ. The plot made for the high-wing configuration (fig. 14(b)) shows that, if the center of gravity was at 28 percent of the mean-aerodynamic-chord station as before, essentially the same static

margin (5 percent $\bar{c}$ at $C_\mu = 0$) could be attained with a horizontal tail having an area equal to only 40 percent of the wing area. For this configuration as before, the static margin would be greater at higher values of C_μ.

Lateral.- The variation of rolling moment, yawing moment, and side force with sideslip angle for the various configurations is presented in figures 7, 9, and 11 for the condition of zero tail incidence. The rolling-moment data in these figures, particularly those in figure 7, are very erratic. The data of figures 7, 9, and 11 also show large asymmetries and large rolling moments at zero sideslip in many cases. These cases generally involve high angles of attack, frequently beyond the stall, or high values of C_μ where the lift is high, and reasonably small percentage differences in lift between the right and left wings can cause large rolling moments. For example, a rolling-moment coefficient of about 0.08 can be produced by a difference in lift coefficient of 0.3 which is about 10 percent of the total lift.

The data of figures 7, 9, and 11 and a summary plot made for $C_\mu = 0$ and 1.48 (fig. 15) show, in general, that for all the configurations tested increasing the momentum coefficient had a stabilizing effect on the yawing moment due to sideslip. In some instances, especially for the mid-wing configuration with the tail off, the model became directionally stable. The vertical tail used on the model provided directional stability at angles of attack up to 10° for all conditions covered in the tests. At an angle of attack of 15°, however, the model was directionally unstable at $C_\mu = 0$, and at an angle of attack of 20° the model had unsatisfactory directional stability characteristics even with power on. The plots of rolling-moment variation with sideslip angle show at low angles of attack a positive dihedral effect ($-Cl_\beta$) in the high-wing configuration (fig. 7) and a neutral dihedral effect (Cl_β essentially zero) for some of the low-wing configurations. At high angles of attack, for example 15° or 20°, the variation of rolling moment with sideslip was very erratic.

APPLICATION OF DATA

A brief analysis was made by using the results of the experimental investigation to determine how high a lift coefficient could be obtained with an airplane of the type represented by the model. It should be realized that the lift coefficient is not the only factor of interest in the case of a take-off, since the take-off distance is markedly affected

by the acceleration of the airplane during the ground roll. No account was taken in the analysis of the ground effect on the aerodynamic characteristics although proximity to the ground is known to have an adverse effect on the lift coefficients obtainable. For this analysis, the same airplane characteristics were used that were used in the preliminary analysis on which the design of the model had been based. This airplane, as previously mentioned, was a 13,500-pound fighter with three engines, each having a static thrust of 2,500 pounds without afterburners and 3,600 pounds with afterburners operating. Two of the engines were pod mounted beneath the wing and one was mounted at the rear of the fuselage.

As a first step in the analysis, the curves of C_L plotted as a function of C_μ for the trim condition of $C_m = 0$ were constructed by interpolation from the data of figure 6. These curves are presented in figure 16 for two angles of attack, 0° and 10°. The ratio of the thrust of the wing engines without afterburning to the weight of the airplane is 0.37. A line representing this thrust-weight ratio is shown in the bottom plot in figure 16. From the intersection of this line with the lift curves, the lift coefficient of the airplane was found to be 2.8 at $\alpha = 0^\circ$ and 3.5 at $\alpha = 10^\circ$. The ratio of the thrust of the tail engine with afterburner operating to that of the wing engine is 0.75. A line representing this ratio is shown in the top plot in figure 16. From the intersection of this line with the drag curves, it can be seen that little excess thrust is left for climb at an angle of attack of 10°, but a considerable amount of excess thrust is available at an angle of attack of 0°. If an interpolation is made between these two conditions and a maximum usable lift coefficient of about 3.0 is assumed, the hypothetical airplane could climb at about 6° (or with a rate of climb of nearly 1000 feet per minute). It should be borne in mind that the model had a full-span flap and had no provision for roll control. The provision of an adequate roll control system might compromise the configuration by causing lower maximum lift coefficients than those obtained in the model tests.

The obvious question that arises is how the lift obtainable with the jet flap compares with that obtainable by simply directing the jet exhaust downward. In considering the case in which the engines are tilted so that the jet exhaust is directed downward, it is necessary to assume a somewhat different configuration in order that the exhaust of all the engines may be directed downward while longitudinal trim is maintained. In the following analysis it is assumed, however, that total weight and the total thrust available from the jet engines are the same as those for the airplane with the jet-augmented flap. If all the engines of such an airplane are tilted 70°, the vertical component of the thrust with afterburners operating would be about 10,000 pounds or three-fourths of the weight. The jets would therefore support three times the lift of the wing or have three times the lift coefficient of the wing. Since the airplane

could easily attain an aerodynamic lift coefficient of 1.0, the total lift coefficient with engines operating would be about 4.0. With the jet deflection of 70° the forward component of the thrust would be 3,700 pounds which is more than adequate to propel the airplane.

It might seem unreasonable to direct the exhaust of afterburning engines directly at the ground in this manner; a similar analysis was, therefore, made for the case in which the exhaust of the engines without afterburning was deflected downward as has been done in England on a Gloster Meteor (ref. 5). In this case if the engine exhaust were deflected downward through an angle of 60°, the vertical component of the thrust would be approximately 6,500 pounds which is nearly one-half the weight of the airplane. The total lift coefficient would therefore be about twice the aerodynamic lift coefficient or about 2.0. With this 60° jet deflection, the forward component of the jet force would be about 3,750 pounds. These analyses for the deflected-jet cases are obviously superficial. More detailed calculations have been found to give approximately the same results.

Since it was realized that not only the lift but the take-off distances of the various configurations were of interest, calculations were made to determine how the take-off distances compared with each other for these various lift augmentation schemes. The following configurations were considered: the three configurations previously mentioned (jet-augmented flap, engines tilted with afterburners on, and jet diverted downward with afterburners off) and a conventional configuration with all engines exhausting straight backward with flap down. The results of the calculations indicated that the various configurations all had approximately the same take-off distance, ranging from about 2,000 to 2,200 feet. In one instance the calculations showed that, if the engines were tilted to 50° with the afterburner operating and the take-off performed with flap up and at an angle of attack of 20°, the take-off distances could probably be reduced to about 1,000 feet. The main point that may be inferred from the analysis is that the lift coefficients and take-off distances obtainable with the jet flap are not markedly different from those obtained by simply directing the jet exhaust downward for an airplane of the general configuration represented by the model. The choice of schemes for using the jet thrust to augment the lift would therefore be mostly dependent on mechanical and operational considerations.

CONCLUSIONS

The following conclusions were drawn from the results of an investigation of the application of a jet-augmented flap to a supersonic fighter class of airplane:

1. With the full-span, external-flow jet-augmented double slotted flap used on the model, lift coefficients were obtained which were as high as would be predicted on the basis of the area and aspect ratio of the exposed part of the wing by using the preliminary design charts and methods of NACA Technical Note 3863.

2. Interpretation of the experimental data in terms of the small supersonic fighter airplane indicated that a maximum usable lift coefficient of about 3.0 could be obtained by using the thrust normally available in an airplane of this class.

3. Analysis indicated that for this airplane simple downward deflection of the jet exhaust to provide a large vertical component of thrust could result in total lift coefficients (aerodynamic lift plus jet lift) of approximately the same magnitude as those obtained with the jet-augmented flap.

4. Analysis indicated that with a horizontal tail located on the chord plane of the wing and having an area of 40 to 45 percent of the wing area and a tail lift coefficient of 1.2, pitching-moment trim and static longitudinal stability could be achieved for both the mid-wing and high-wing configurations.

Langley Research Center,
National Aeronautics and Space Administration,
Langley Field, Va., June 26, 1959.

REFERENCES

1. Campbell, John P., and Johnson, Joseph L., Jr.: Wind-Tunnel Investigation of an External-Flow Jet-Augmented Slotted Flap Suitable for Application to Airplanes With Pod-Mounted Jet Engines. NACA TN 3898, 1956.

2. Johnson, Joseph L., Jr.: Wind-Tunnel Investigation of the Static Longitudinal Stability and Trim Characteristics of a Sweptback-Wing Jet-Transport Model Equipped With an External-Flow Jet-Augmented Flap. NACA TN 4177, 1958.

3. Johnson, Joseph L., Jr.: Wind-Tunnel Investigation at Low Speeds of Flight Characteristics of a Sweptback-Wing Jet-Transport Airplane Model Equipped With an External-Flow Jet-Augmented Slotted Flap. NACA TN 4255, 1958.

4. Lowry, John G., and Vogler, Raymond D.: Wind-Tunnel Investigation at Low Speeds To Determine the Effect of Aspect Ratio and End Plates on a Rectangular Wing With Jet Flaps Deflected 85°. NACA TN 3863, 1956.

5. Ashwood, P. F., and Lean, D.: Jet Deflection Flight Tests. Shell Aviation News, Sept. 1958, pp. 14-18.

TABLE I.- GEOMETRIC CHARACTERISTICS OF MODEL TESTED

Wing:	
Area, sq in.	432
Aspect ratio	3.0
Mean aerodynamic chord, in.	12.45
Airfoil section	Modified NACA 65-003
Flap chord (total of both segments), percent wing chord	37.5
Flap span, percent wing span	100
Root chord, in.	16.0
Tip chord, in.	8.00
Span, in.	36.00
Taper ratio	0.5
Sweep of 0.65 chord, deg	0
Fuselage:	
Length, in.	84.73
Diameter (maximum), in.	8.12
Horizontal tail:	
Area, sq in.	108
Length (distance from $0.40\bar{c}$ of wing to $0.25\bar{c}$ of tail), wing chords	2.5
Span, in.	18.00
Root chord, in.	8.00
Tip chord, in.	4.00
Mean aerodynamic chord, in.	6.23
Aspect ratio	3.0
Sweep of 0.25 chord, deg	25
Taper ratio	0.5
Airfoil section	NACA 65-003
Vertical tail:	
Exposed area, sq in.	68.69
Exposed span, in.	8.50
Root chord at fuselage intersection, in.	9.50
Tip chord, in.	6.00
Sweep of leading edge, deg	25

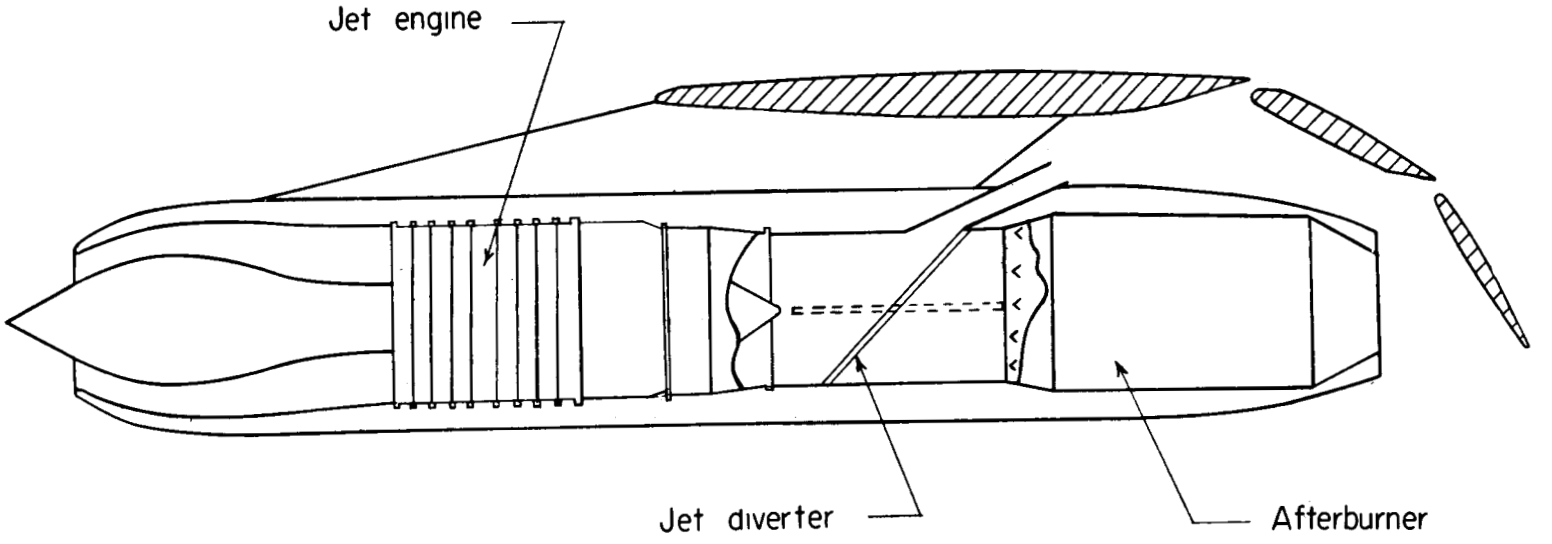

Figure 1.- Schematic diagram of the proposed engine and jet-exhaust-diverter arrangement.

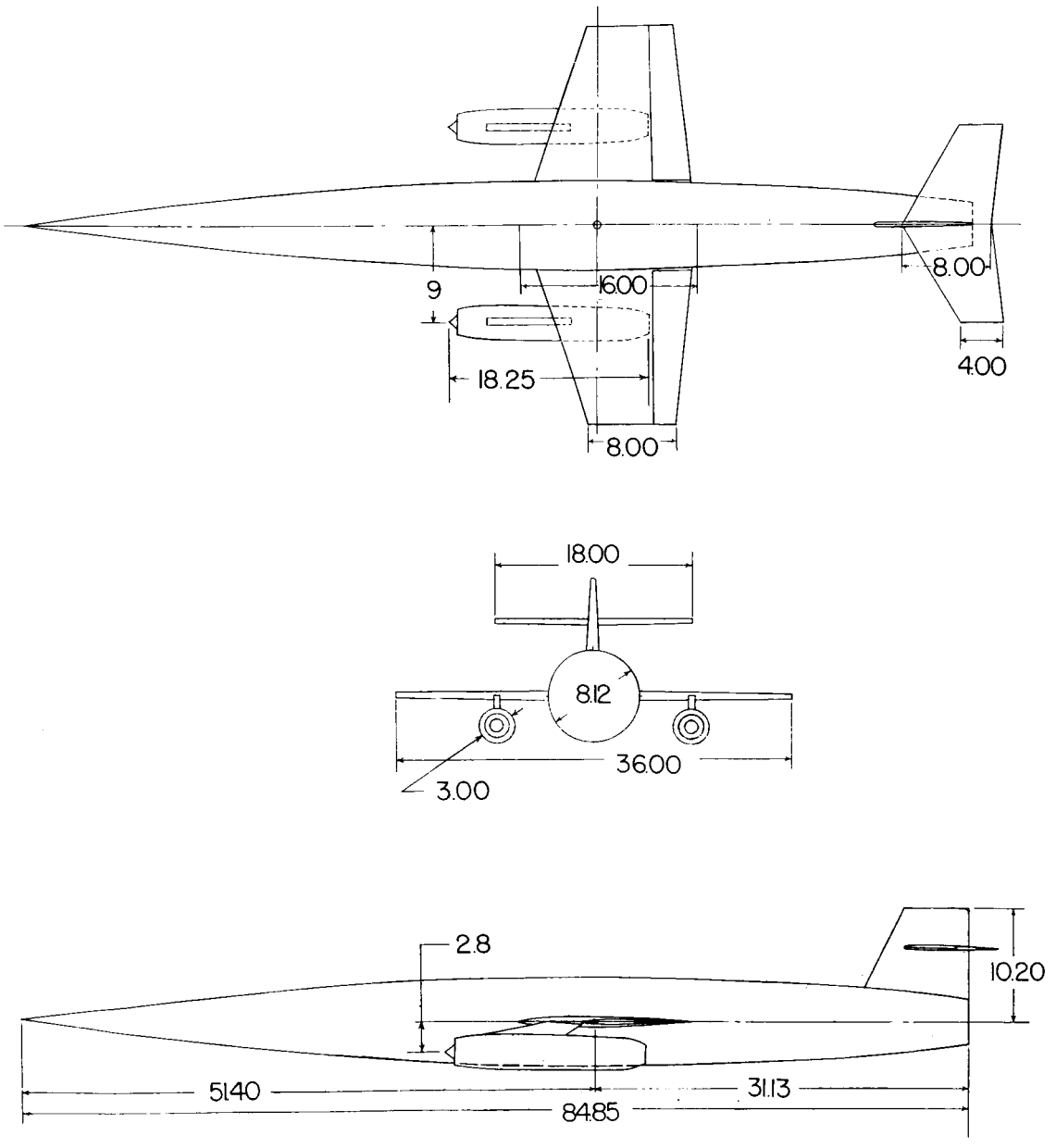

(a) Three-view drawing of the model with the mid-wing configuration and the 0.255 tail.

Figure 2.- Sketches of the model. All dimensions are in inches.

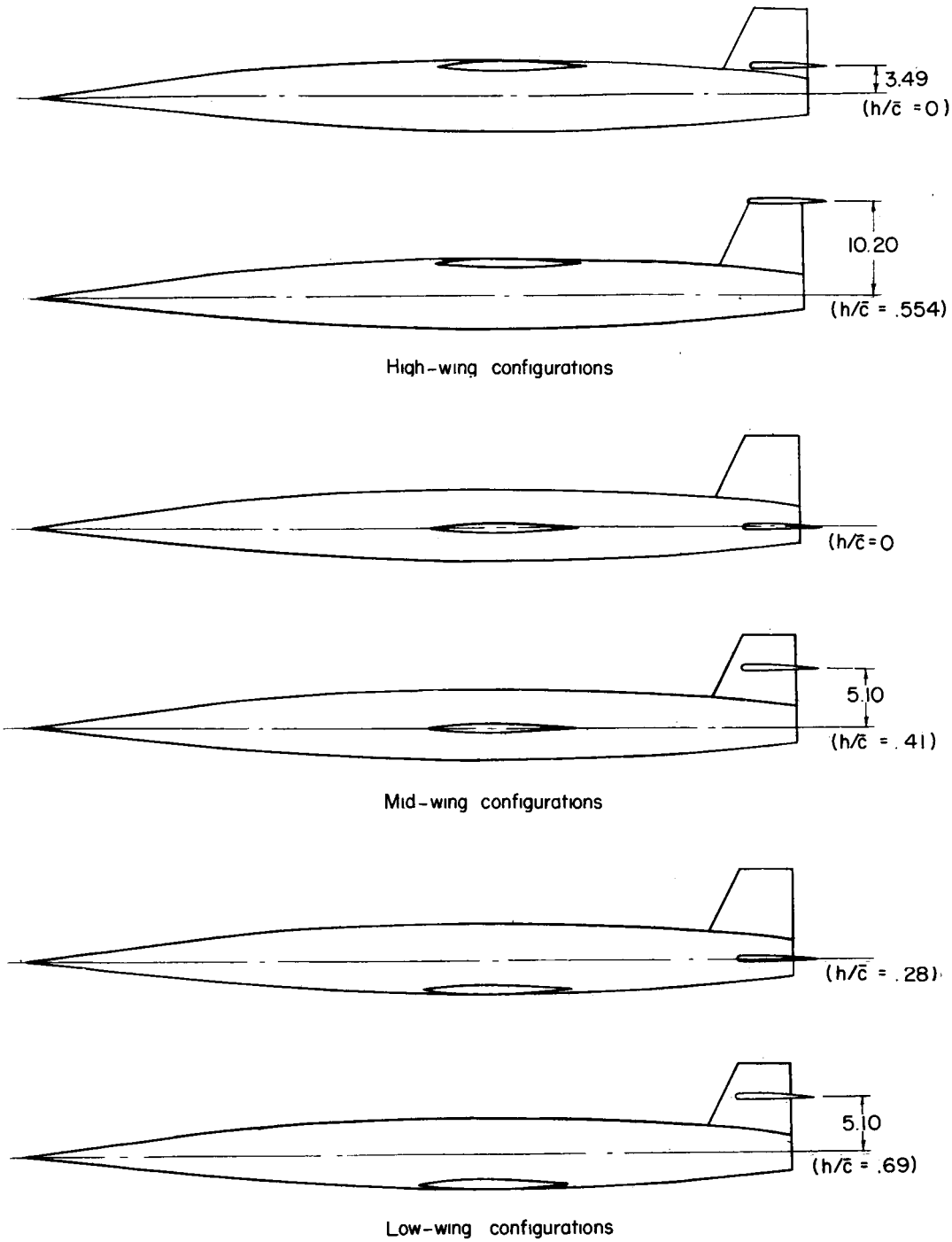

(b) Sketch showing various wing and tail positions covered in the tests.

Figure 2.- Concluded.

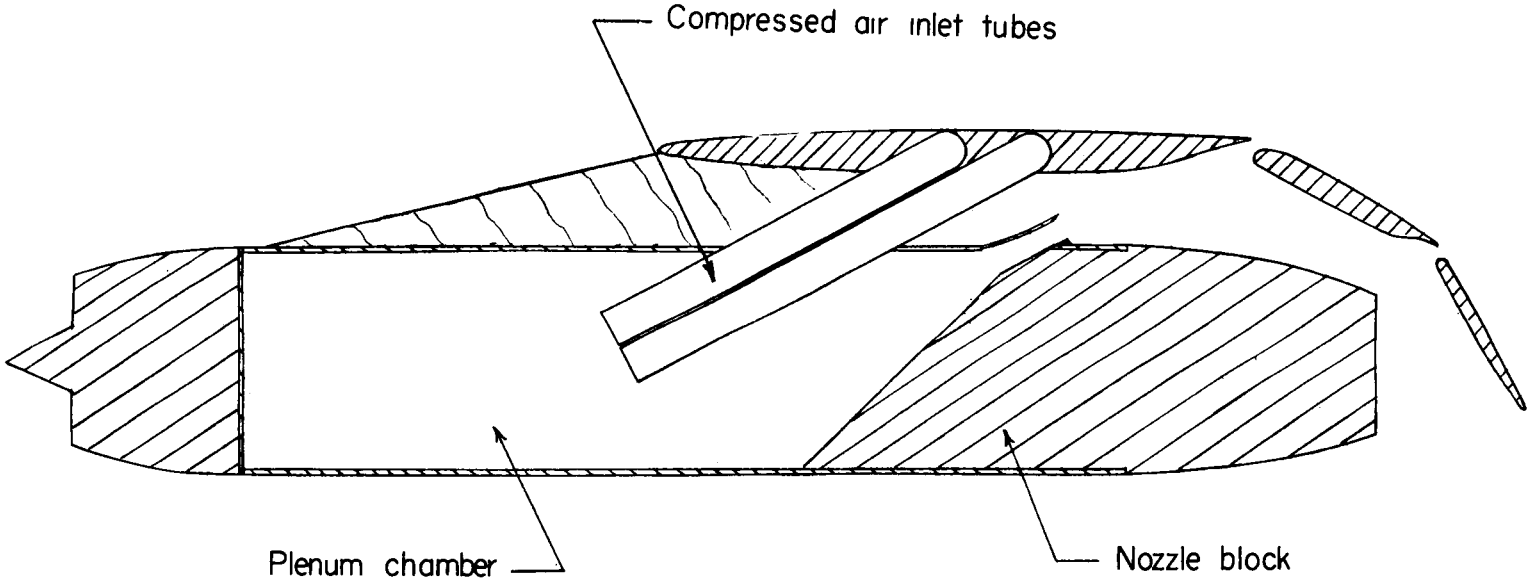

Figure 3.- Internal arrangement of the nacelle of the model tested.

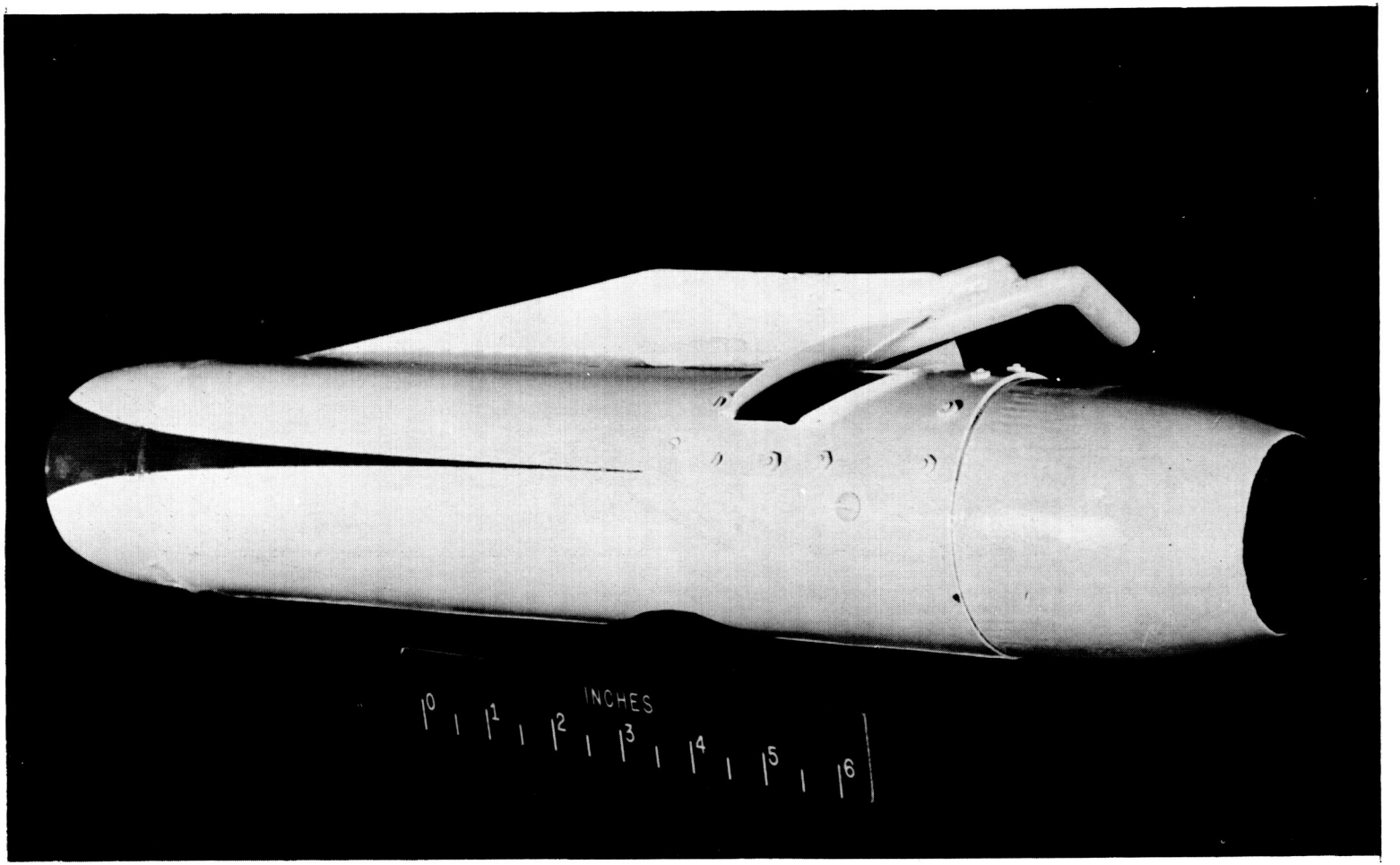

Figure 4. Nacelle of model tested. L-58-3566

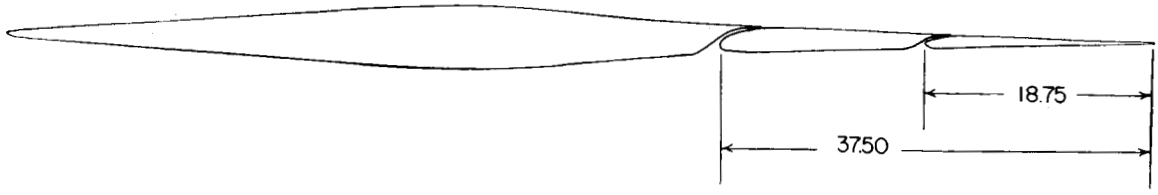

(a) Flaps retracted.

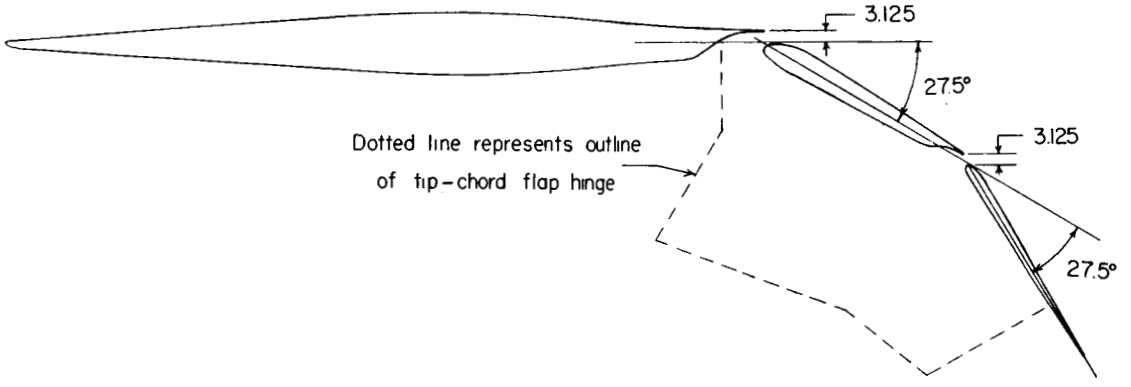

(b) Flaps extended.

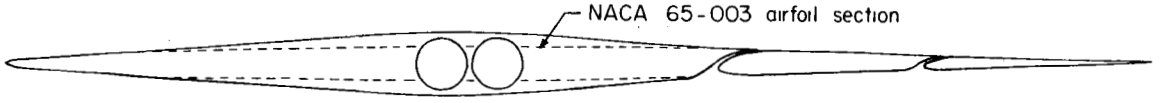

(c) Comparison of model airfoil section with NACA 65-003 airfoil section.

Figure 5.- Wing sections of the model tested. All dimensions are in percent wing chord unless otherwise indicated.

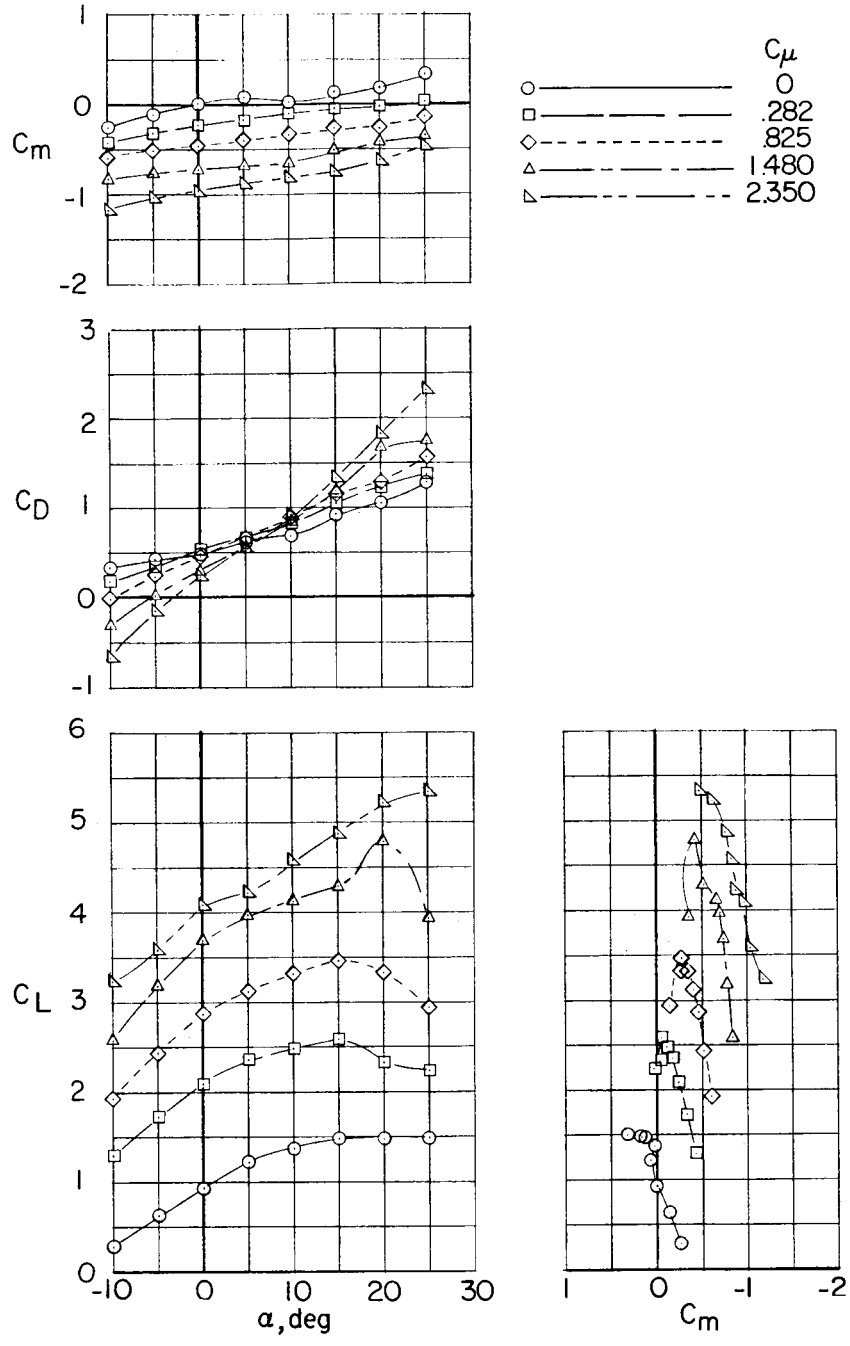

(a) Vertical tail off.

Figure 6.- Longitudinal stability and trim characteristics of the high-wing configuration. $\delta_f = 55^\circ$.

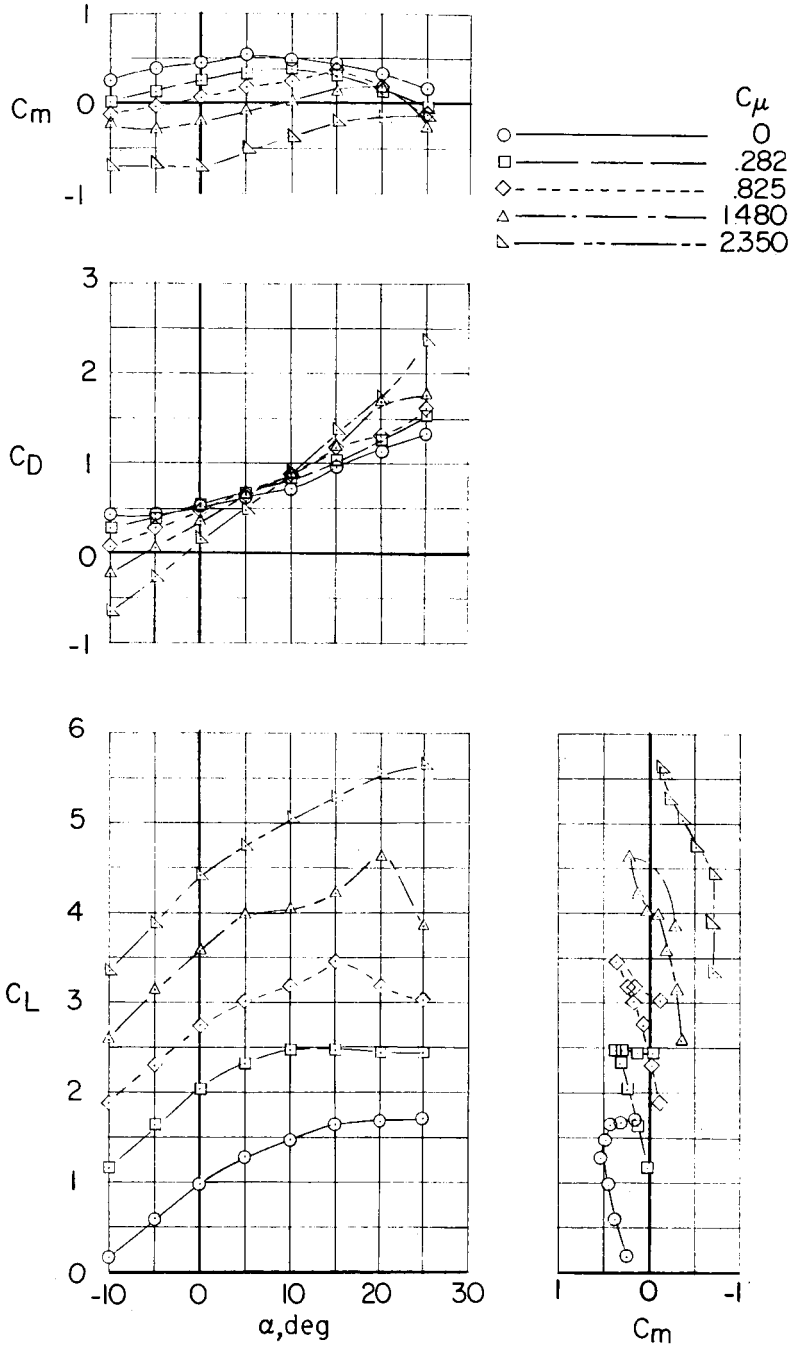

(b) $\frac{h}{\bar{c}} = 0$; $i_t = 0^\circ$.

Figure 6.- Continued.

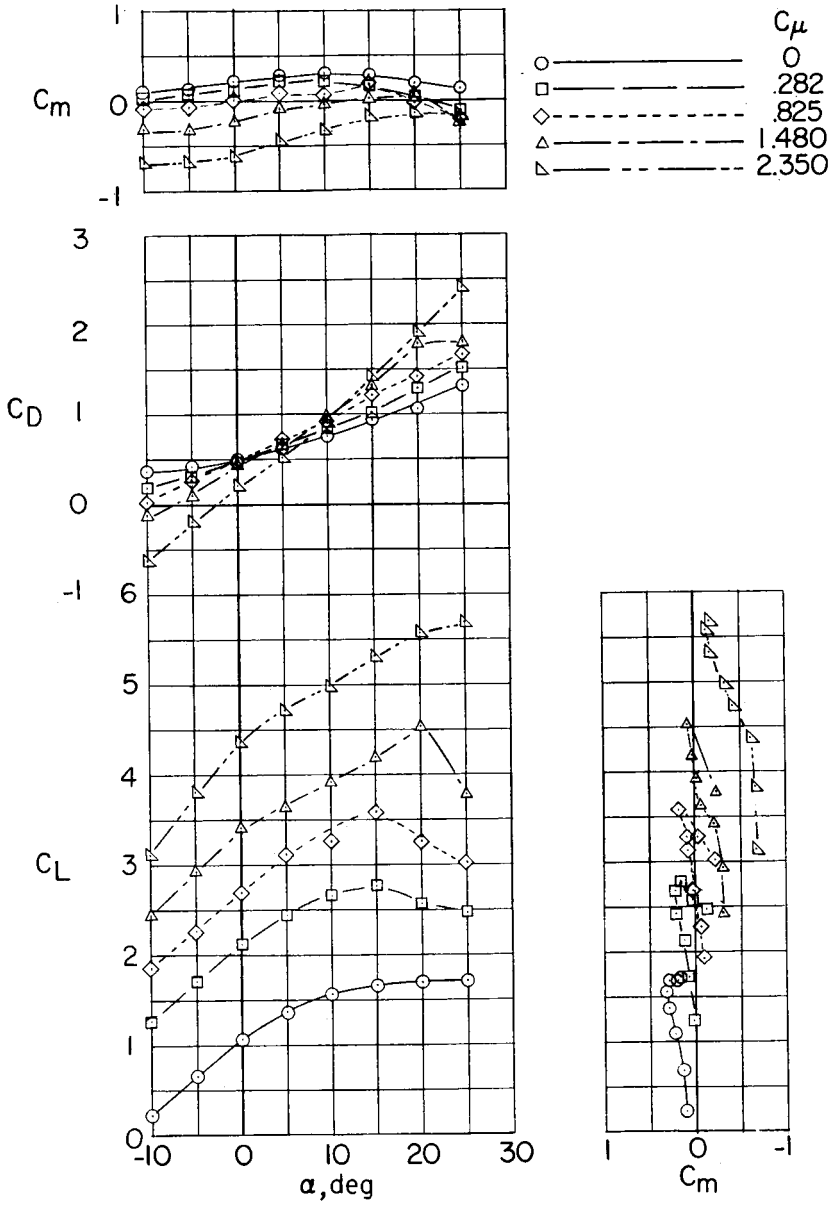

(c) $\frac{h}{\bar{c}} = 0$; $i_t = 5^\circ$.

Figure 6.- Continued.

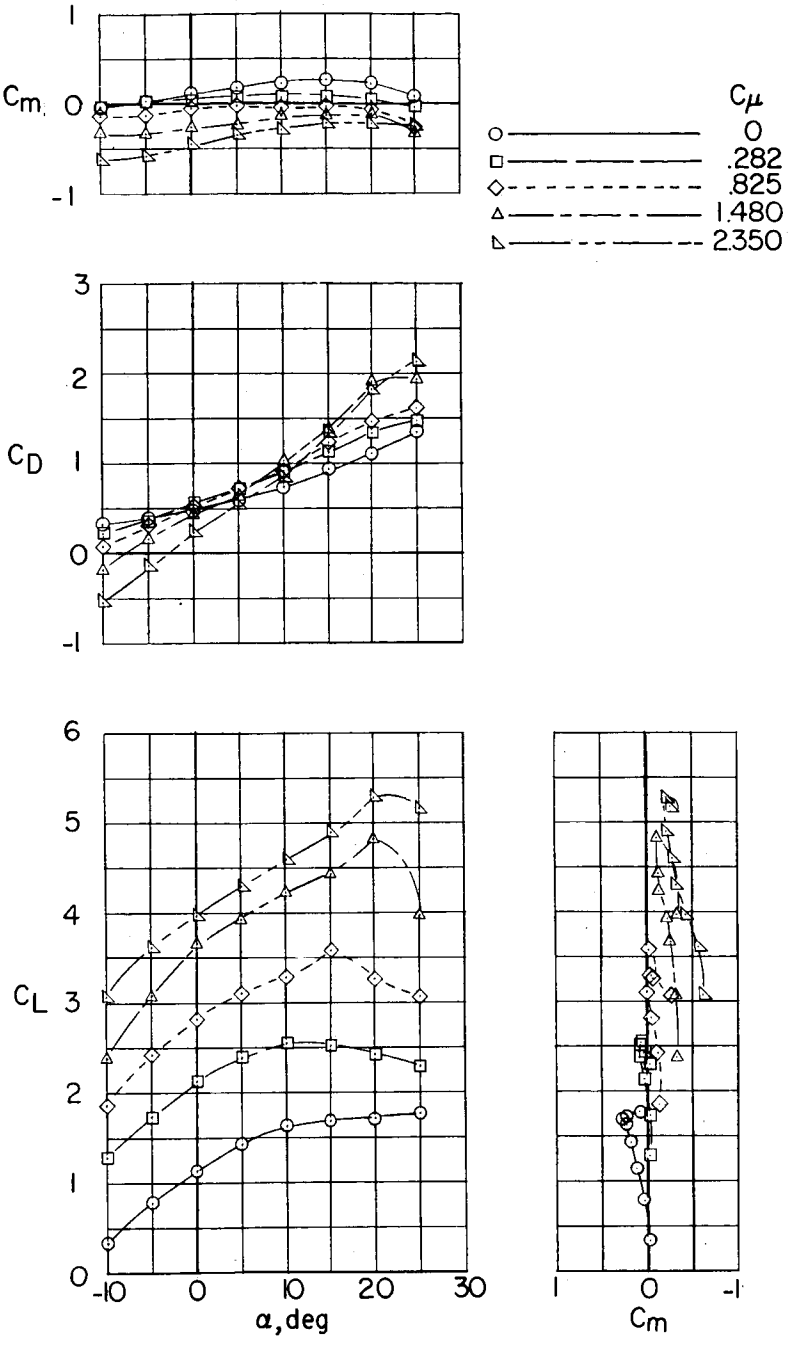

(d) $\frac{h}{\bar{c}} = 0$; $i_t = 10^\circ$.

Figure 6.- Continued.

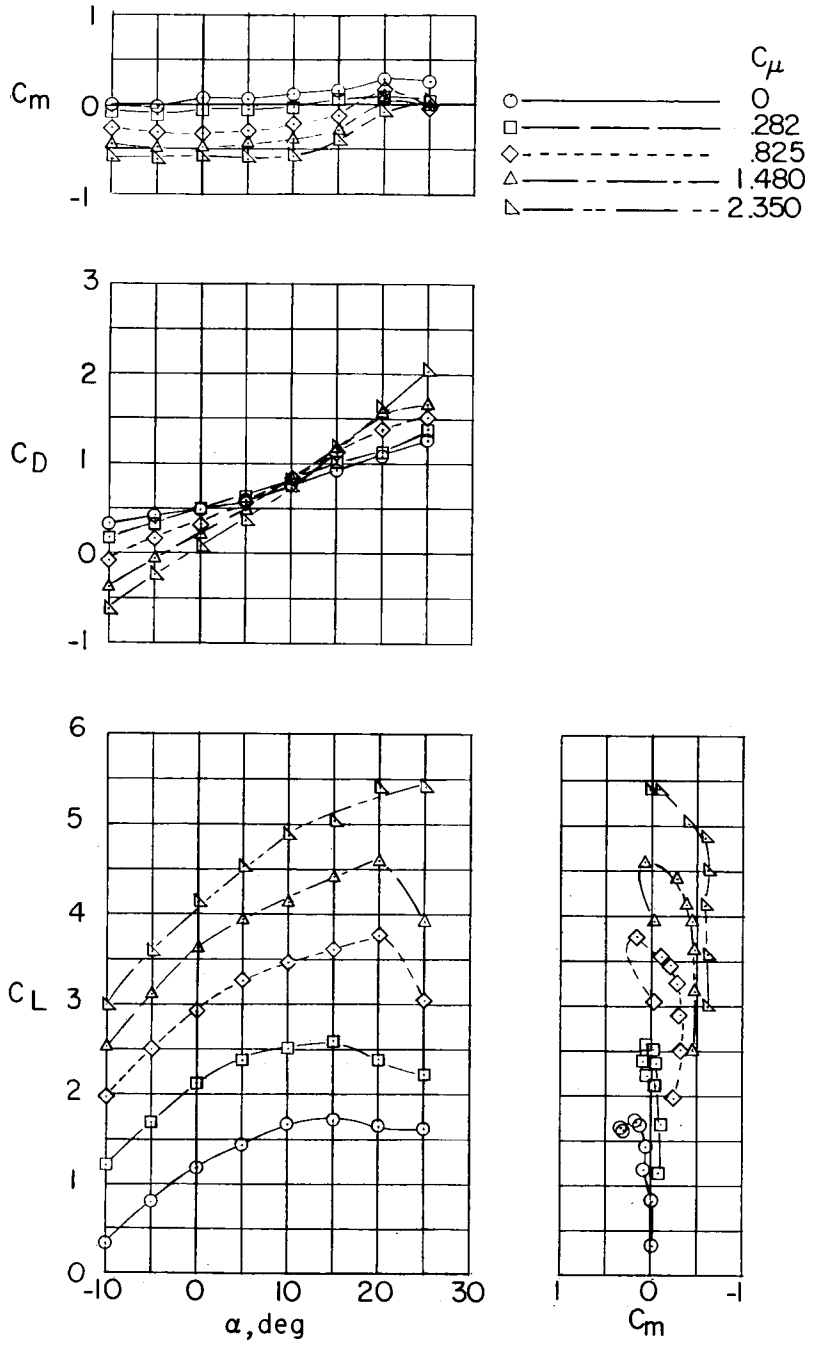

(g) $\frac{h}{c} = 0.554$; $i_t = 5°$.

Figure 6.- Continued.

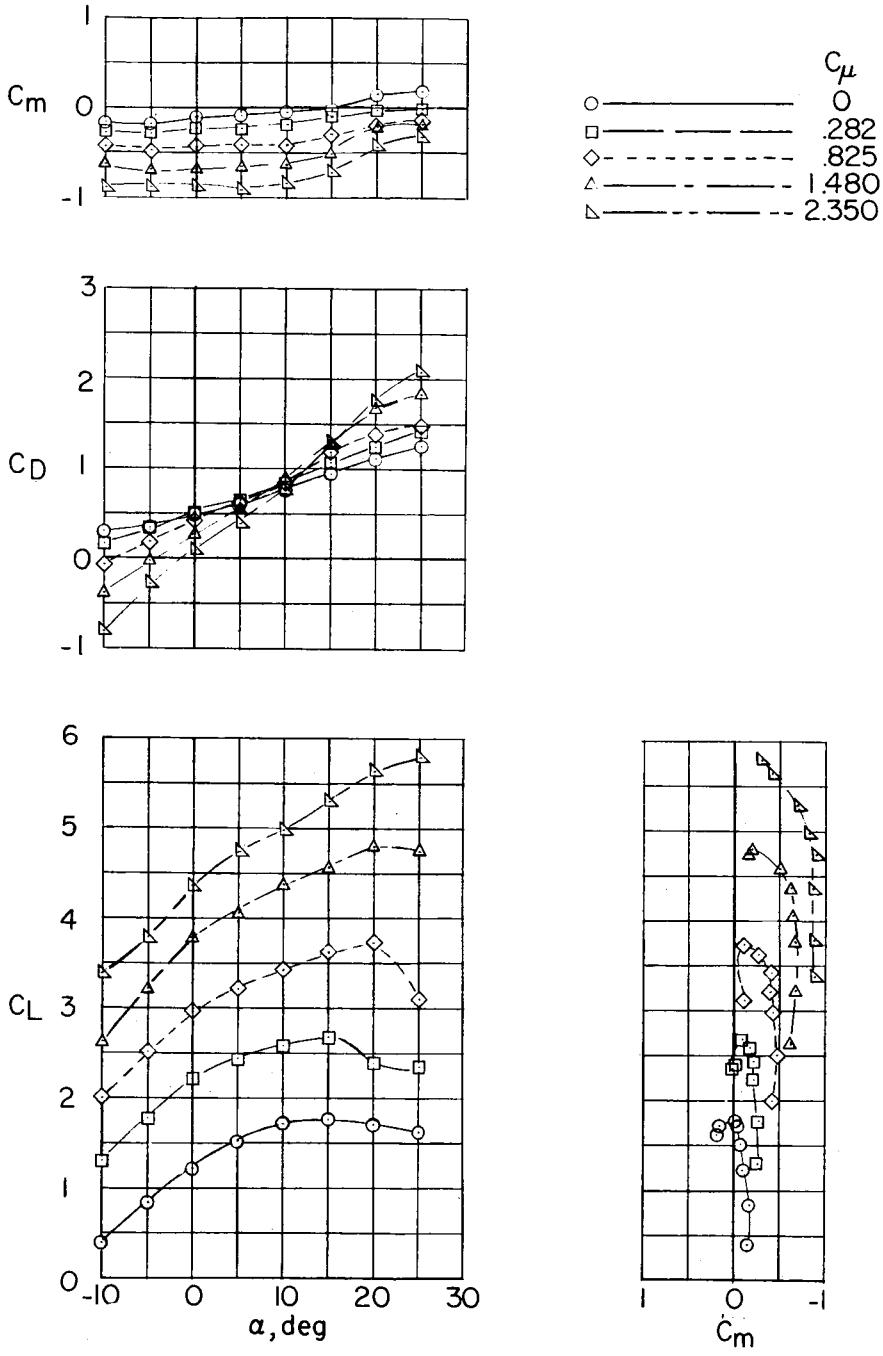

(h) $\frac{h}{c} = 0.554$; $i_t = 10^\circ$.

Figure 6.- Continued.

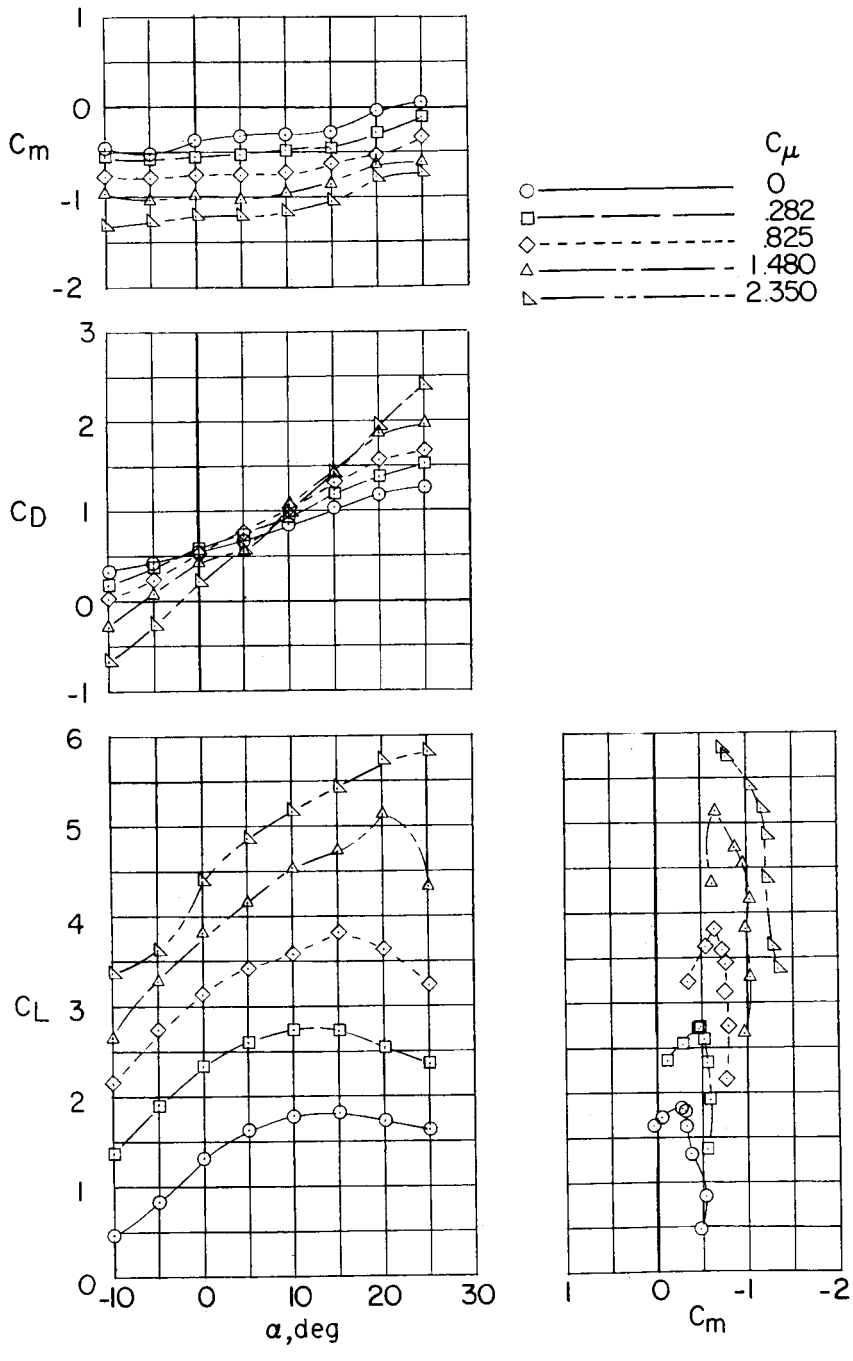

(i) $\frac{h}{c} = 0.554$; $i_t = 20^\circ$.

Figure 6.- Concluded.

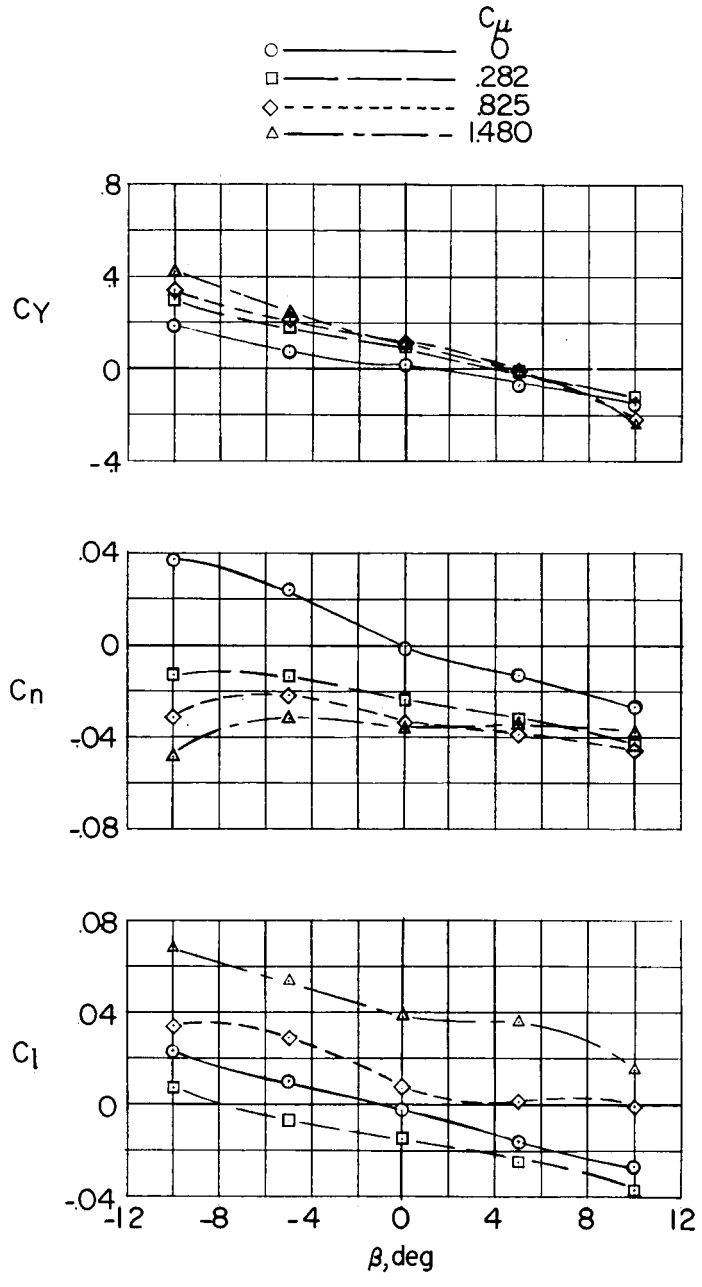

(a) Vertical tail off; $\alpha = 0^\circ$.

Figure 7.- Variation of rolling moment, yawing moment, and side force with sideslip angle for the high-wing configuration. $\delta_f = 55^\circ$; $i_t = 0^\circ$.

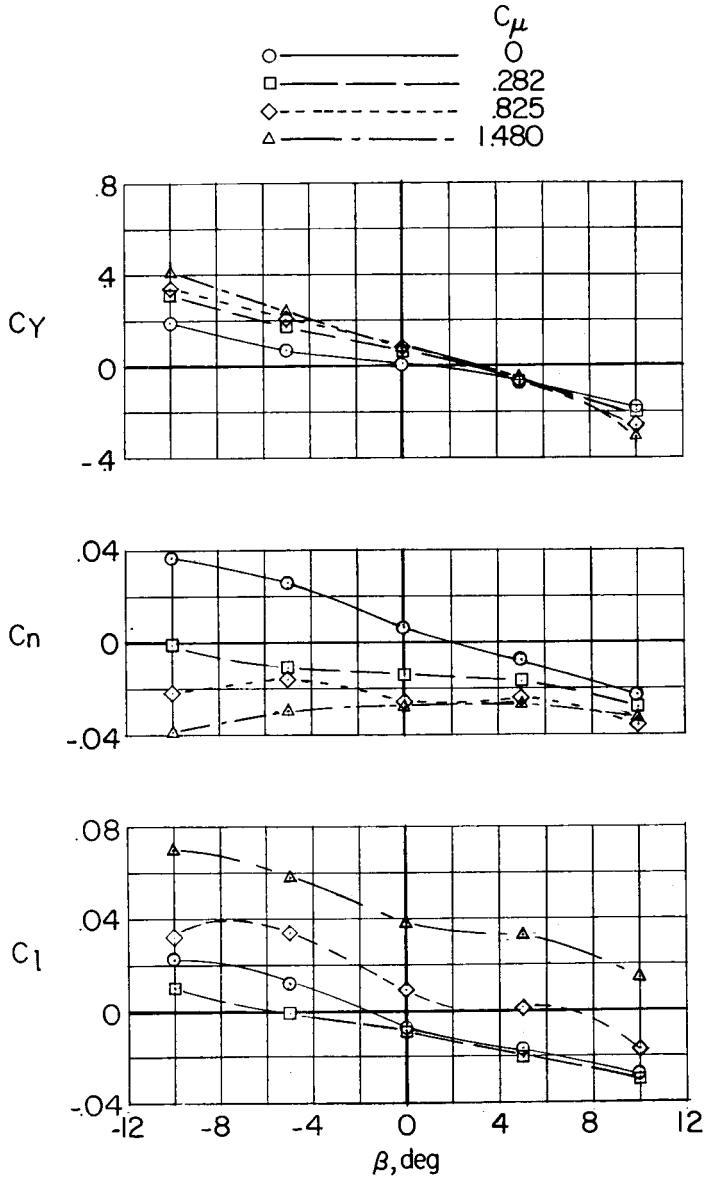

(b) Vertical tail off; $\alpha = 5^\circ$.

Figure 7.- Continued.

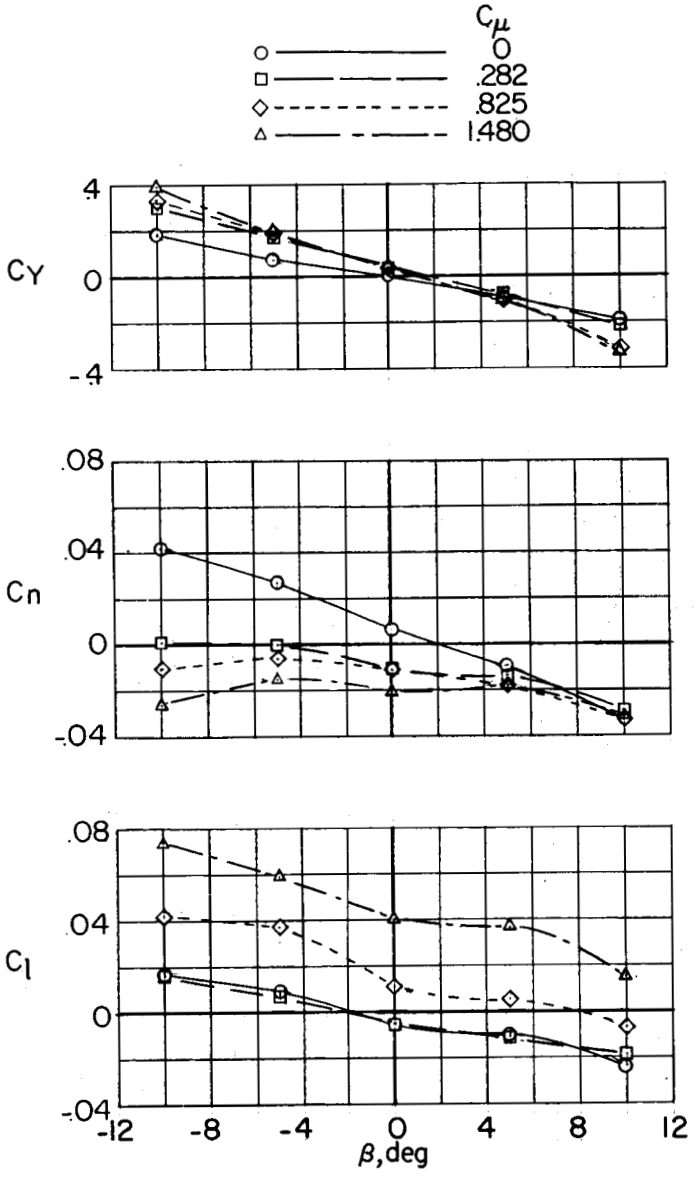

(c) Vertical tail off; $\alpha = 10^\circ$.

Figure 7.- Continued.

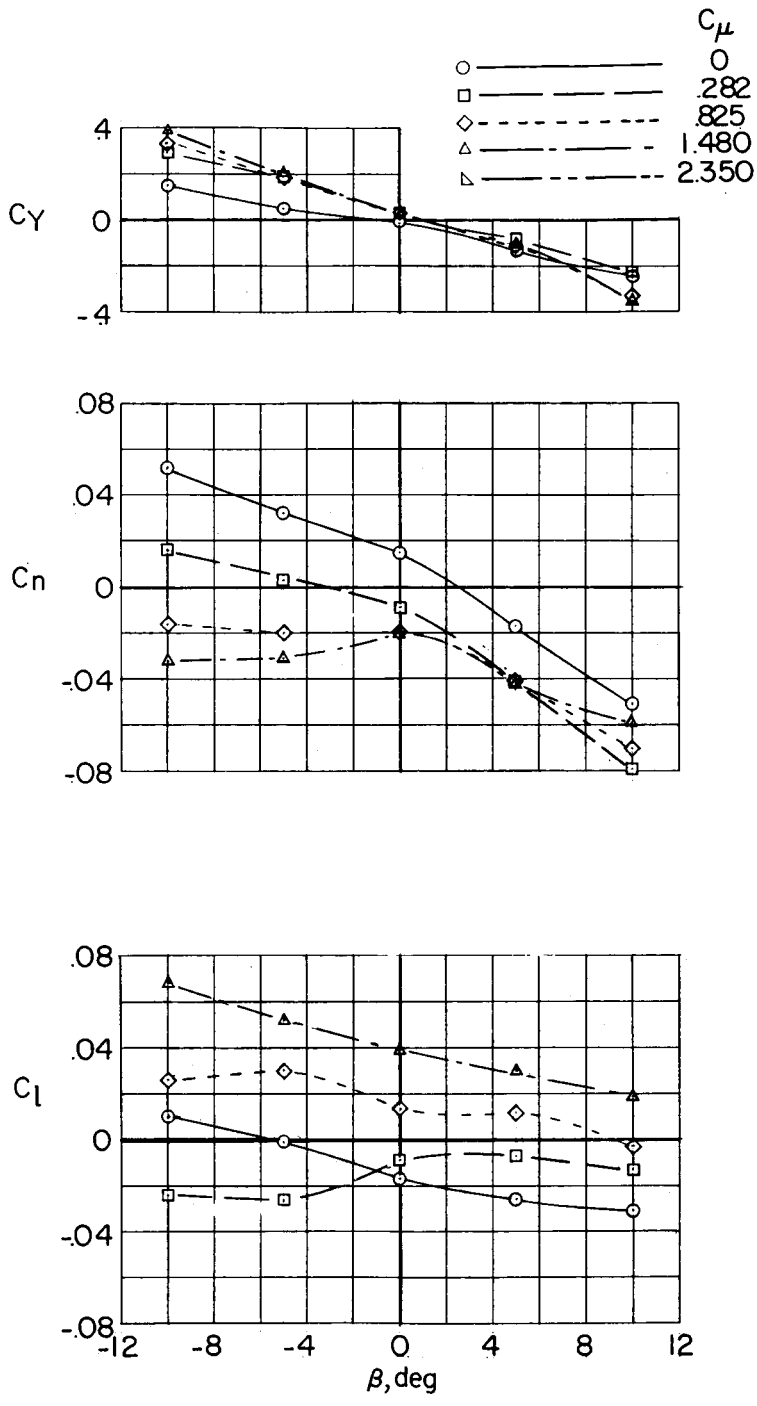

(d) Vertical tail off; $\alpha = 15^\circ$.

Figure 7.- Continued.

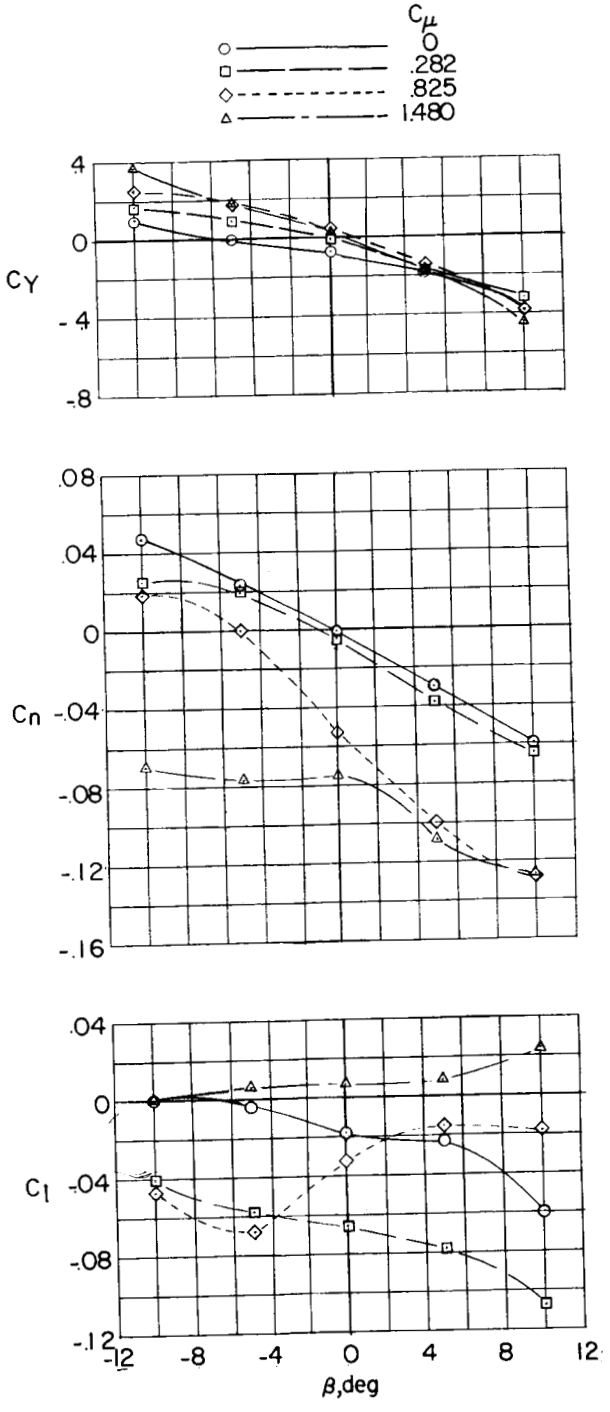

(e) Vertical tail off; $\alpha = 20^\circ$.

Figure 7.- Continued.

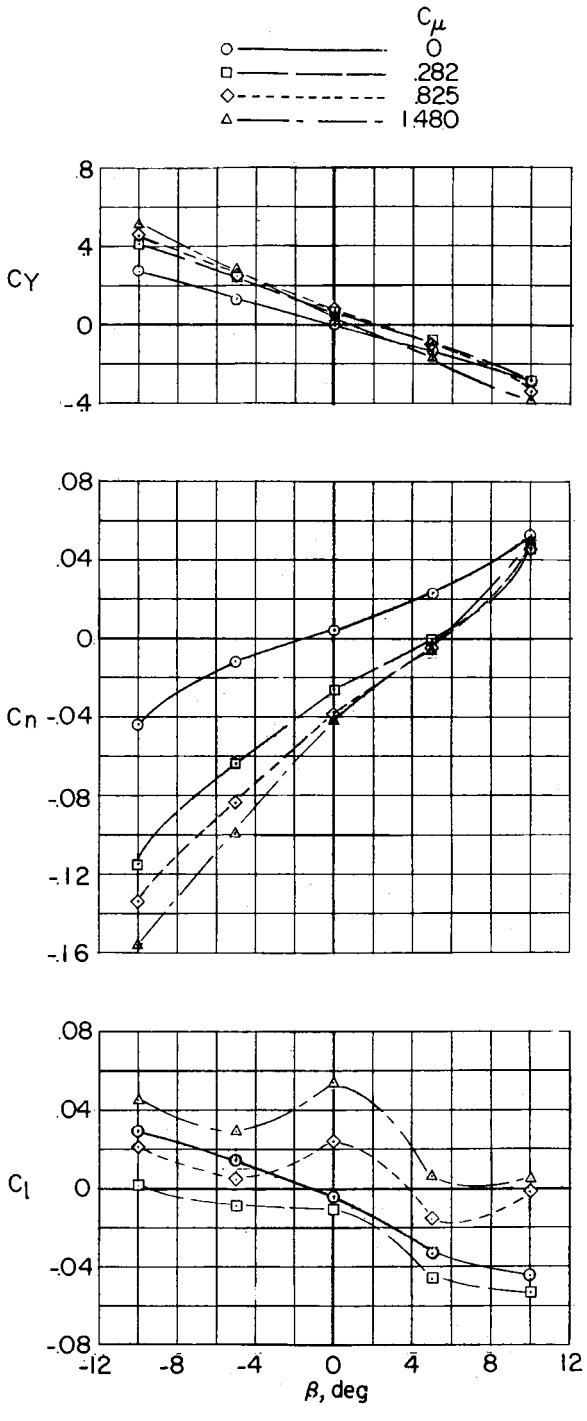

(f) $\frac{h}{\bar{c}} = 0$; $\alpha = 0^\circ$.

Figure 7.- Continued.

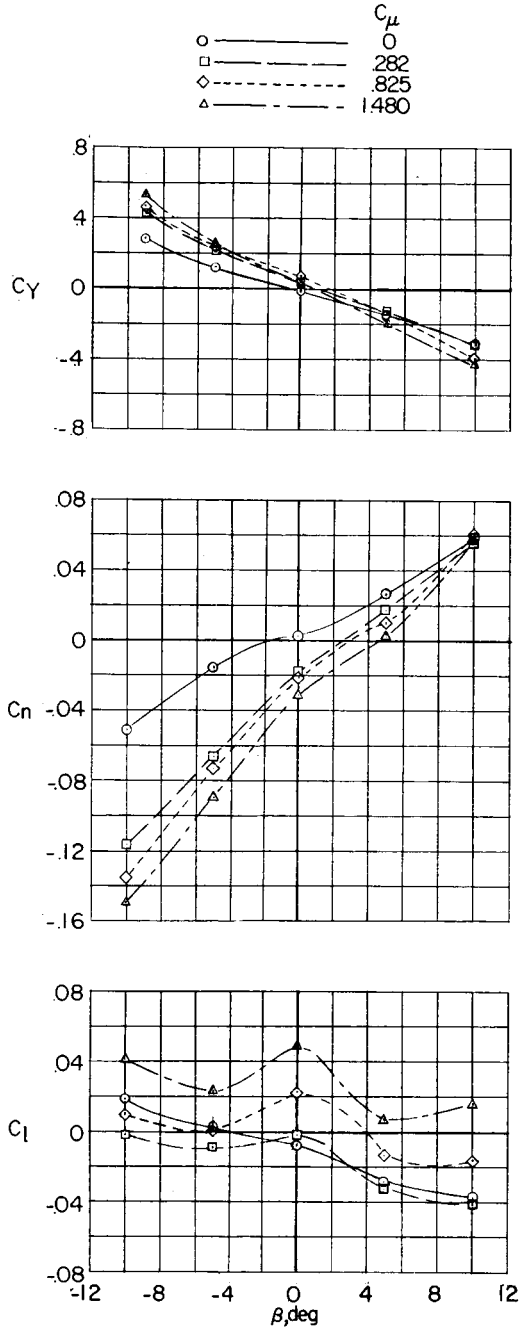

(g) $\frac{h}{c} = 0$; $\alpha = 5^\circ$.

Figure 7.- Continued.

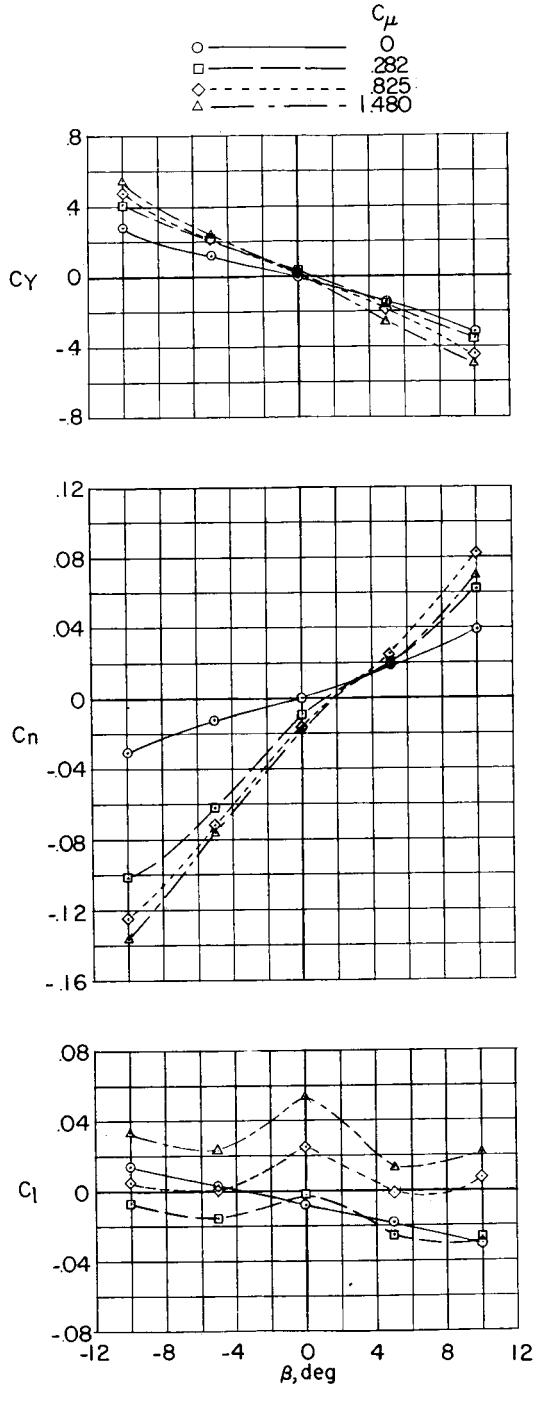

(h) $\frac{h}{c} = 0$; $\alpha = 10^\circ$.

Figure 7.- Continued.

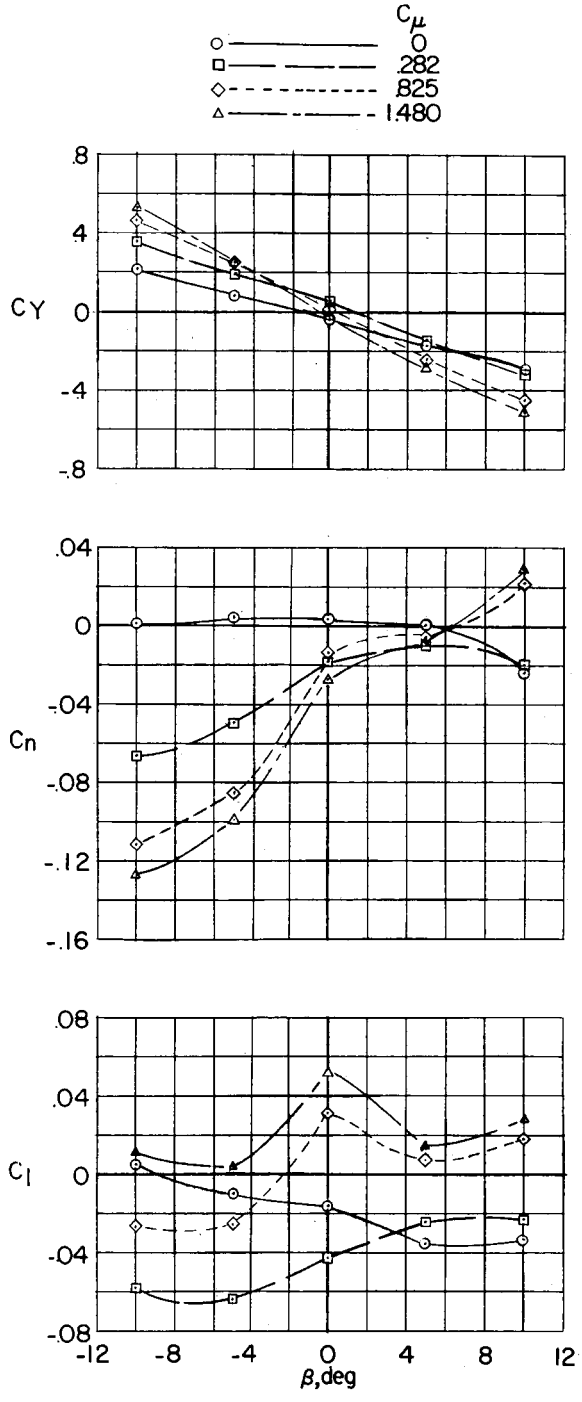

(i) $\frac{h}{\bar{c}} = 0$; $\alpha = 15^\circ$.

Figure 7.- Continued.

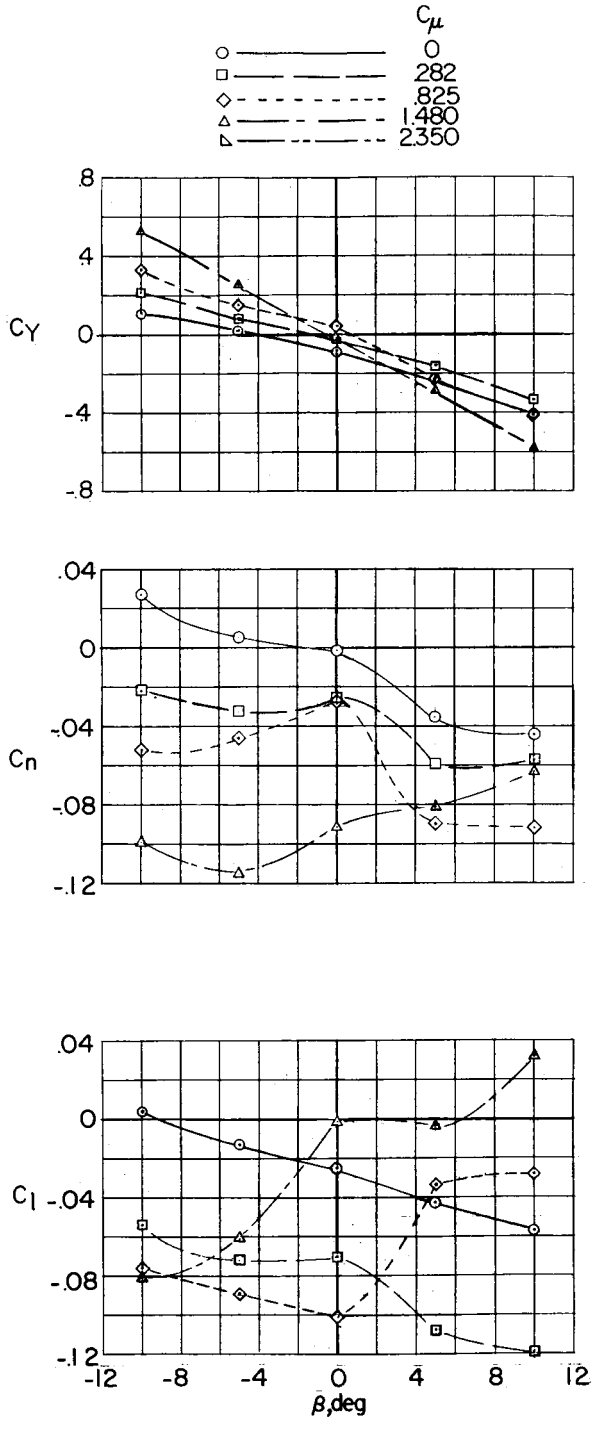

(j) $\frac{h}{\bar{c}} = 0$; $\alpha = 20^\circ$.

Figure 7.- Concluded.

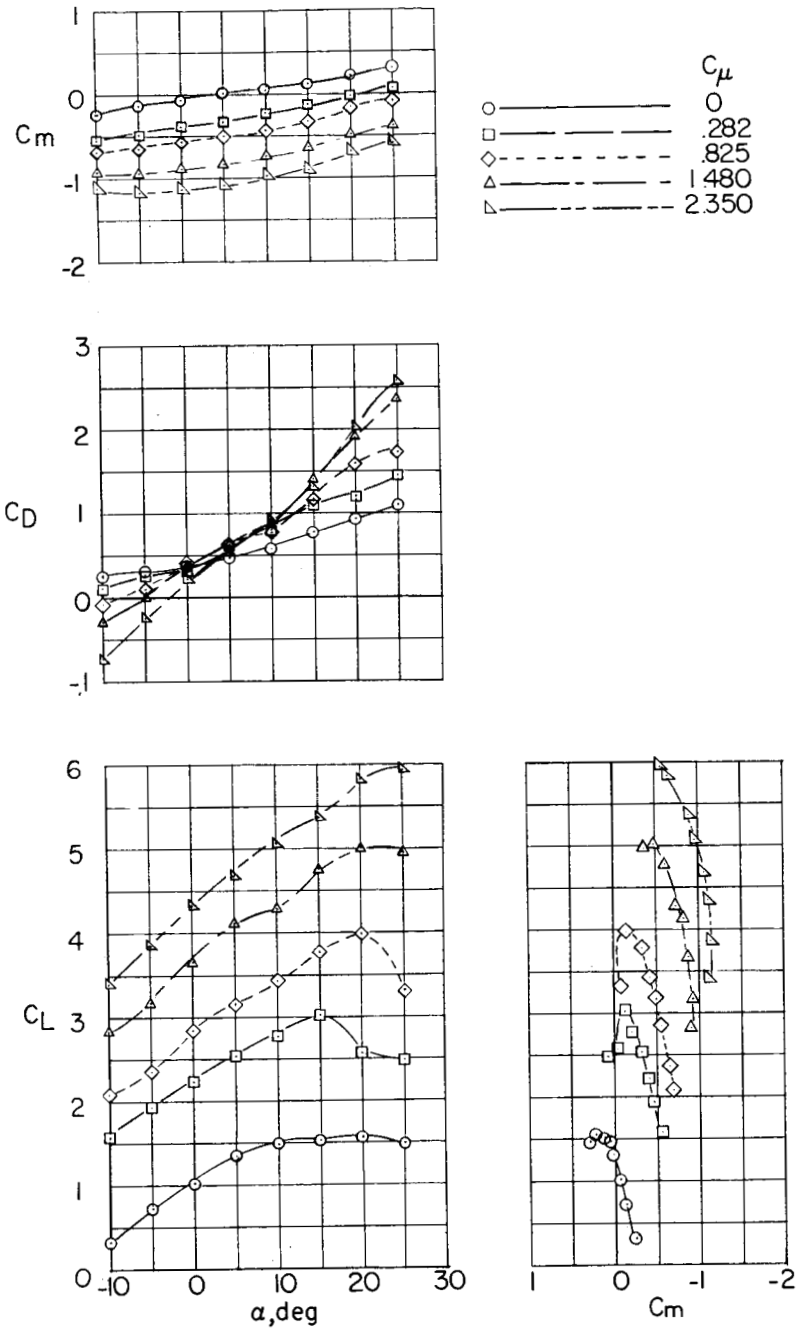

(a) Vertical tail off.

Figure 8.- Longitudinal stability and trim characteristics of the mid-wing configuration. $\delta_f = 55^\circ$.

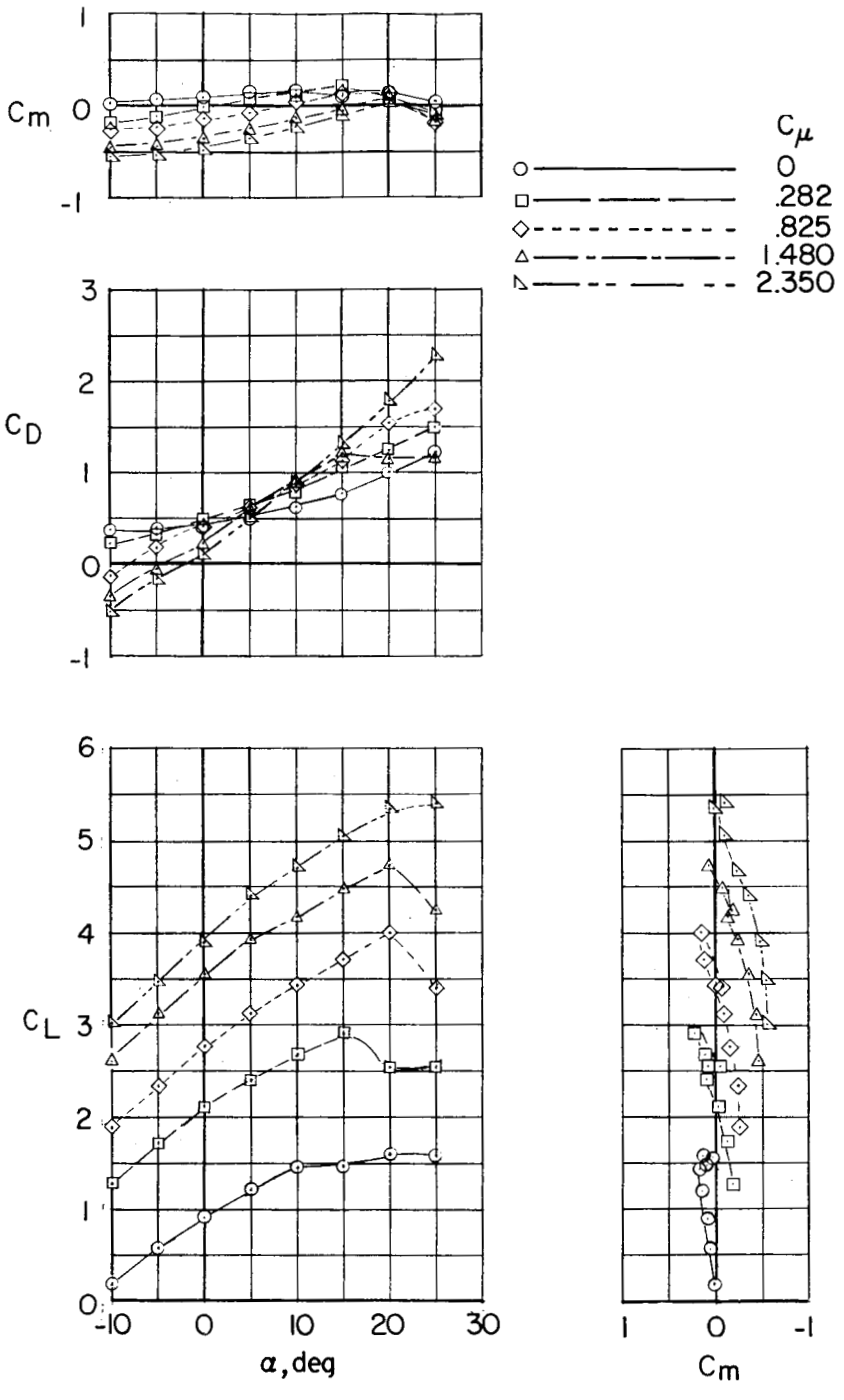

(b) $\frac{h}{\bar{c}} = 0$; $i_t = 0^o$.

Figure 8.- Continued.

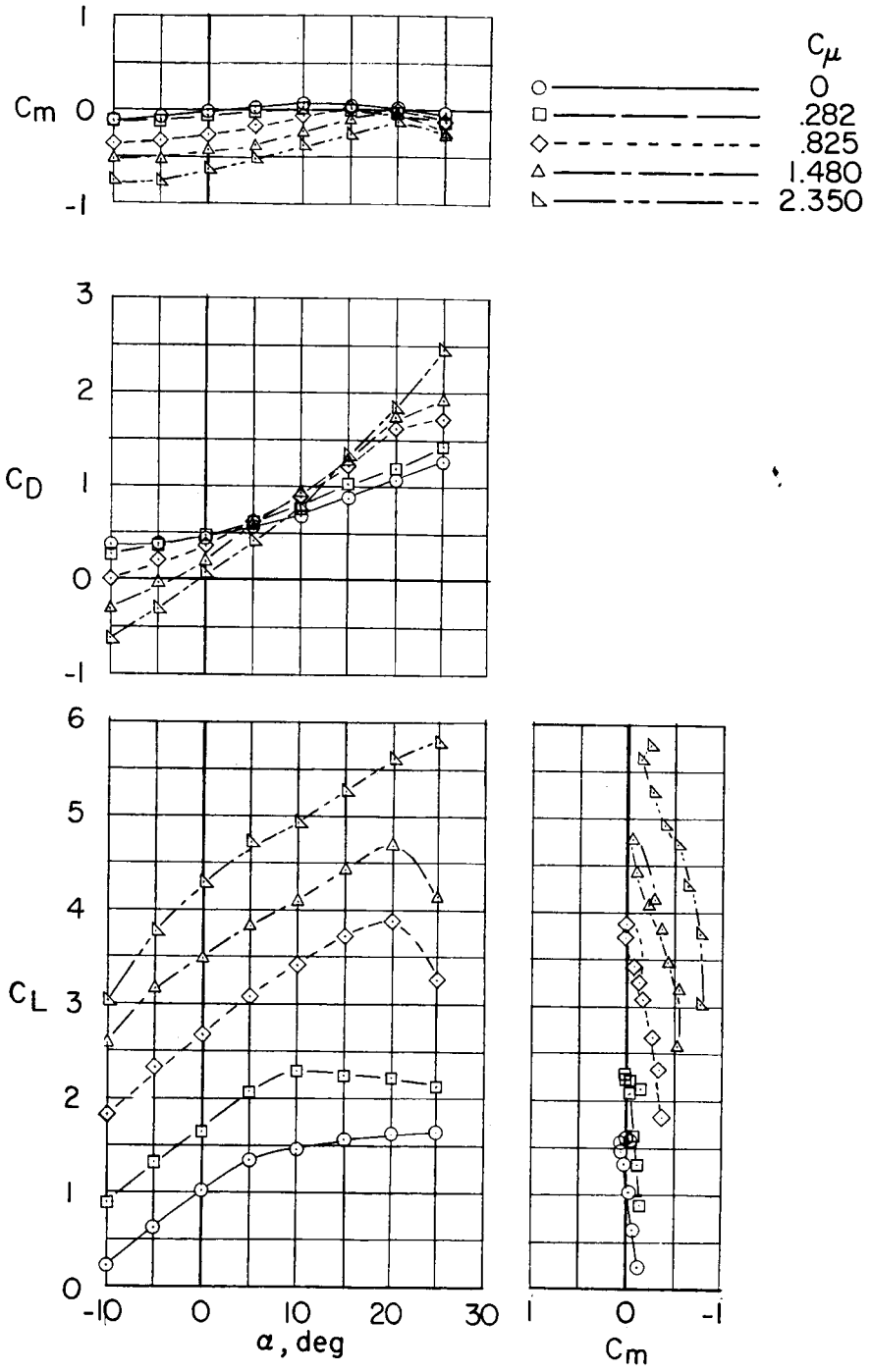

(c) $\frac{h}{\bar{c}} = 0$; $i_t = 5^\circ$.

Figure 8.- Continued.

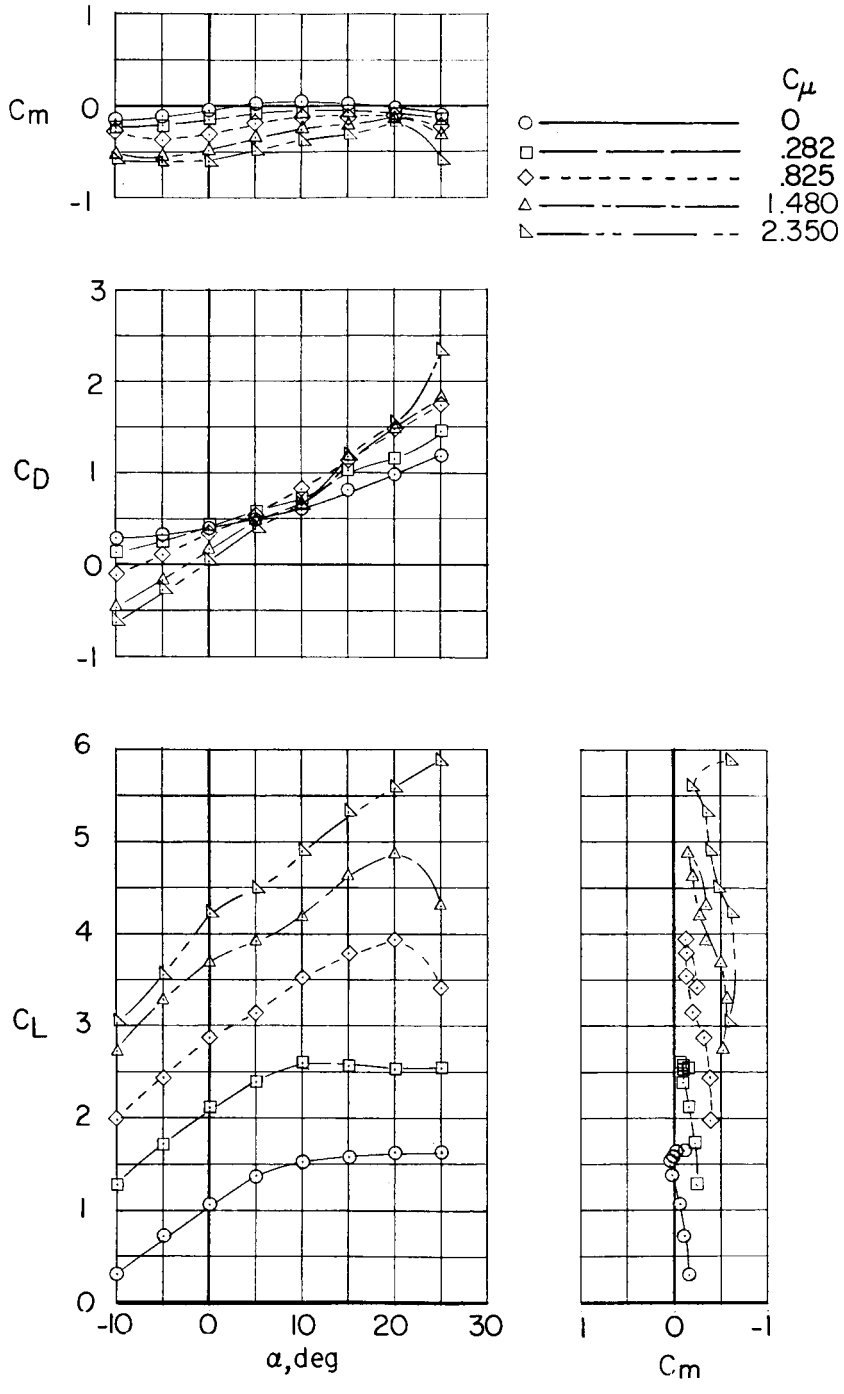

(d) $\frac{h}{c} = 0$; $i_t = 10^\circ$.

Figure 8.- Continued.

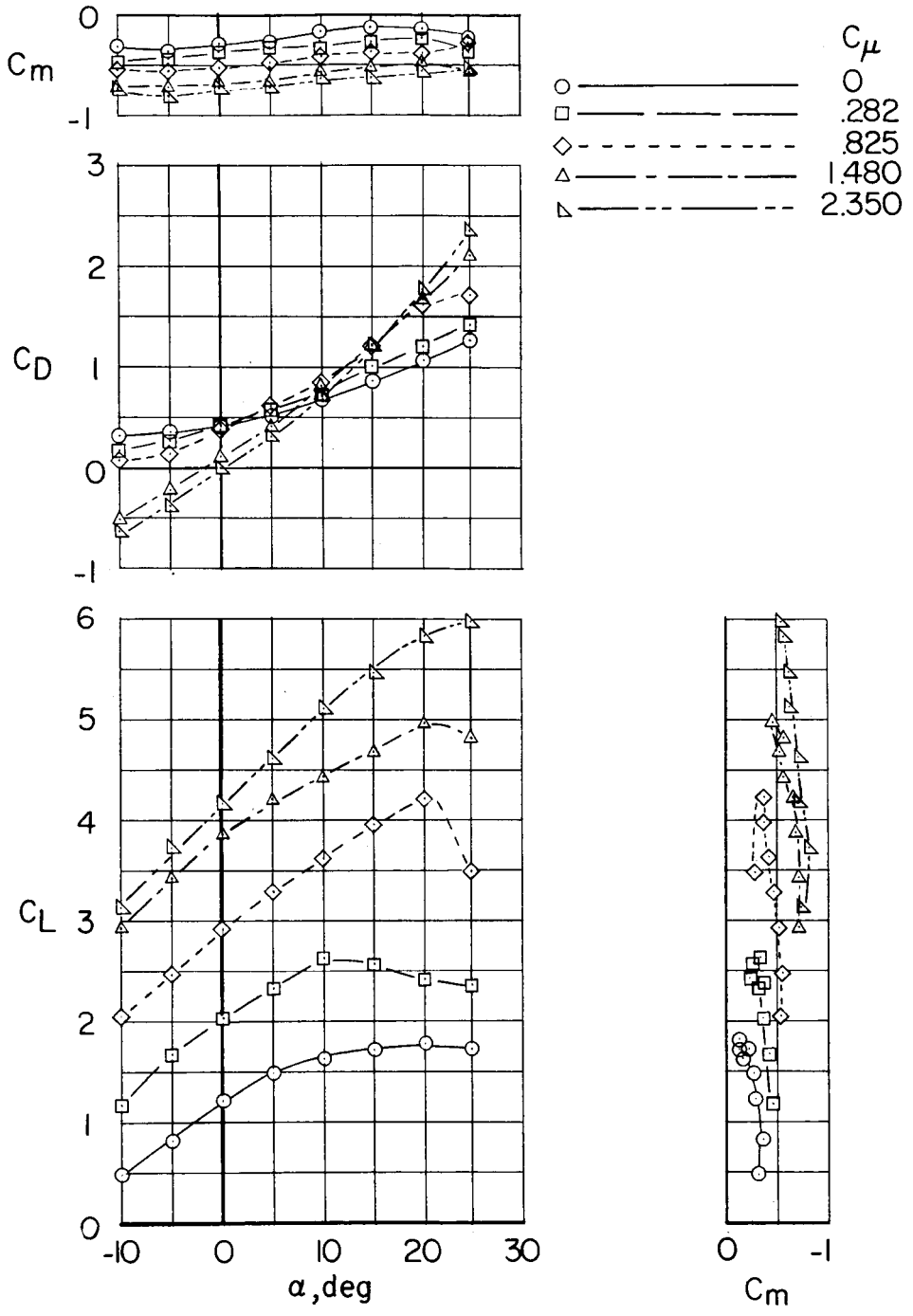

(e) $\frac{h}{c} = 0$; $i_t = 20^\circ$.

Figure 8.- Continued.

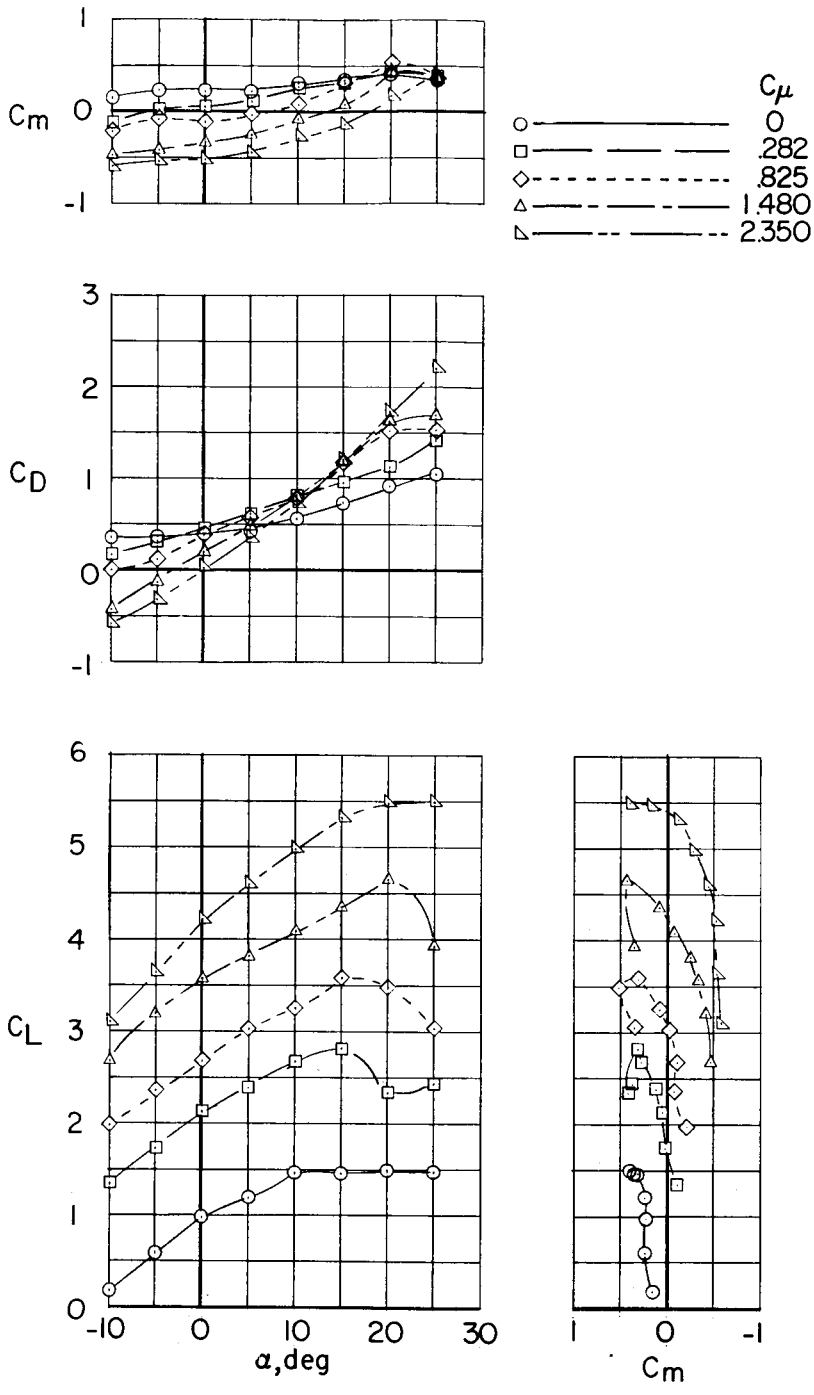

(f) $\frac{h}{\bar{c}} = 0.41$; $i_t = 0^\circ$.

Figure 8.- Continued.

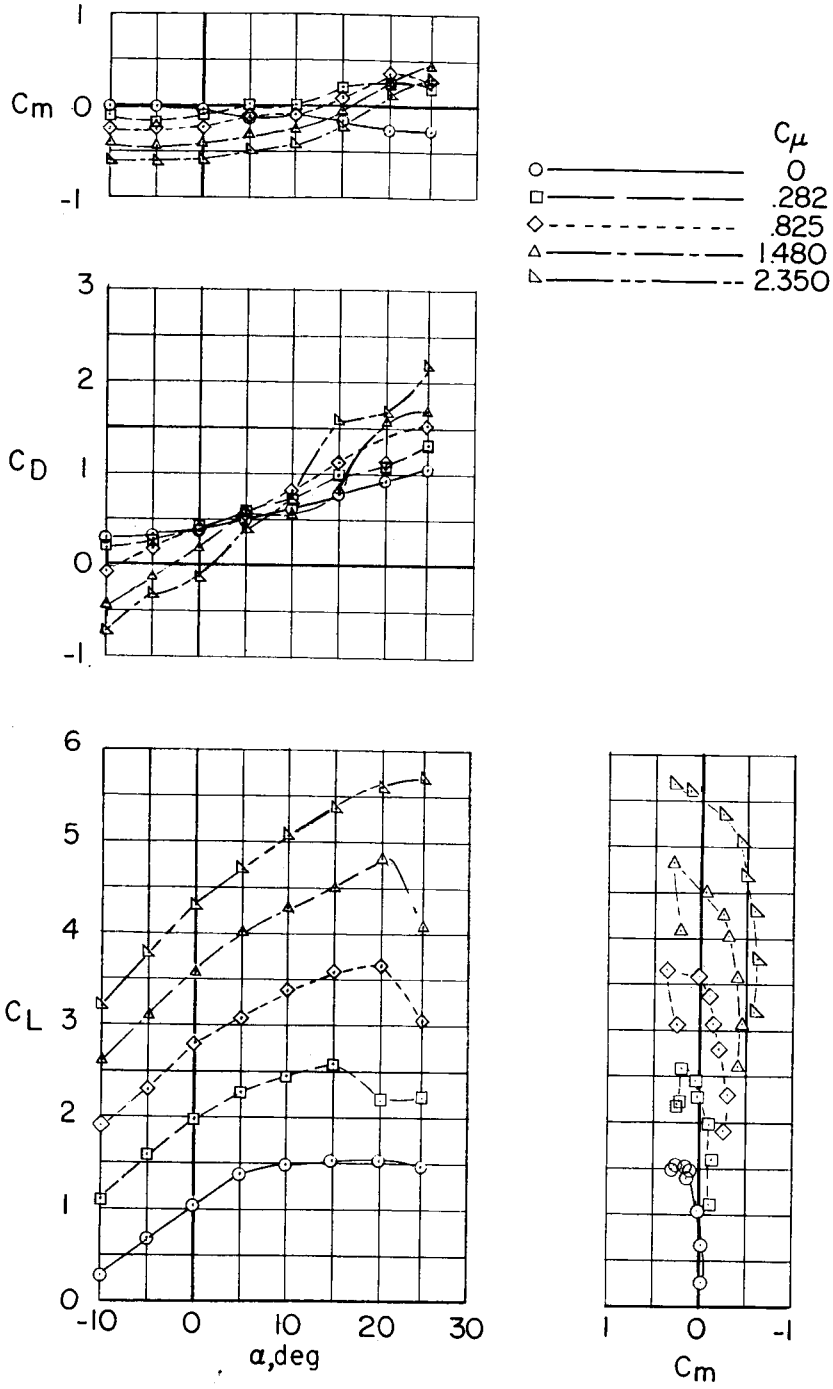

(g) $\frac{h}{\bar{c}} = 0.41$; $i_t = 5^\circ$.

Figure 8.- Continued.

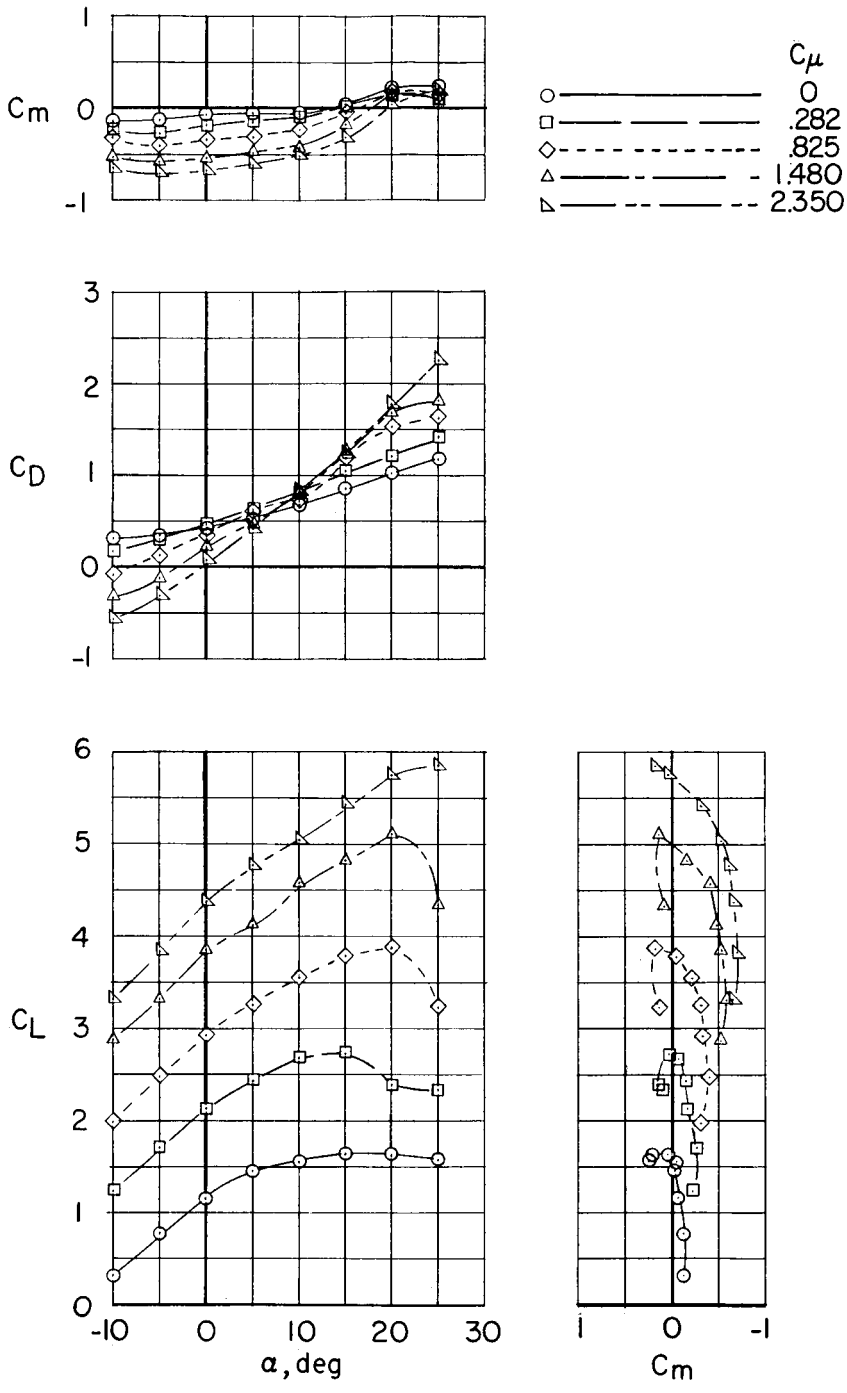

(h) $\frac{h}{c} = 0.41$; $i_t = 10^\circ$.

Figure 8.- Continued.

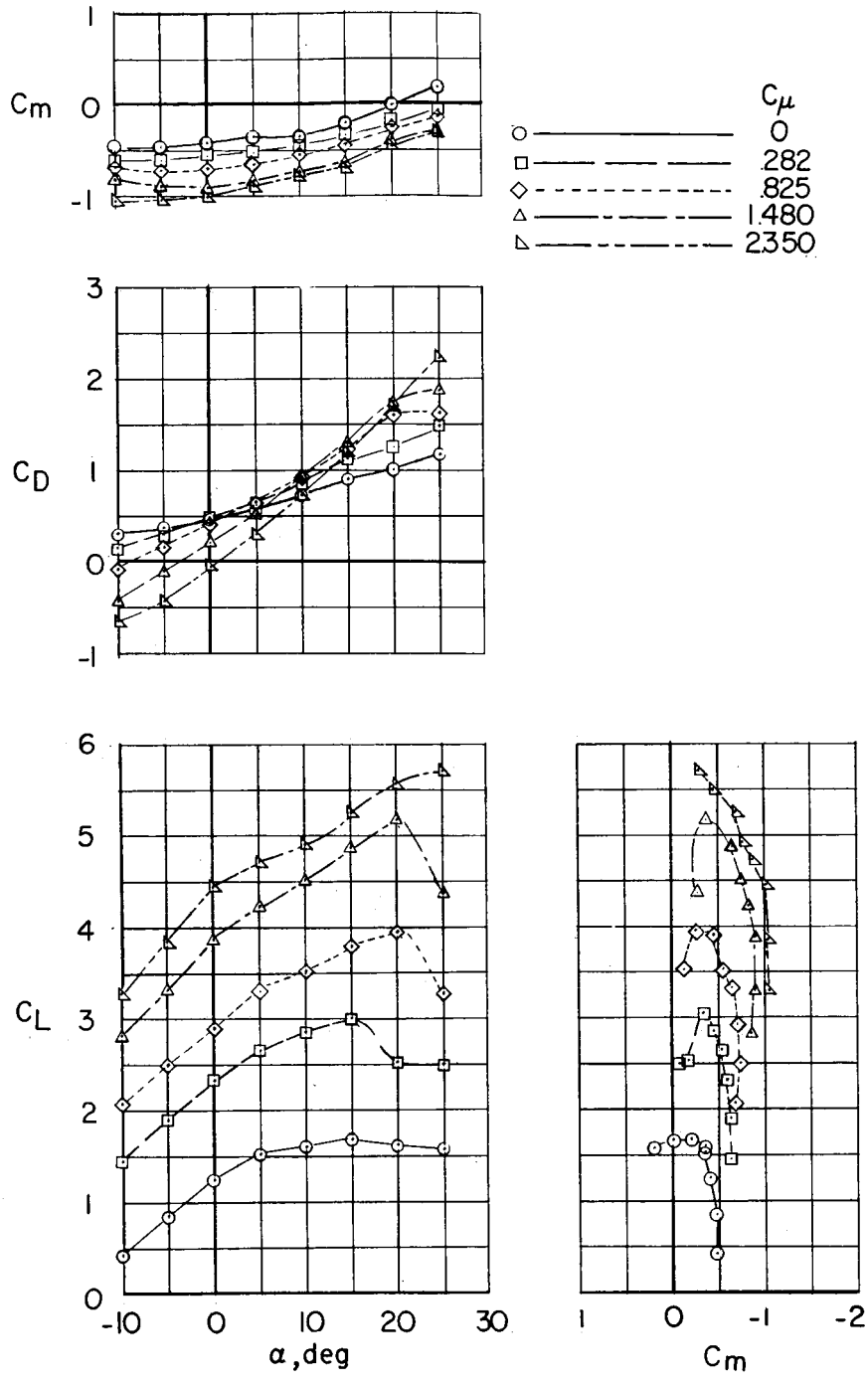

(i) $\frac{h}{c} = 0.41$; $i_t = 20^\circ$.

Figure 8.- Concluded.

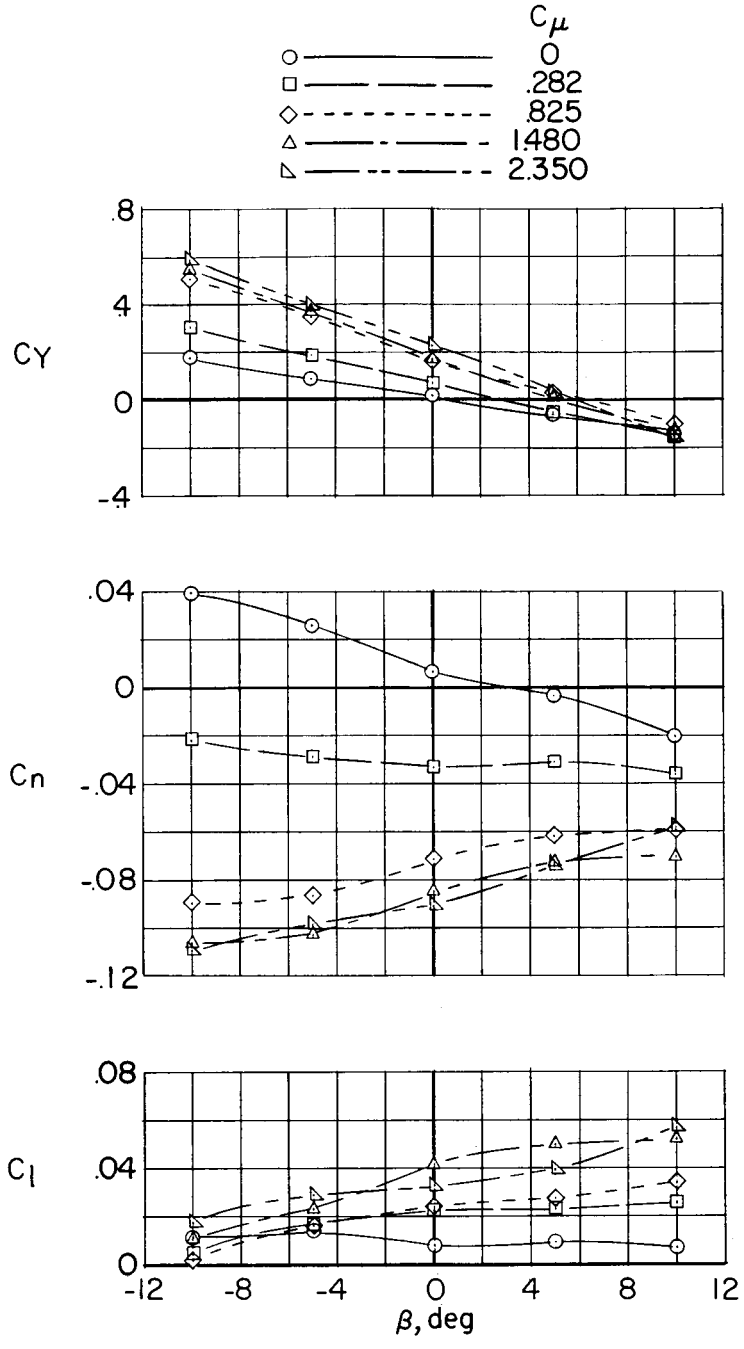

(a) Vertical tail off; $\alpha = 0^{\circ}$.

Figure 9.- Variation of rolling moment, yawing moment, and side force with sideslip angle for the mid-wing configuration. $\delta_f = 55^{\circ}$; $i_t = 0^{\circ}$.

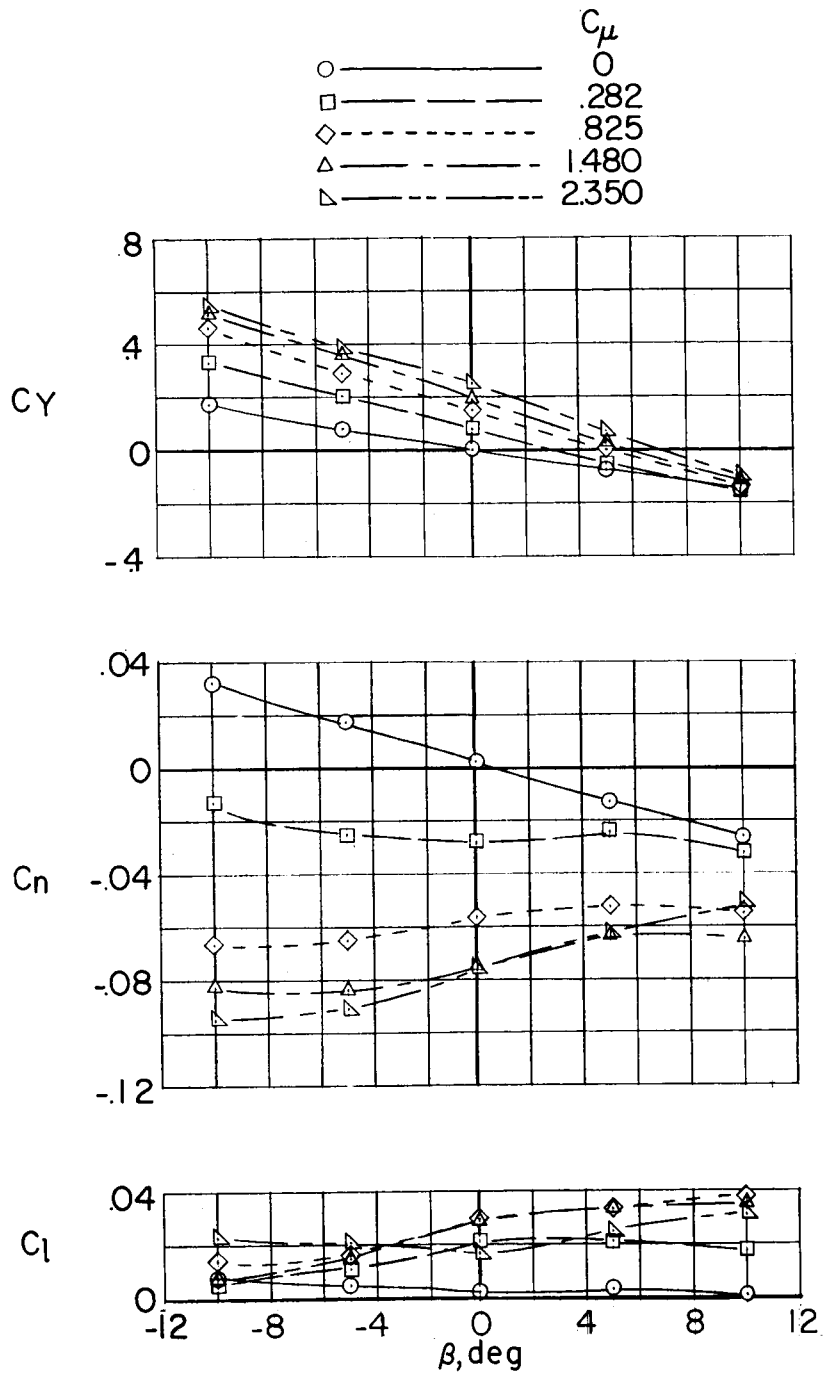

(b) Vertical tail off; $\alpha = 5^\circ$.

Figure 9.- Continued.

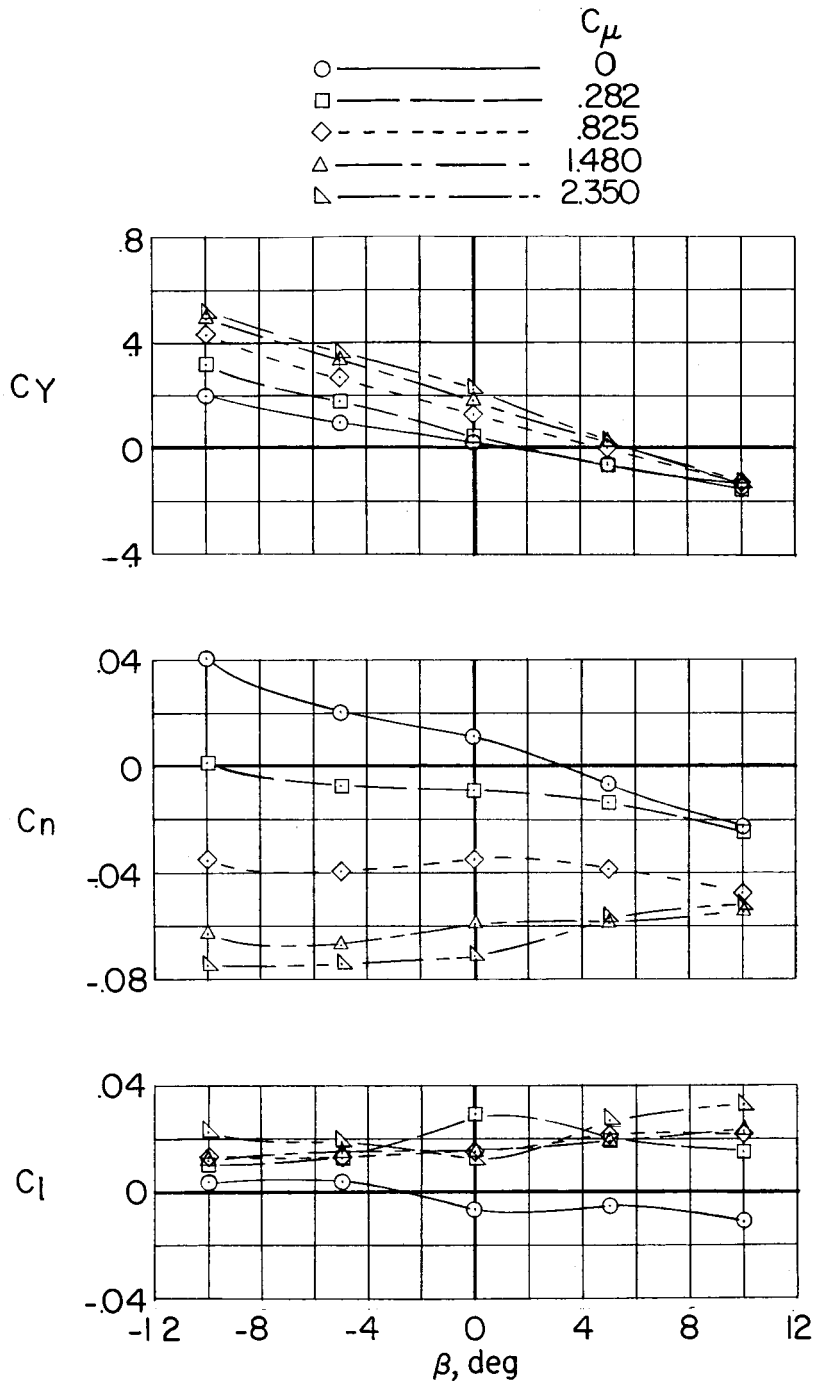

(c) Vertical tail off; $\alpha = 10^{\circ}$.

Figure 9.- Continued.

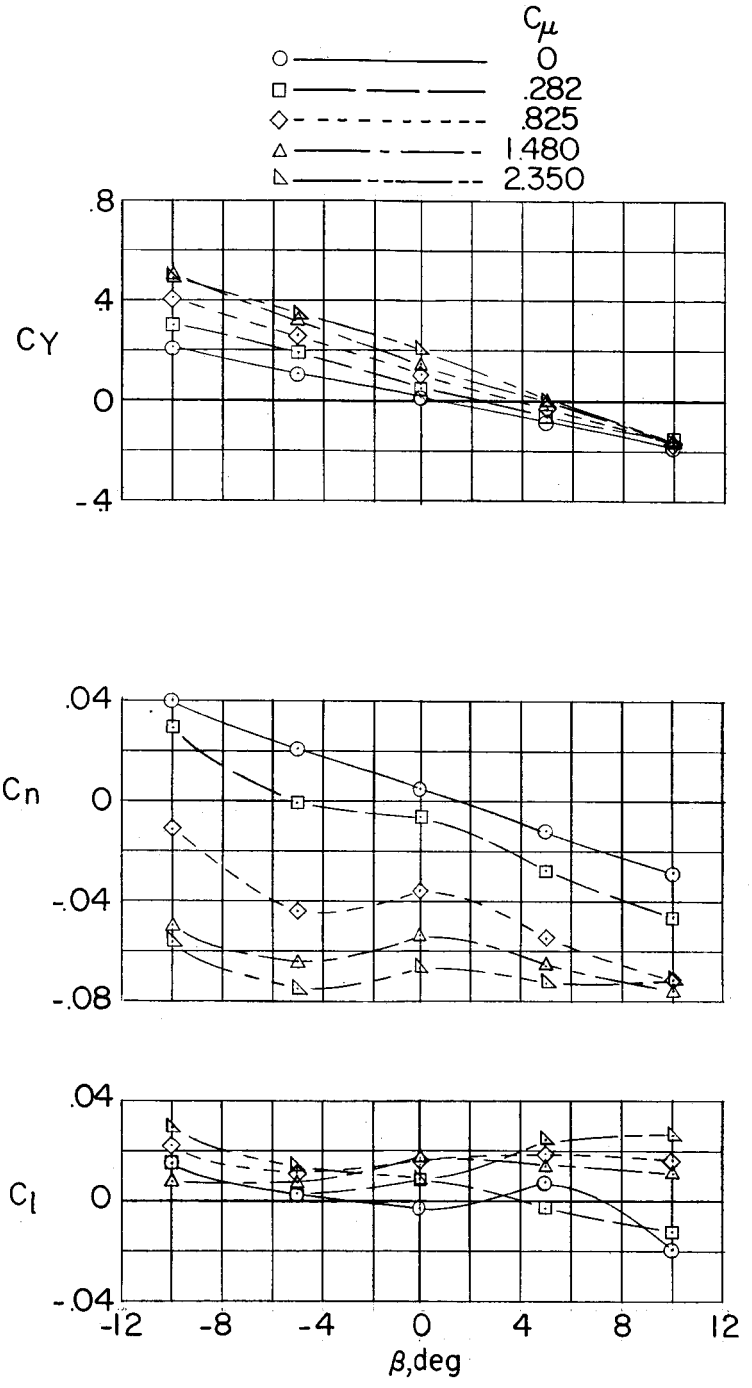

(d) Vertical tail off; $\alpha = 15^\circ$.

Figure 9.- Continued.

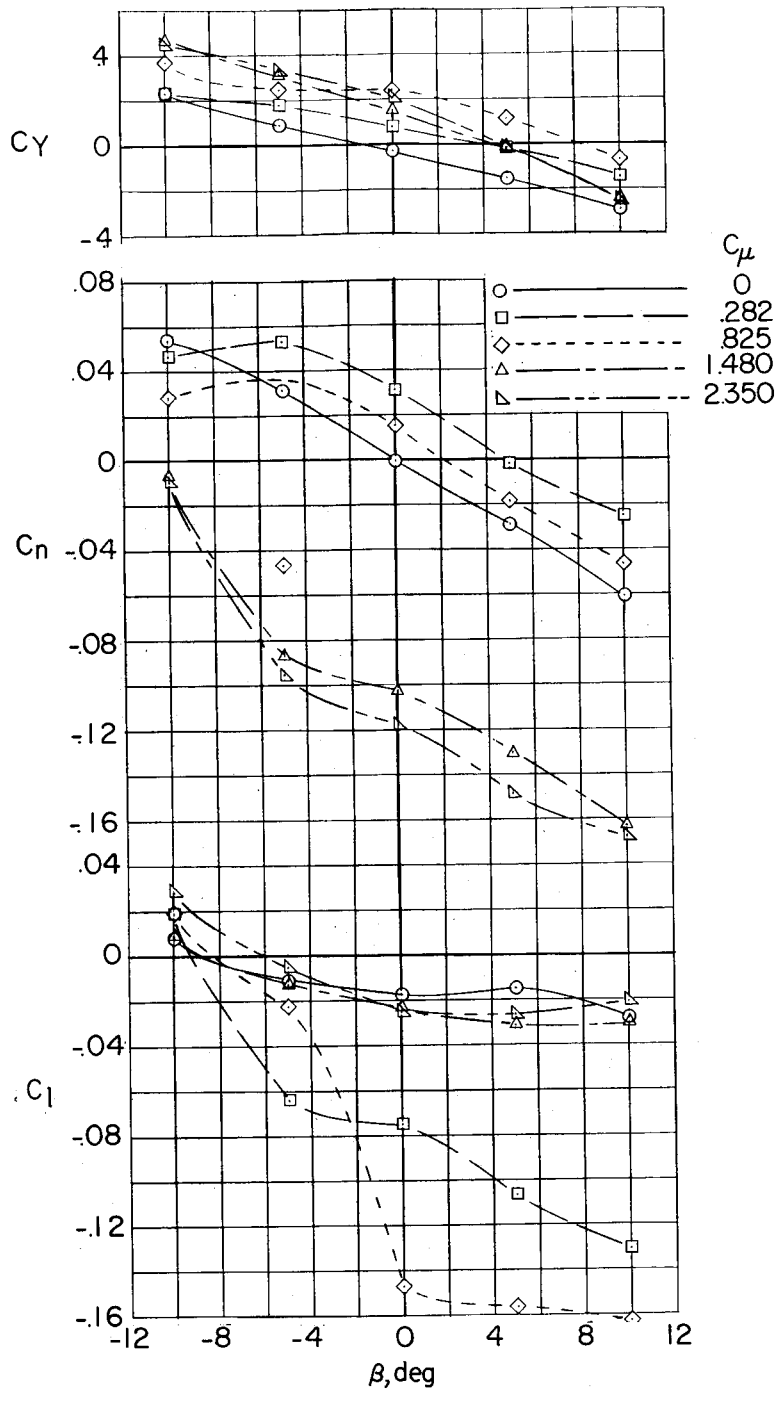

(e) Vertical tail off; $\alpha = 20^\circ$.

Figure 9.- Continued.

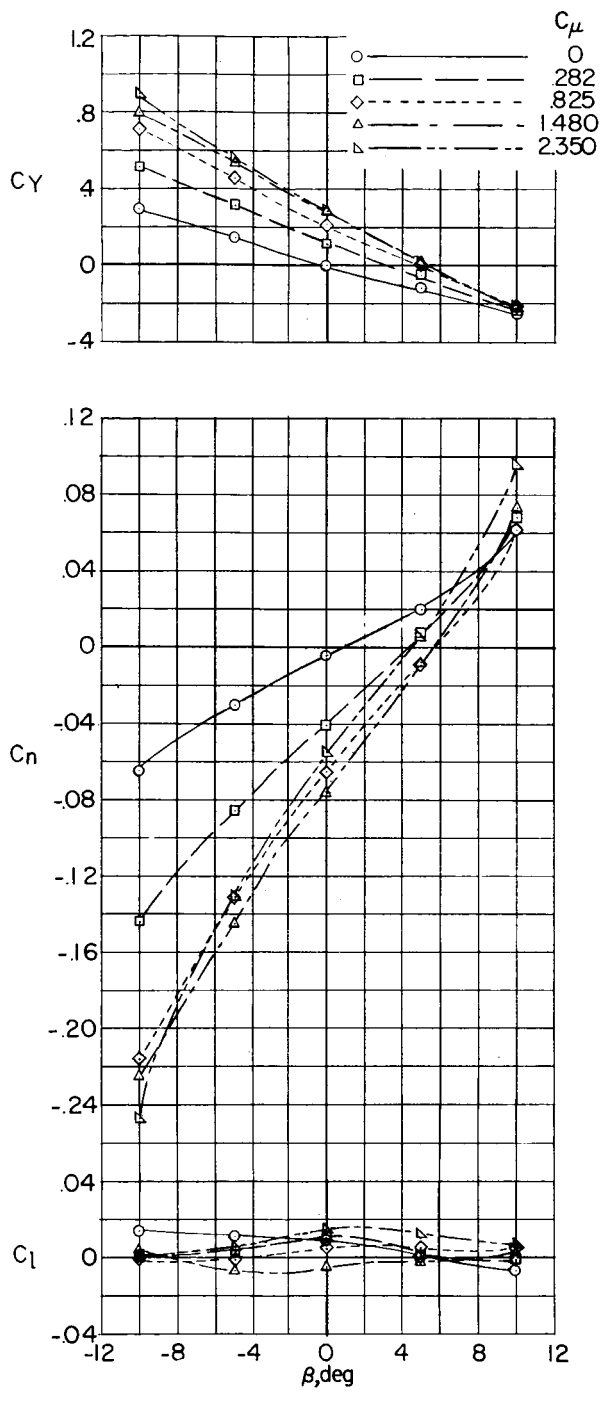

(f) $\frac{h}{\bar{c}} = 0$; $\alpha = 0^\circ$.

Figure 9.- Continued.

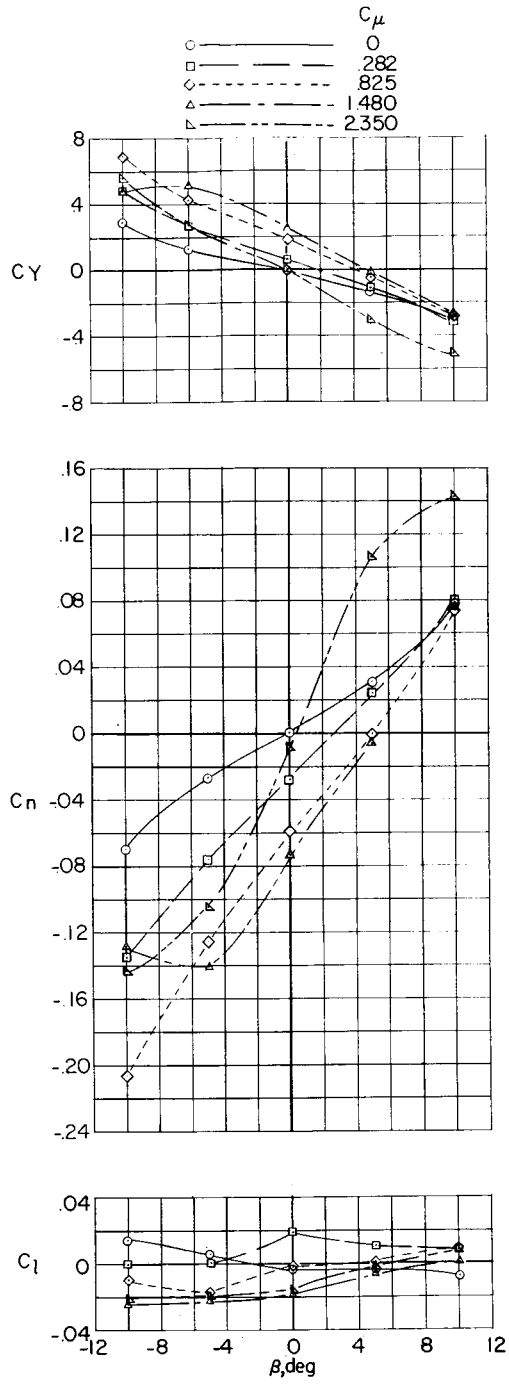

(g) $\frac{h}{\bar{c}} = 0$; $\alpha = 5^\circ$.

Figure 9.- Continued.

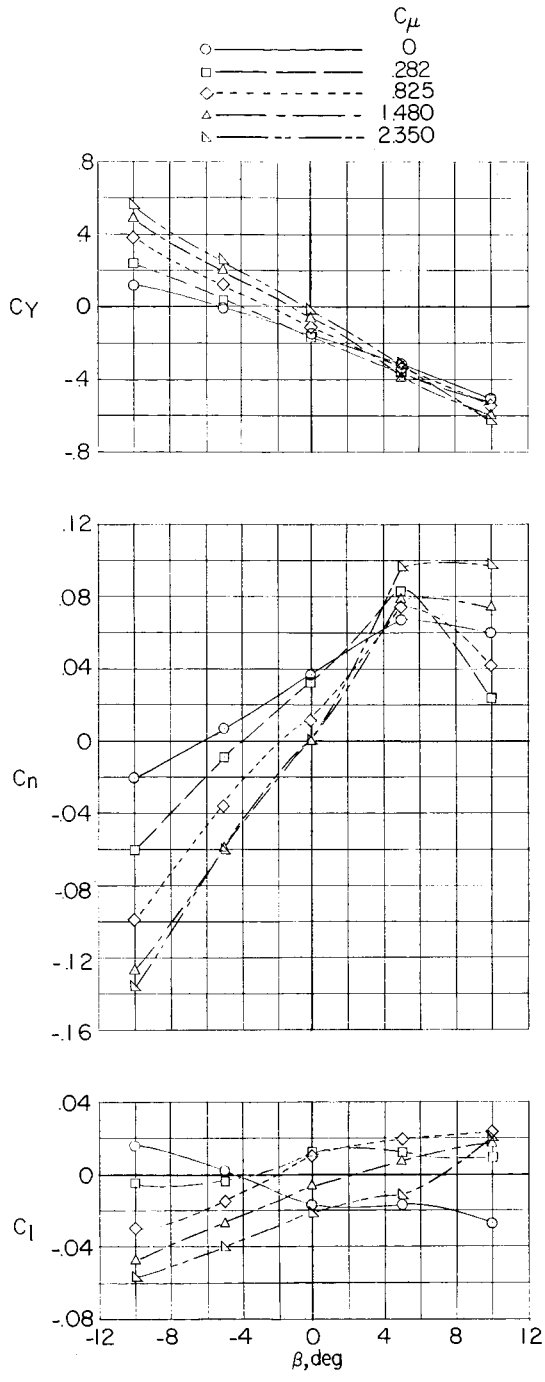

(h) $\frac{h}{\bar{c}} = 0$; $\alpha = 10^\circ$.

Figure 9.- Continued.

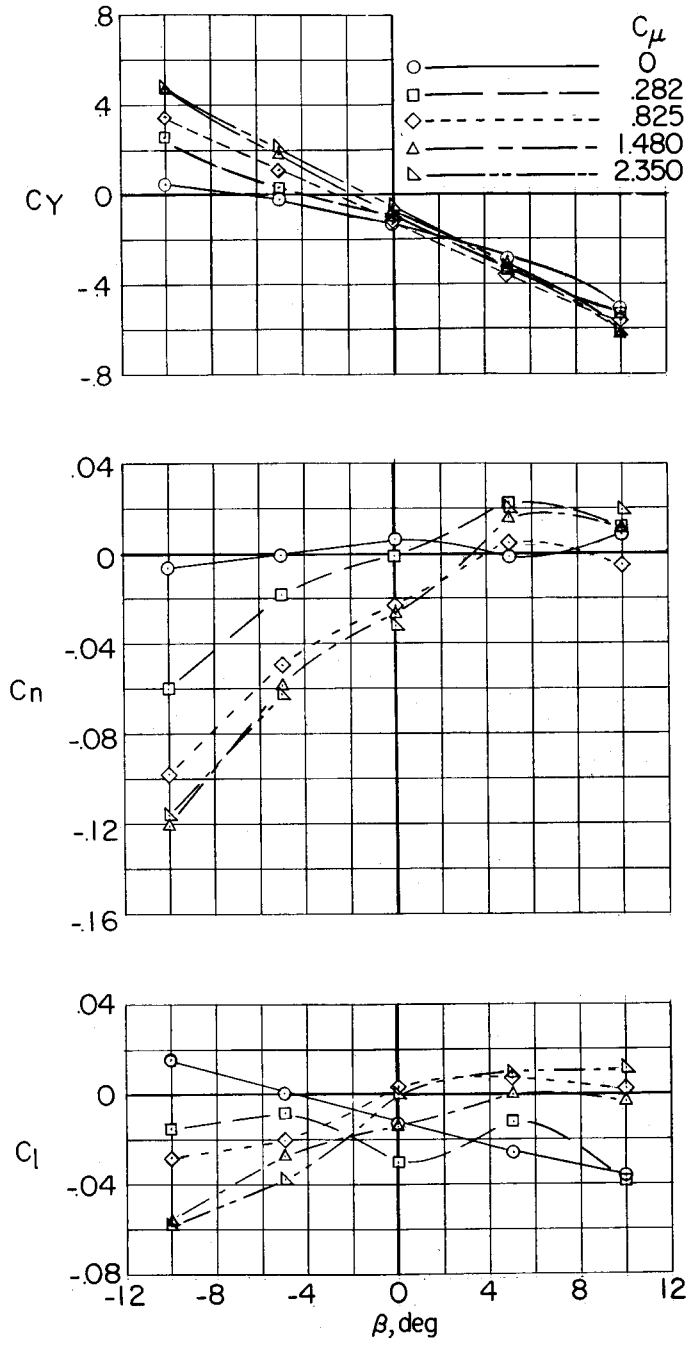

(i) $\frac{h}{c} = 0$; $\alpha = 15^\circ$.

Figure 9.- Continued.

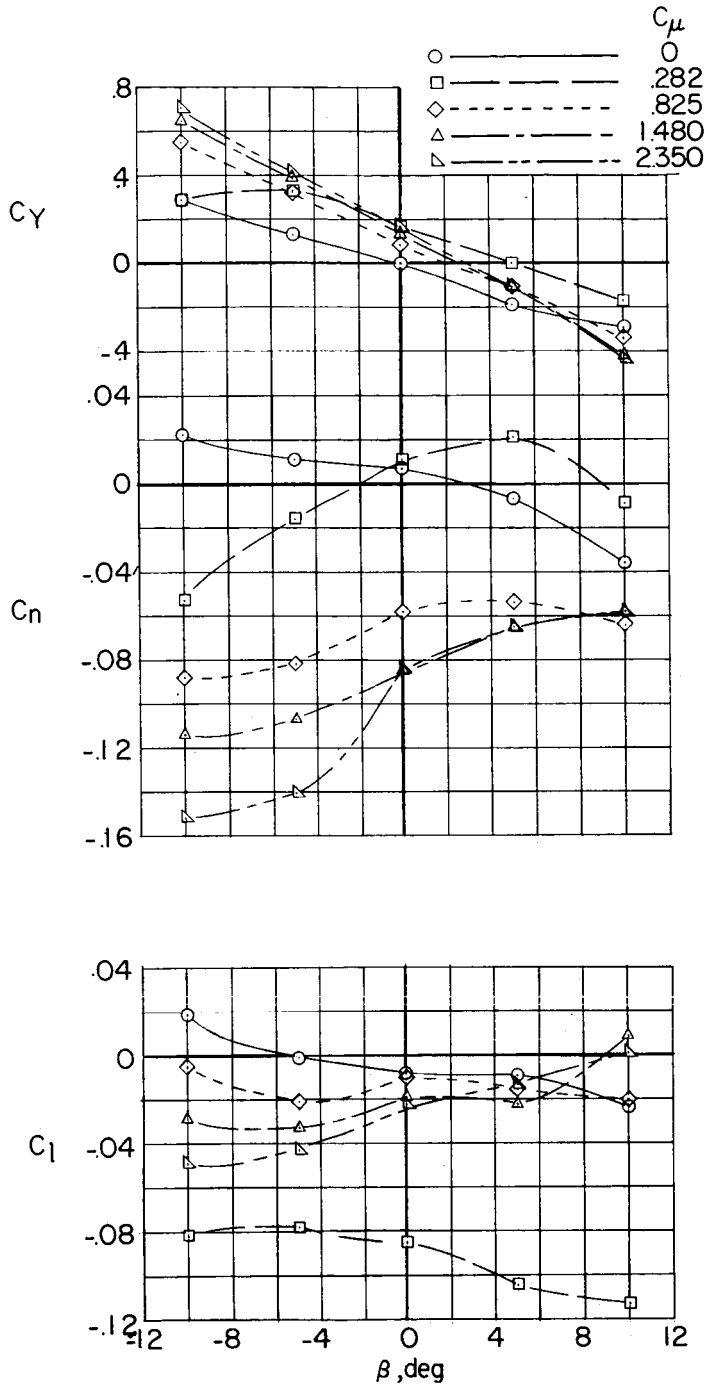

(j) $\frac{h}{\bar{c}} = 0^\circ$; $\alpha = 20^\circ$.

Figure 9.- Concluded.

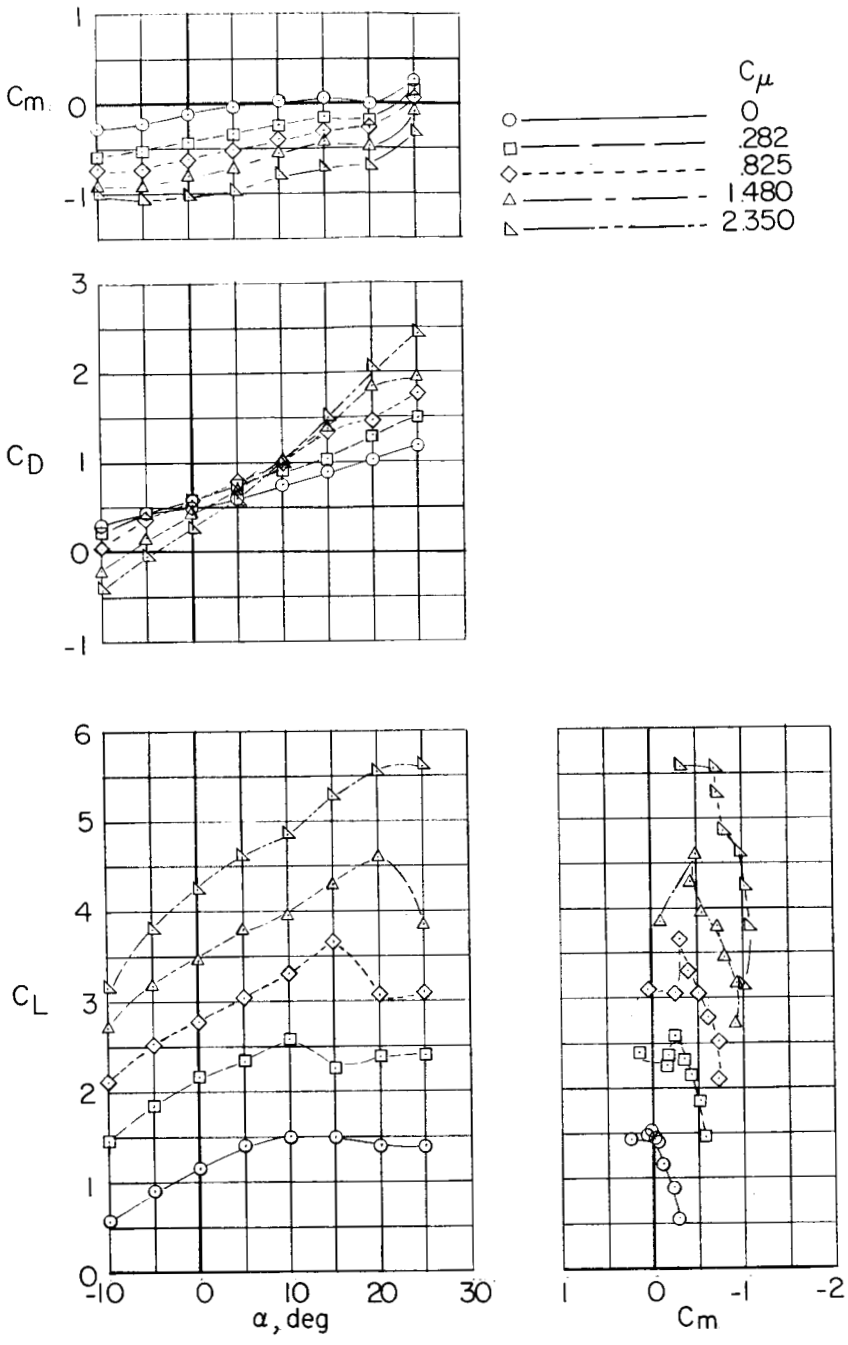

(a) Vertical tail off.

Figure 10.- Longitudinal stability and trim characteristics of the low-wing configuration. $\delta_f = 55^\circ$.

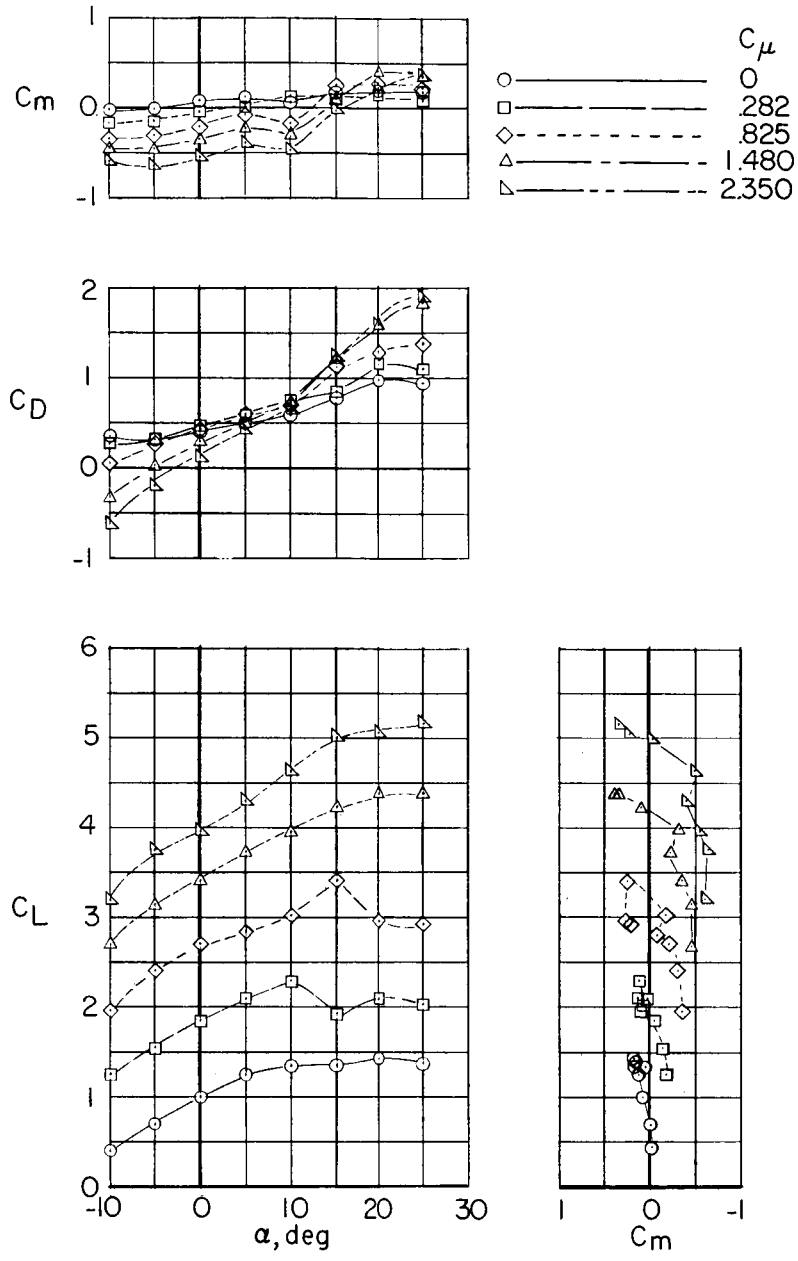

(b) $\frac{h}{\bar{c}} = 0.28$; $i_t = 0°$.

Figure 10.- Continued.

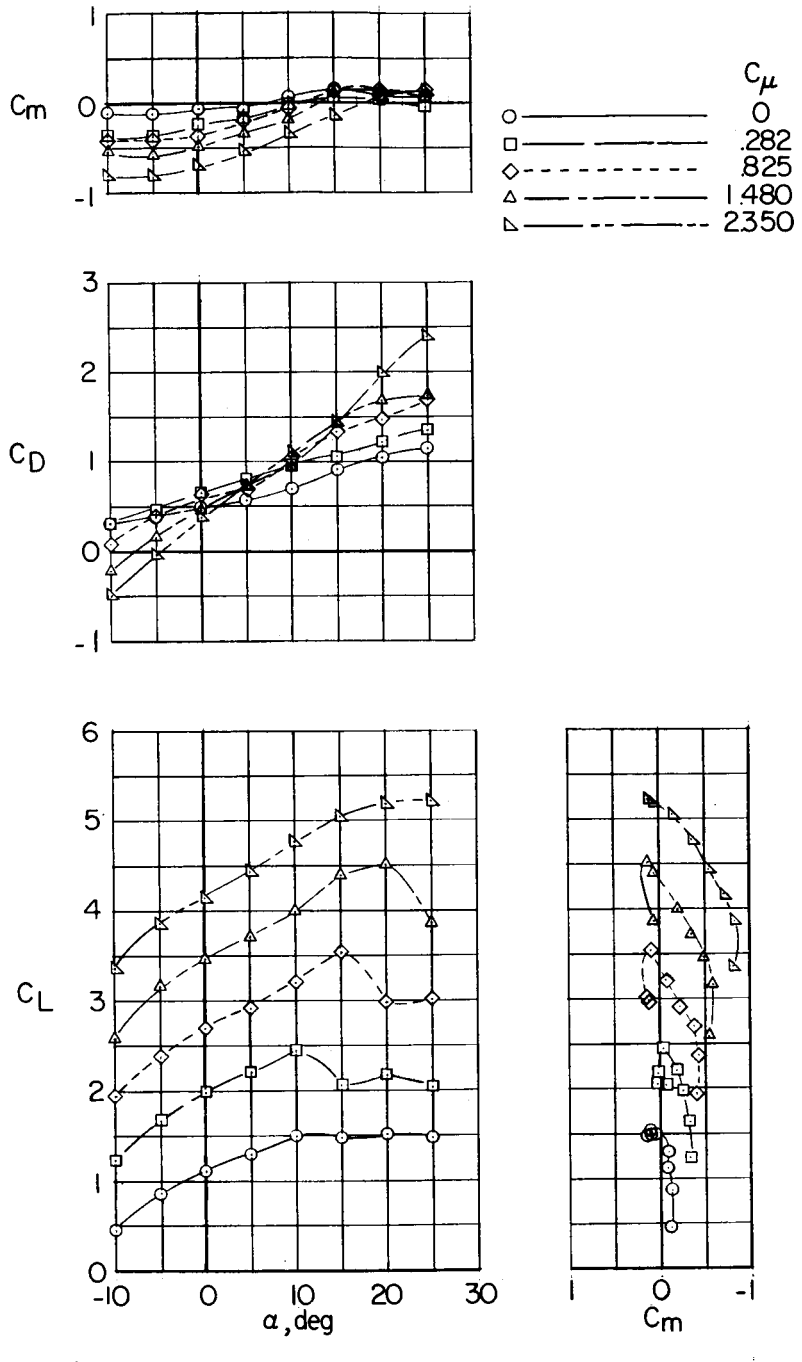

(c) $\frac{h}{\bar{c}} = 0.28$; $i_t = 5^\circ$.

Figure 10.- Continued.

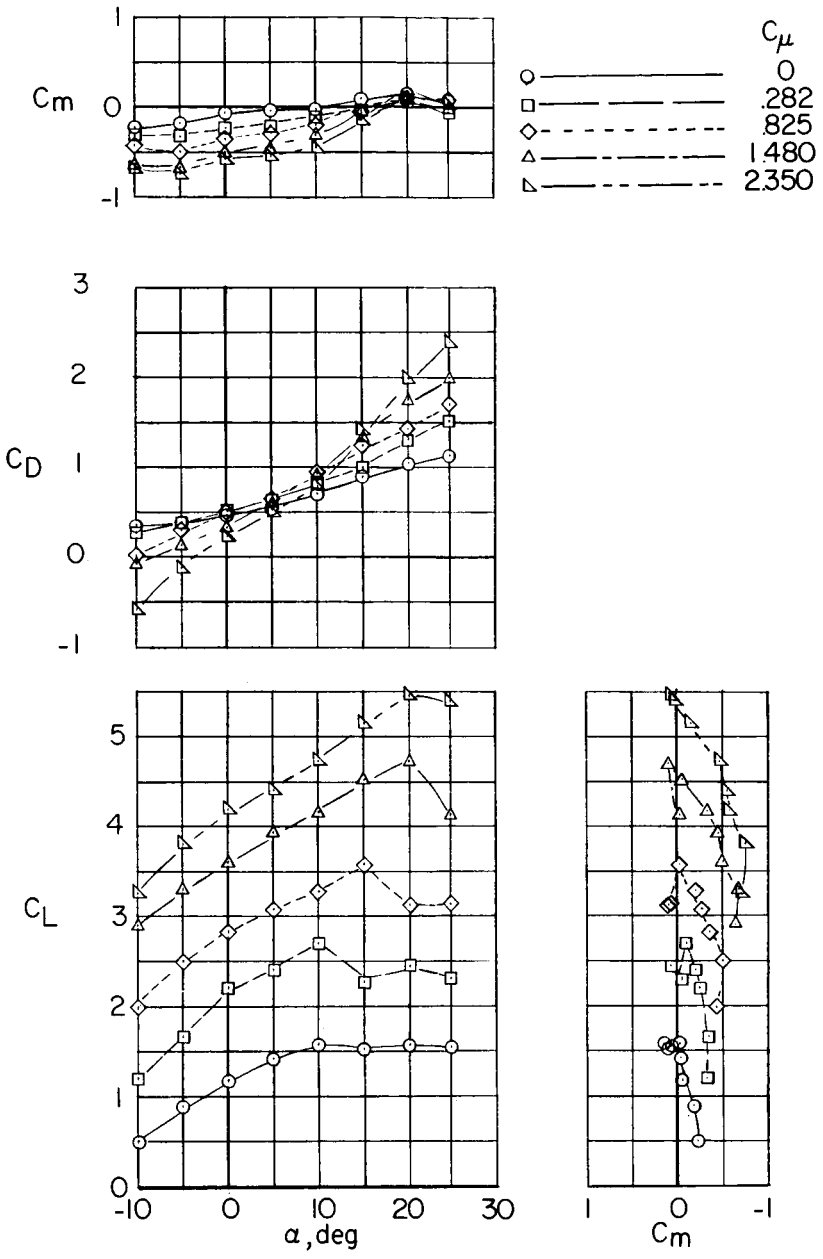

(d) $\frac{h}{\bar{c}} = 0.28$; $i_t = 10^\circ$.

Figure 10.- Continued.

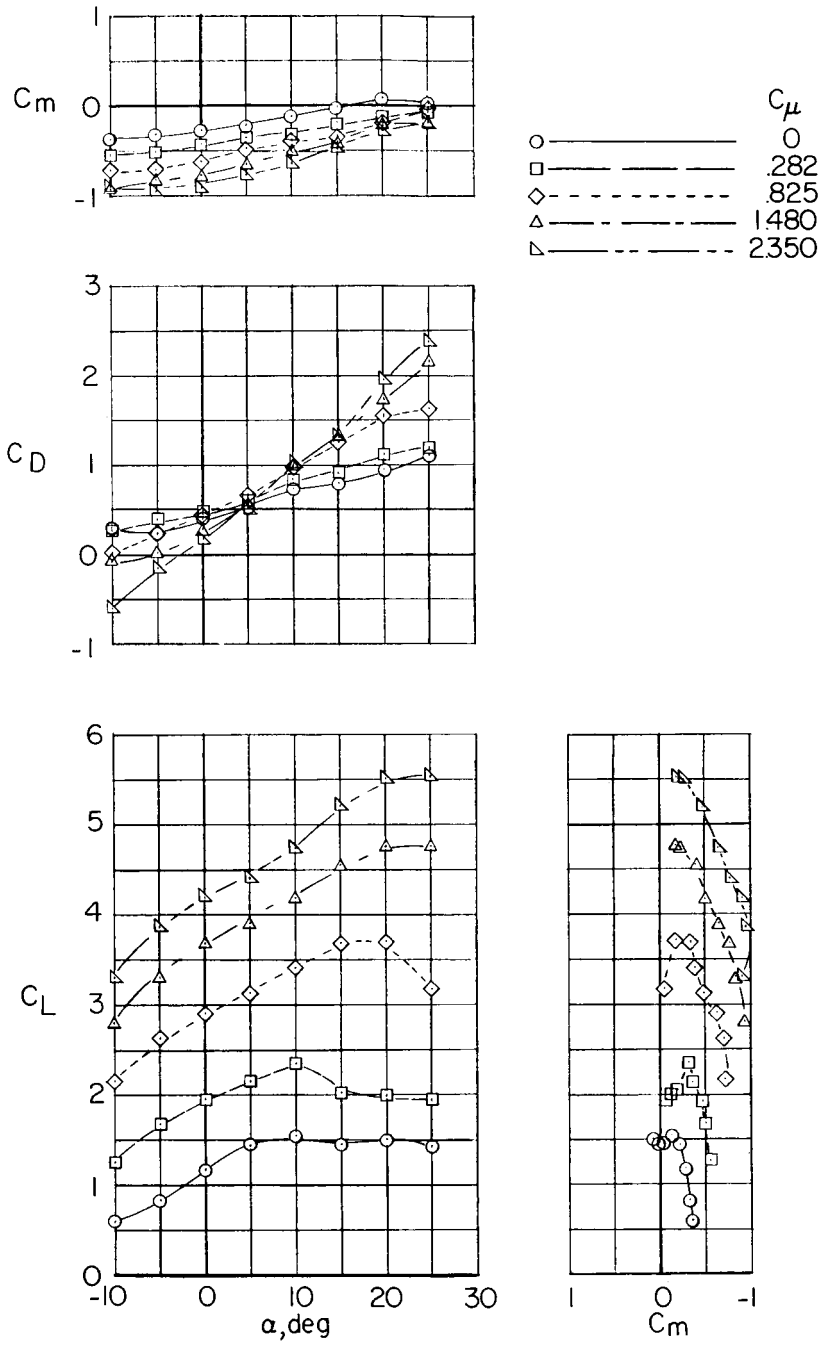

(e) $\frac{h}{\bar{c}} = 0.28$; $i_t = 20°$.

Figure 10.- Continued.

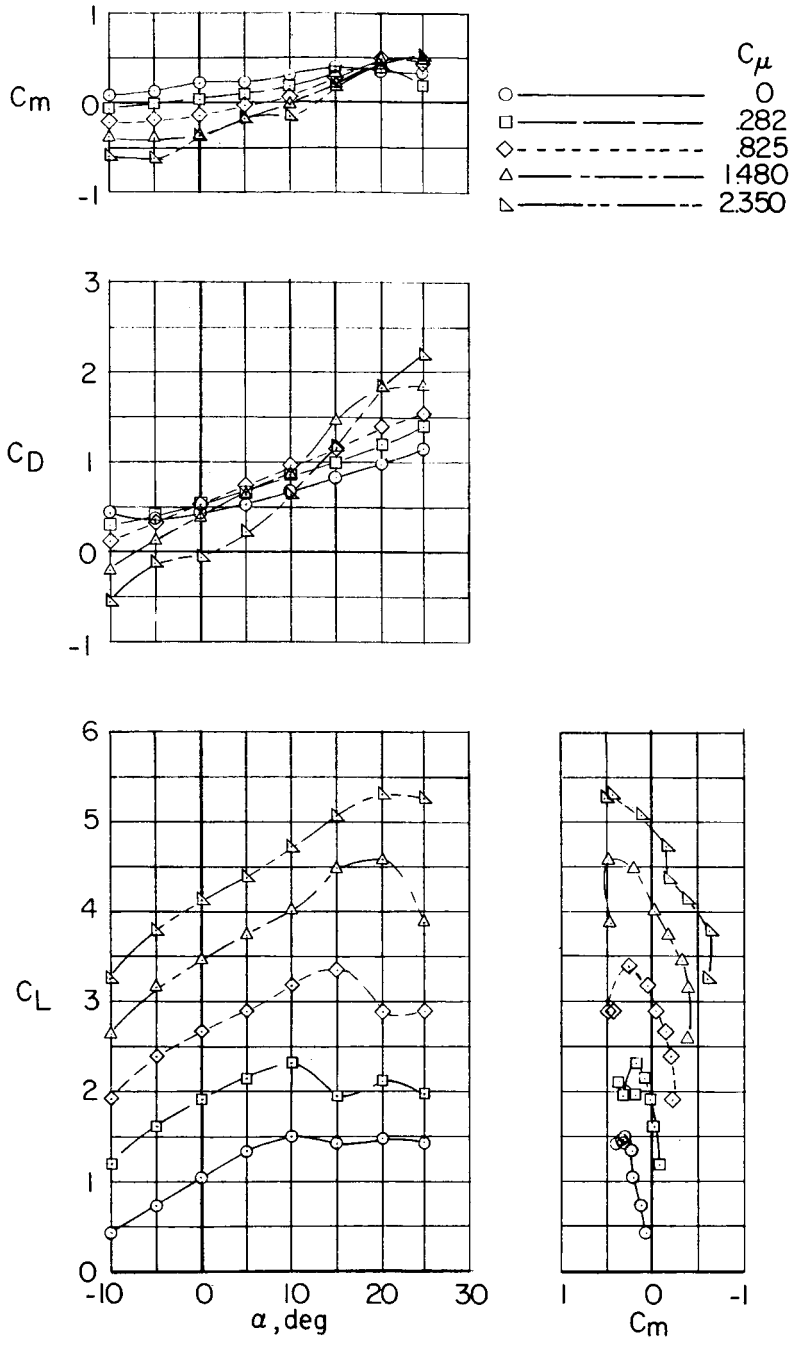

(f) $\frac{h}{c} = 0.69$; $i_t = 0^\circ$.

Figure 10.- Continued.

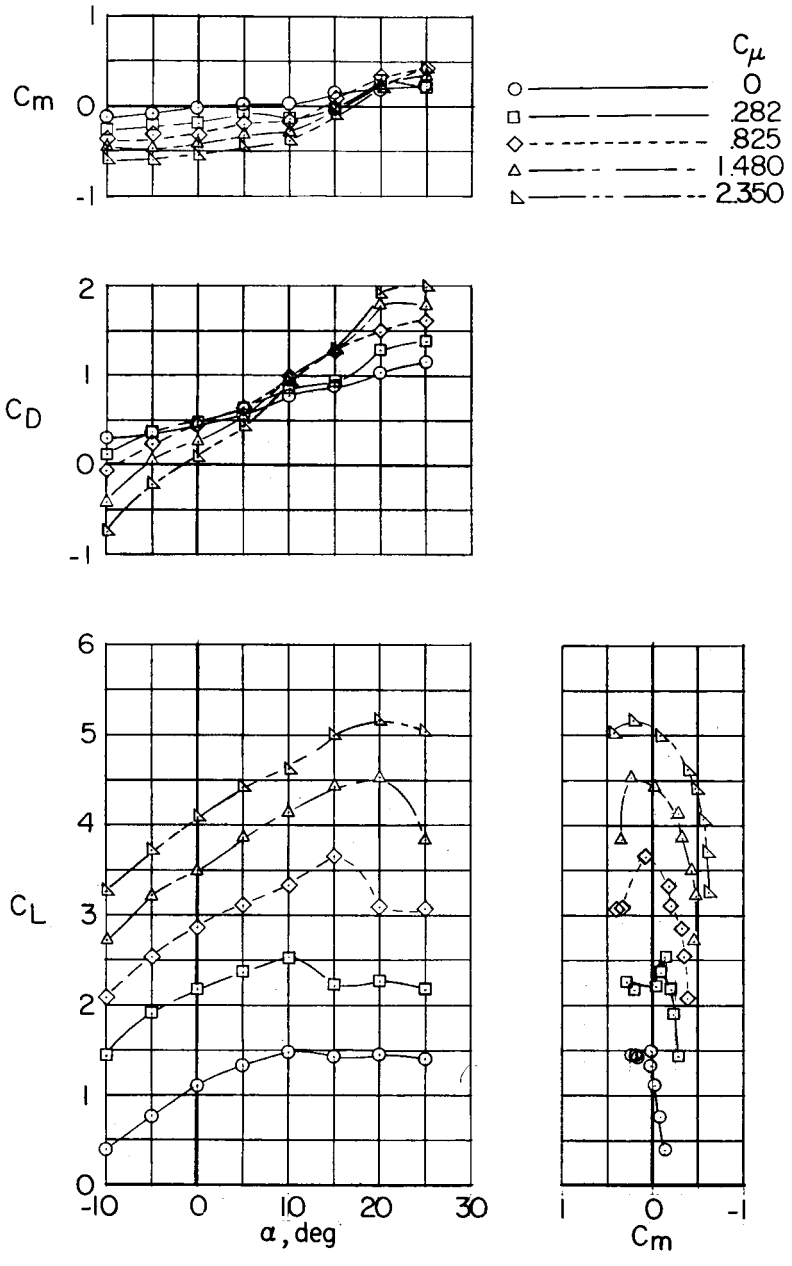

(g) $\frac{h}{\bar{c}} = 0.69$; $i_t = 5^\circ$.

Figure 10.- Continued.

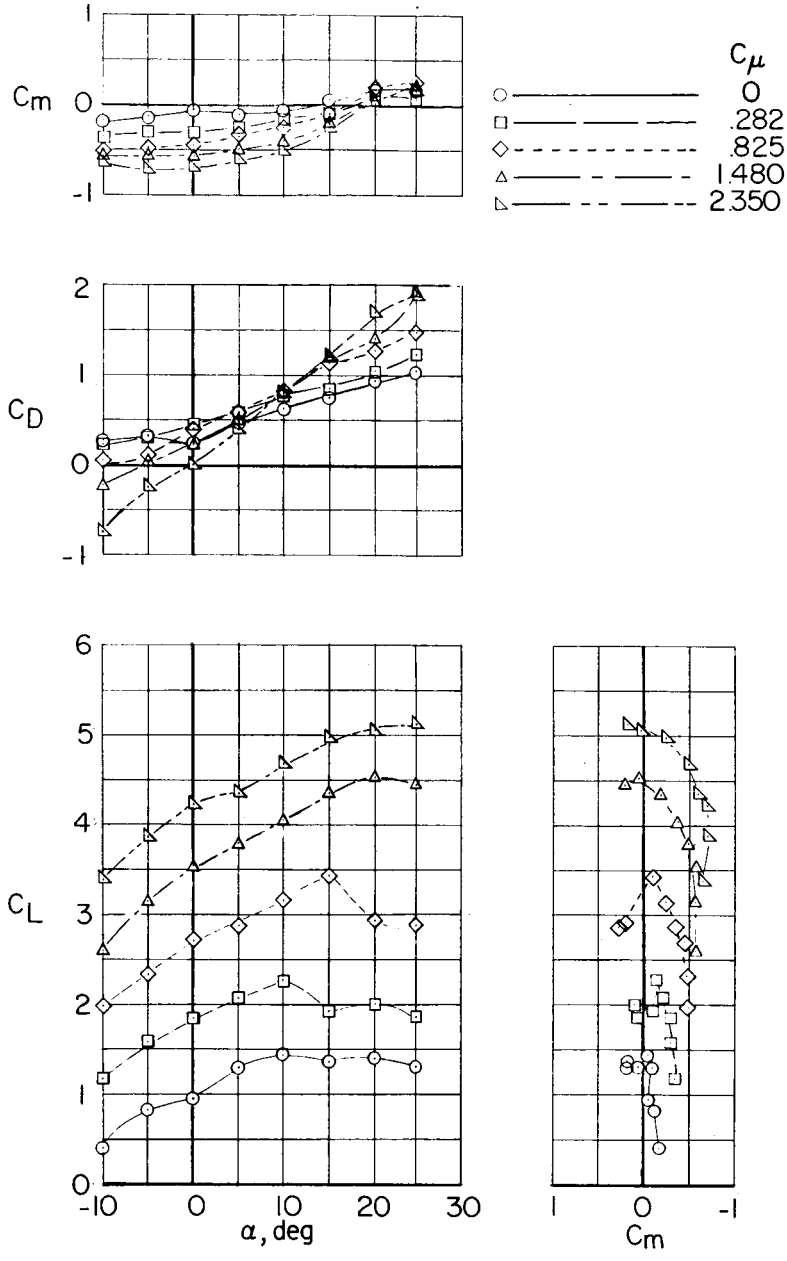

(h) $\frac{h}{c} = 0.69$; $i_t = 10^\circ$.

Figure 10.- Continued.

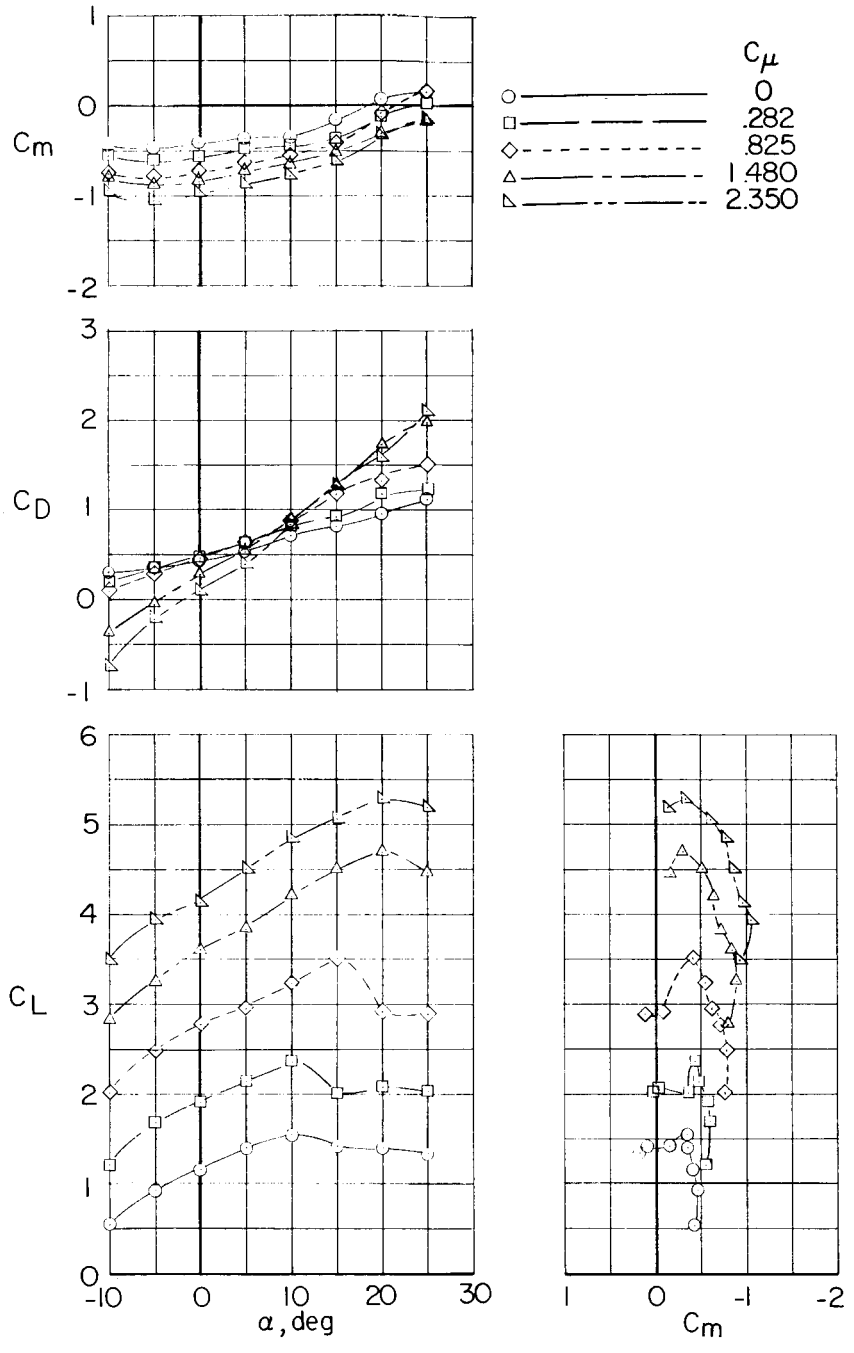

(i) $\frac{h}{\bar{c}} = 0.69$; $i_t = 20^\circ$.

Figure 10.- Concluded.

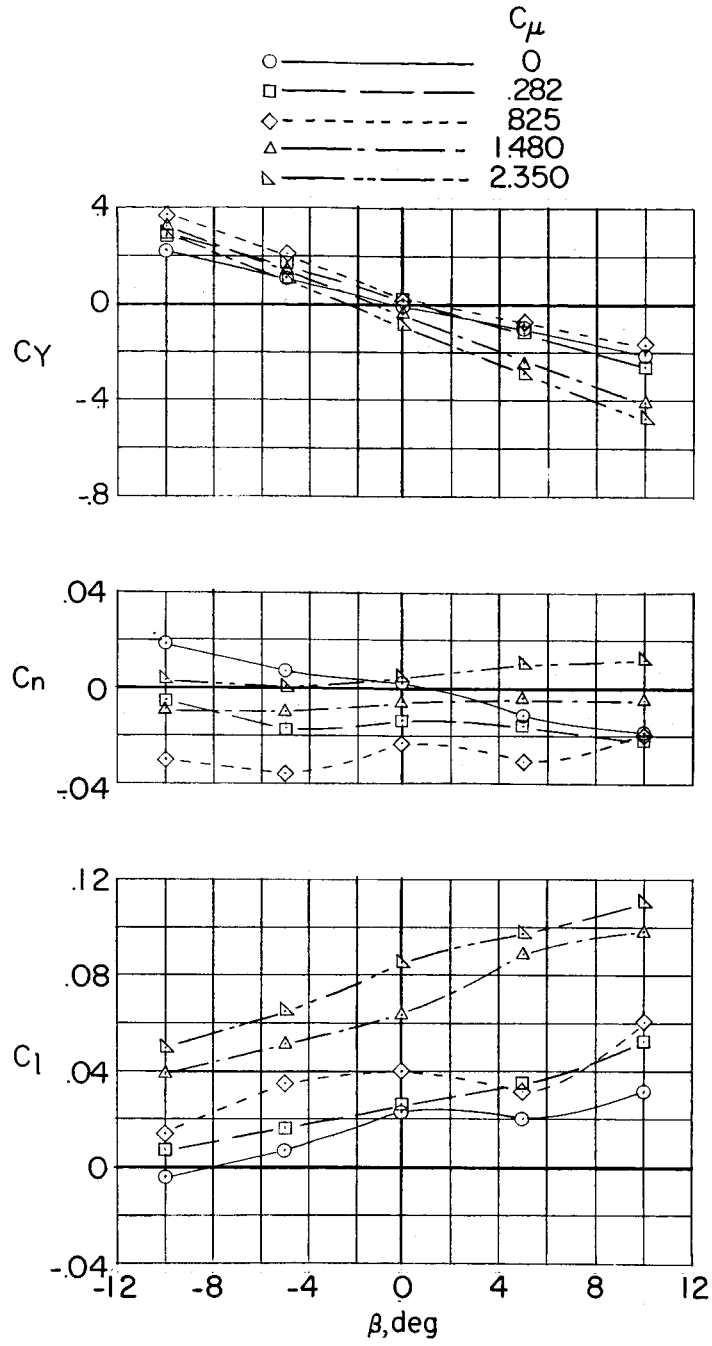

(a) Vertical tail off; $\alpha = 0^\circ$.

Figure 11.- Variation of rolling moment, yawing moment, and side force with sideslip angle for the low-wing configuration. $\delta_f = 55^\circ$; $i_t = 0^\circ$.

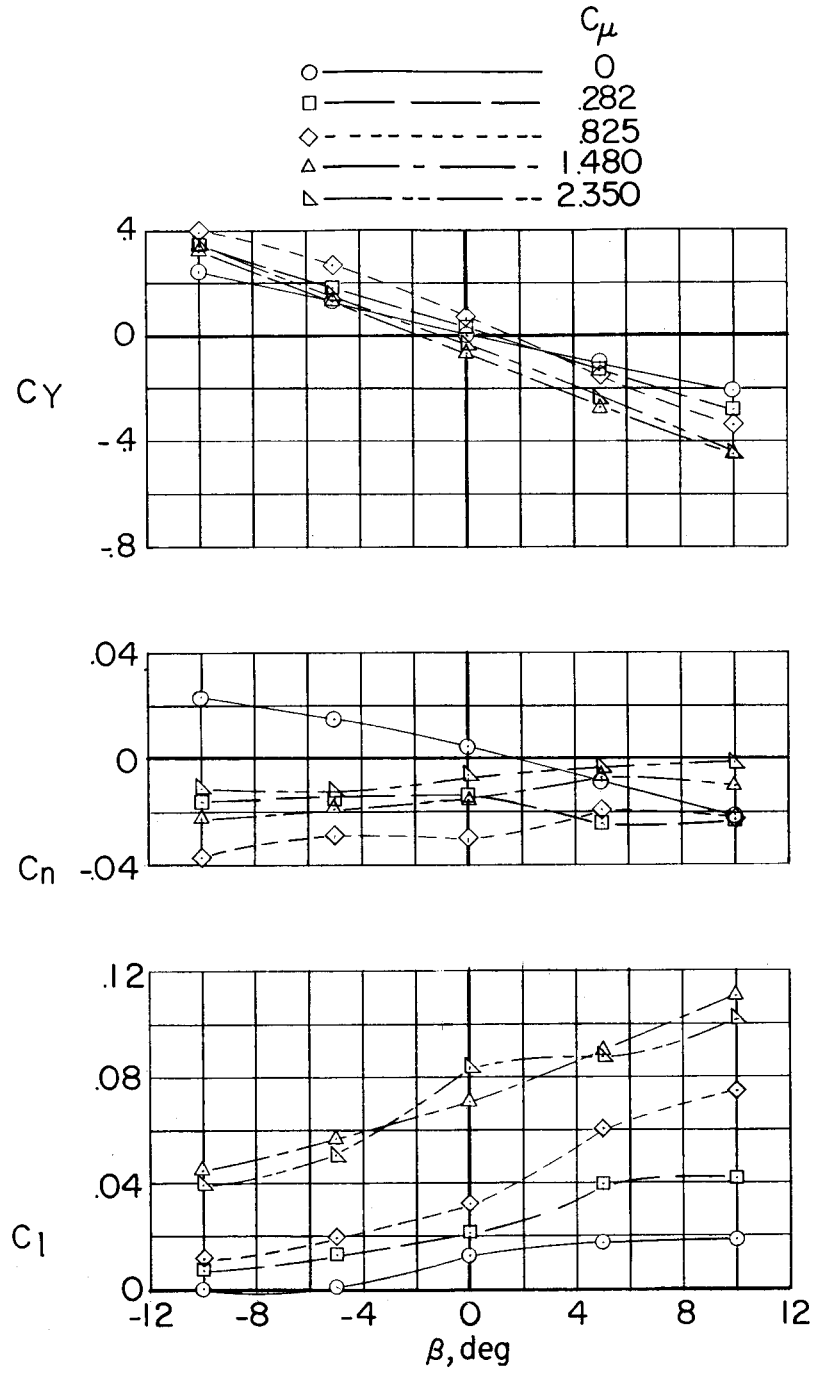

(b) Vertical tail off; $\alpha = 5^{\circ}$.

Figure 11.- Continued.

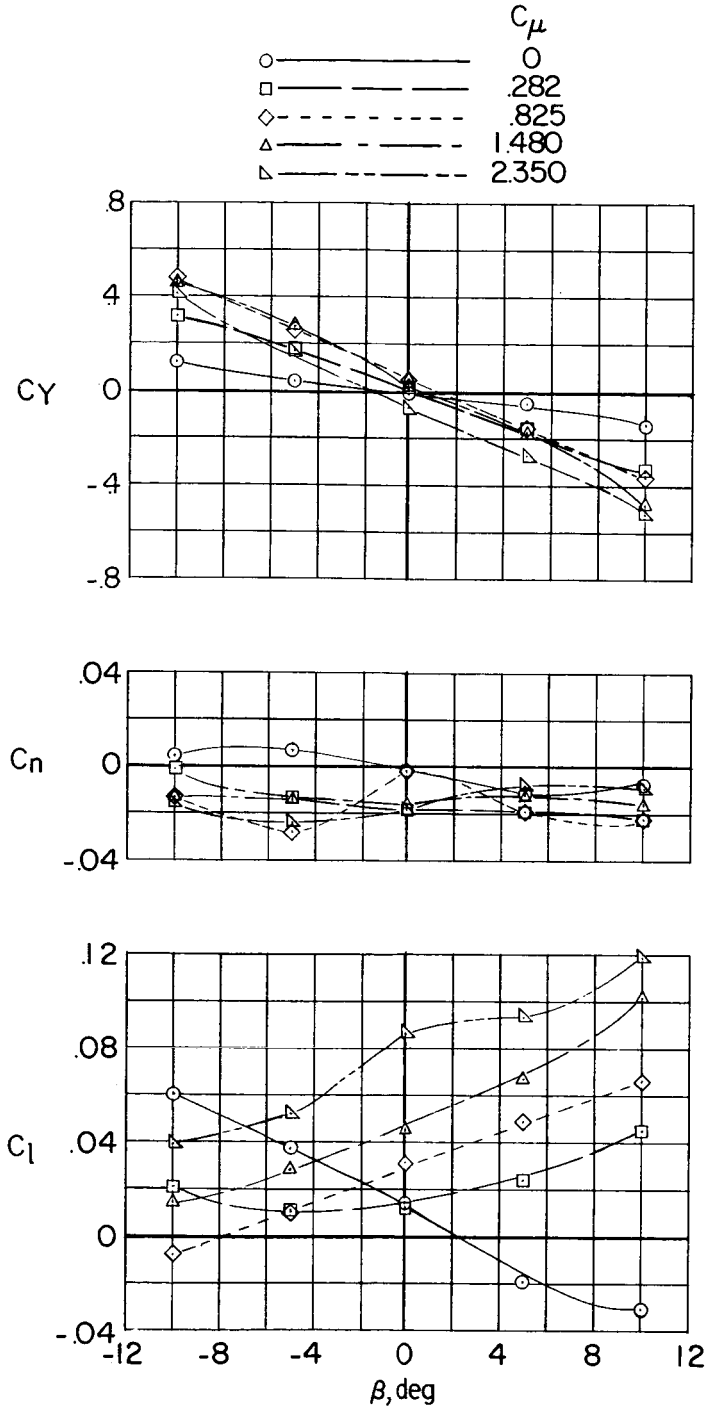

(c) Vertical tail off; $\alpha = 10^\circ$.

Figure 11.- Continued.

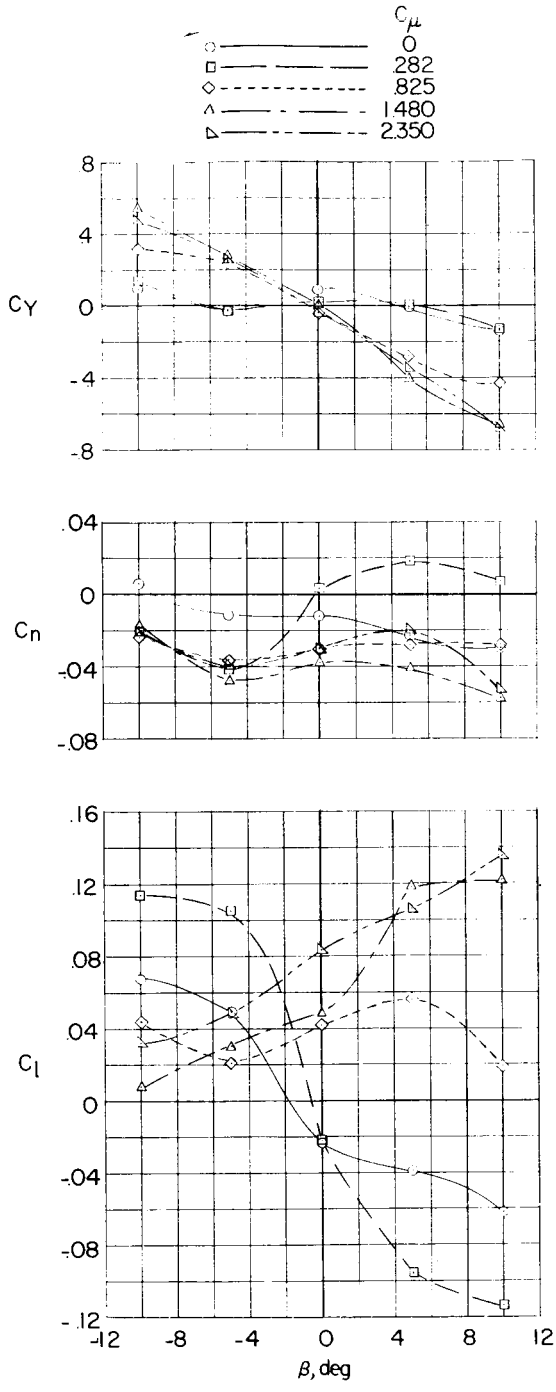

(d) Vertical tail off; $\alpha = 15^\circ$.

Figure 11.- Continued.

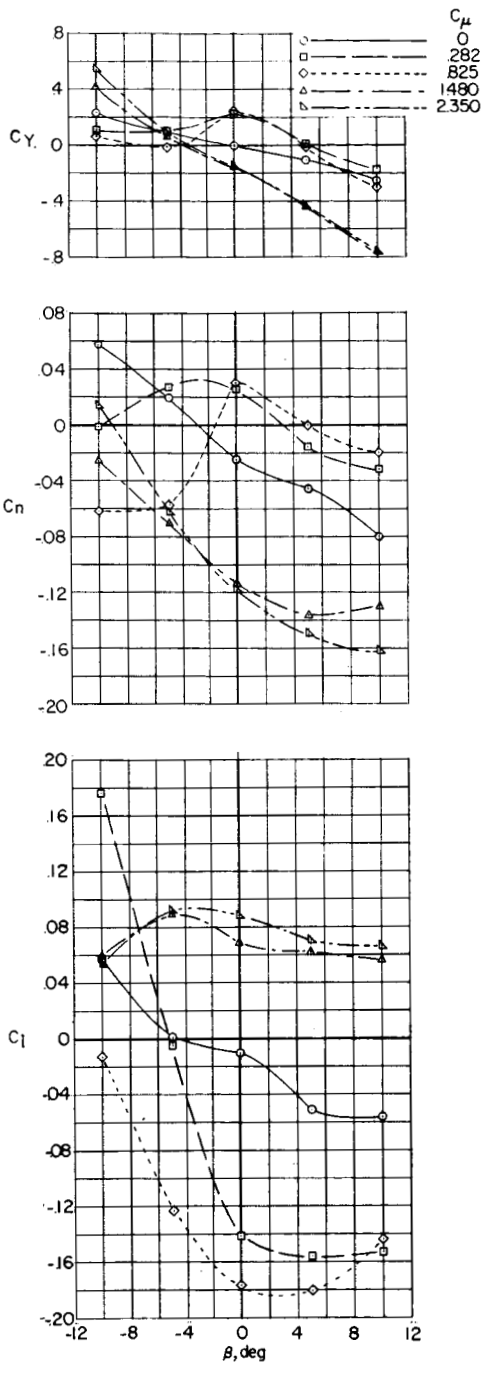

(e) Vertical tail off; $\alpha = 20^\circ$.

Figure 11.- Continued.

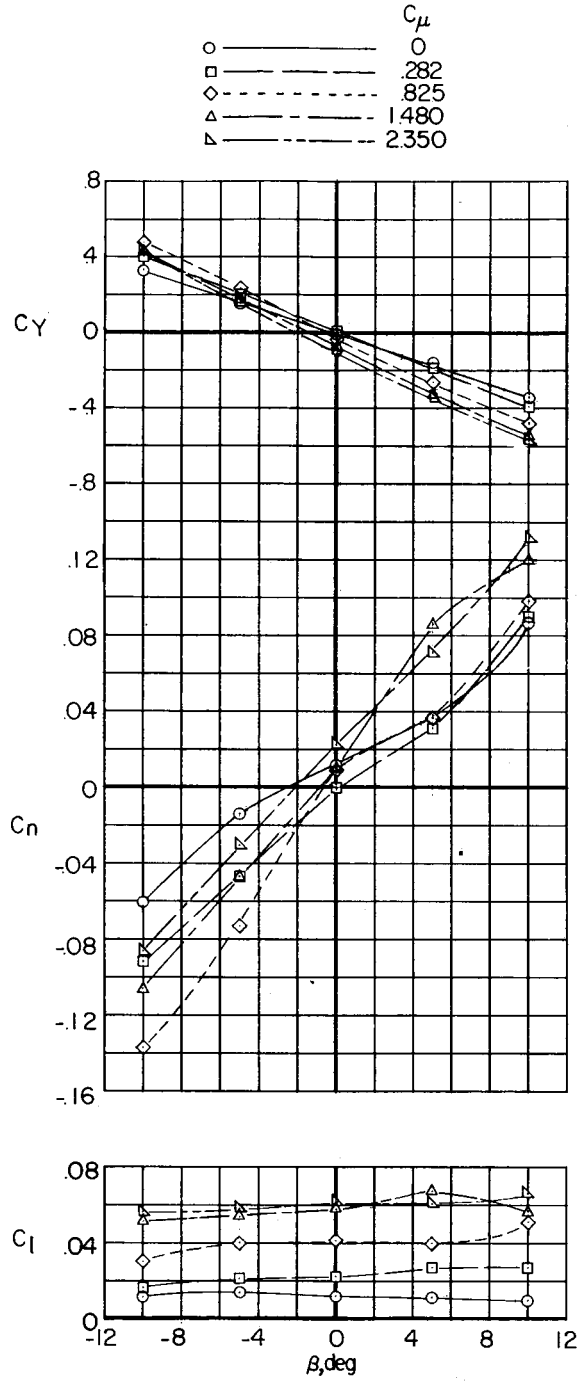

(f) $\frac{h}{\bar{c}} = 0.28$; $\alpha = 0^\circ$.

Figure 11.- Continued.

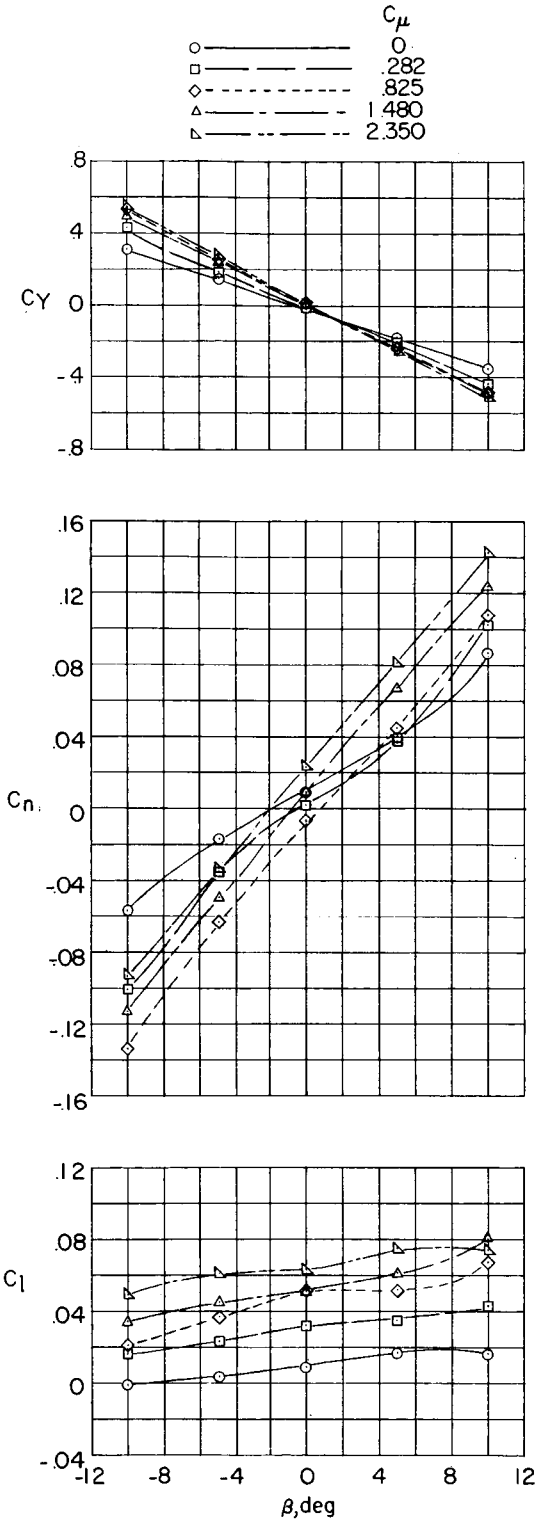

(g) $\frac{h}{c} = 0.28$; $\alpha = 5^\circ$.

Figure 11.- Continued.

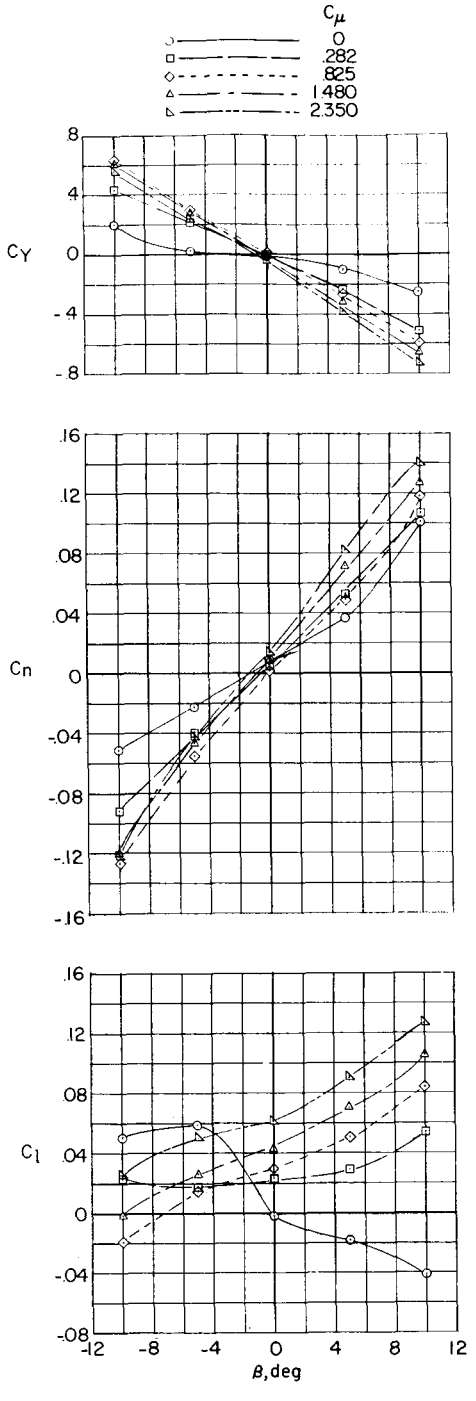

(h) $\frac{h}{\bar{c}} = 0.28$; $\alpha = 10^\circ$.

Figure 11.- Continued.

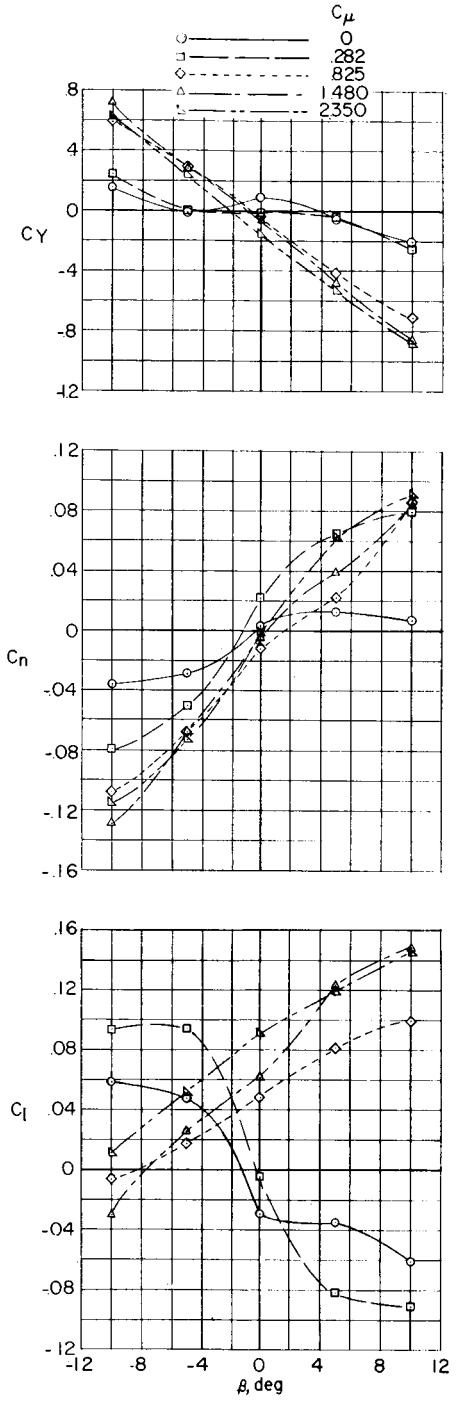

(i) $\frac{h}{c} = 0.28$; $\alpha = 15^\circ$.

Figure 11.- Continued.

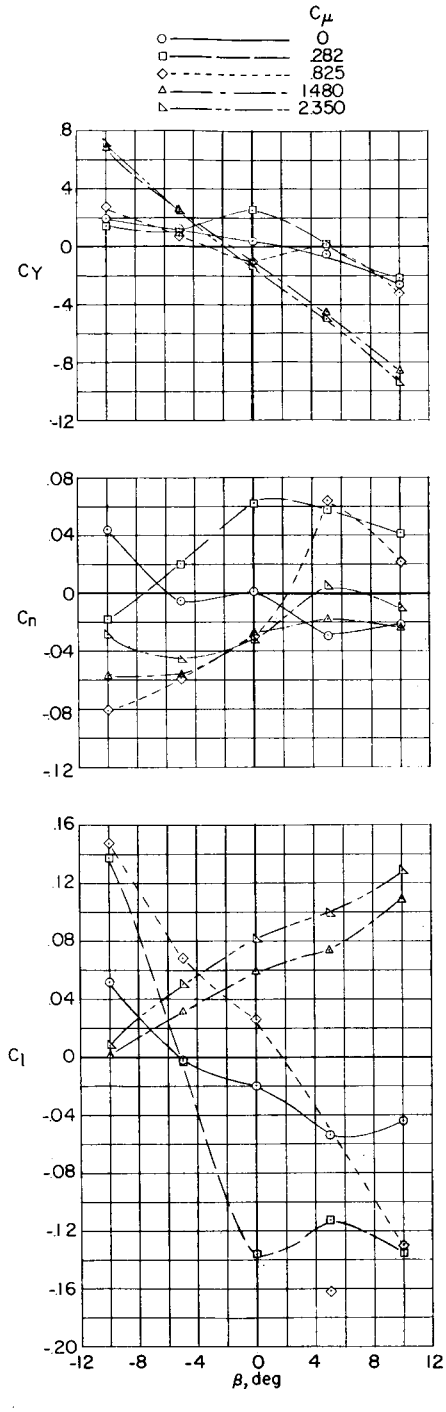

(j) $\frac{h}{\bar{c}} = 0.28$; $\alpha = 20^\circ$.

Figure 11.- Concluded.

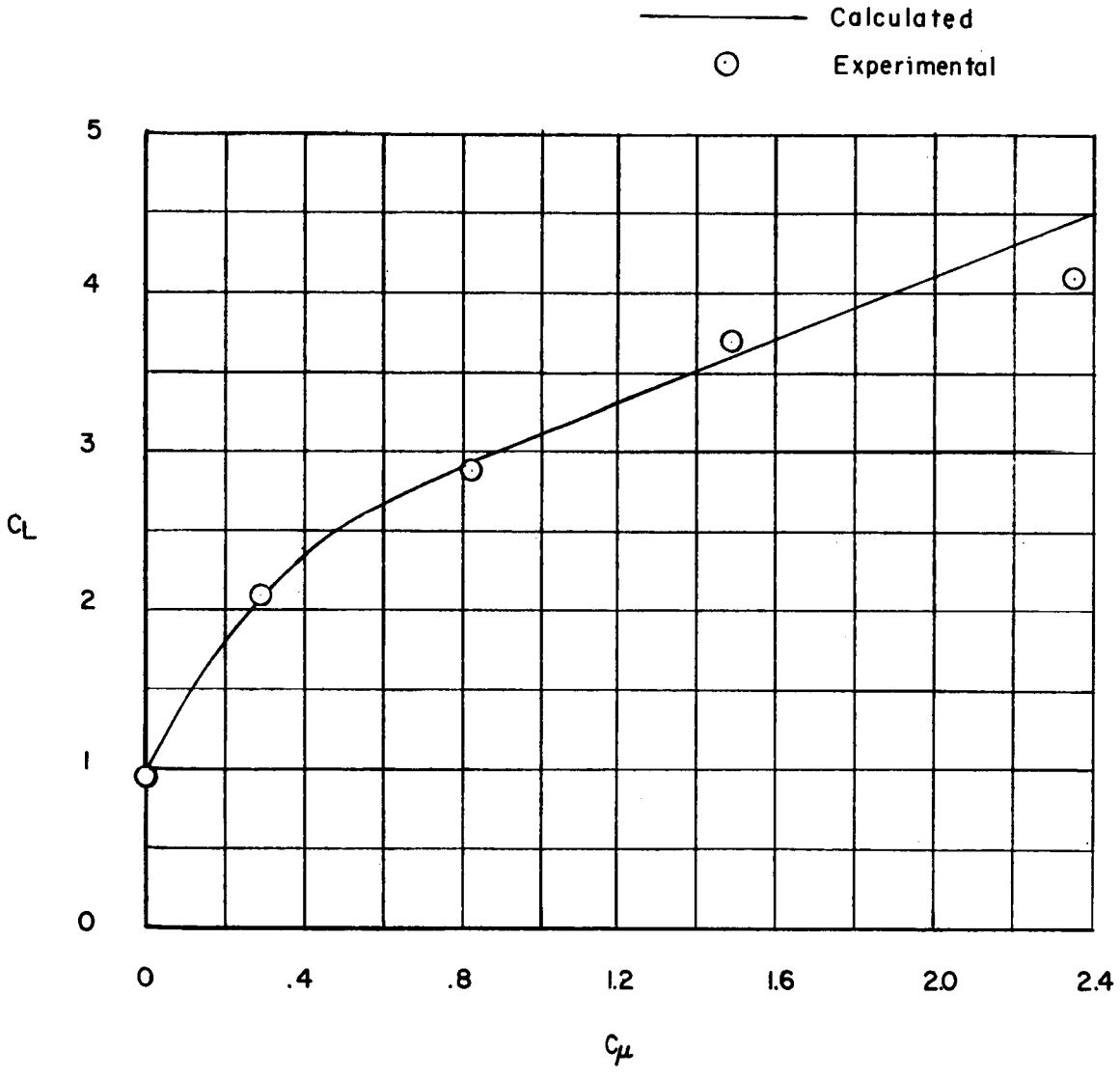

Figure 12.- Comparison of calculated and measured lift for the high-wing—tail-off configuration at $\alpha = 0^\circ$.

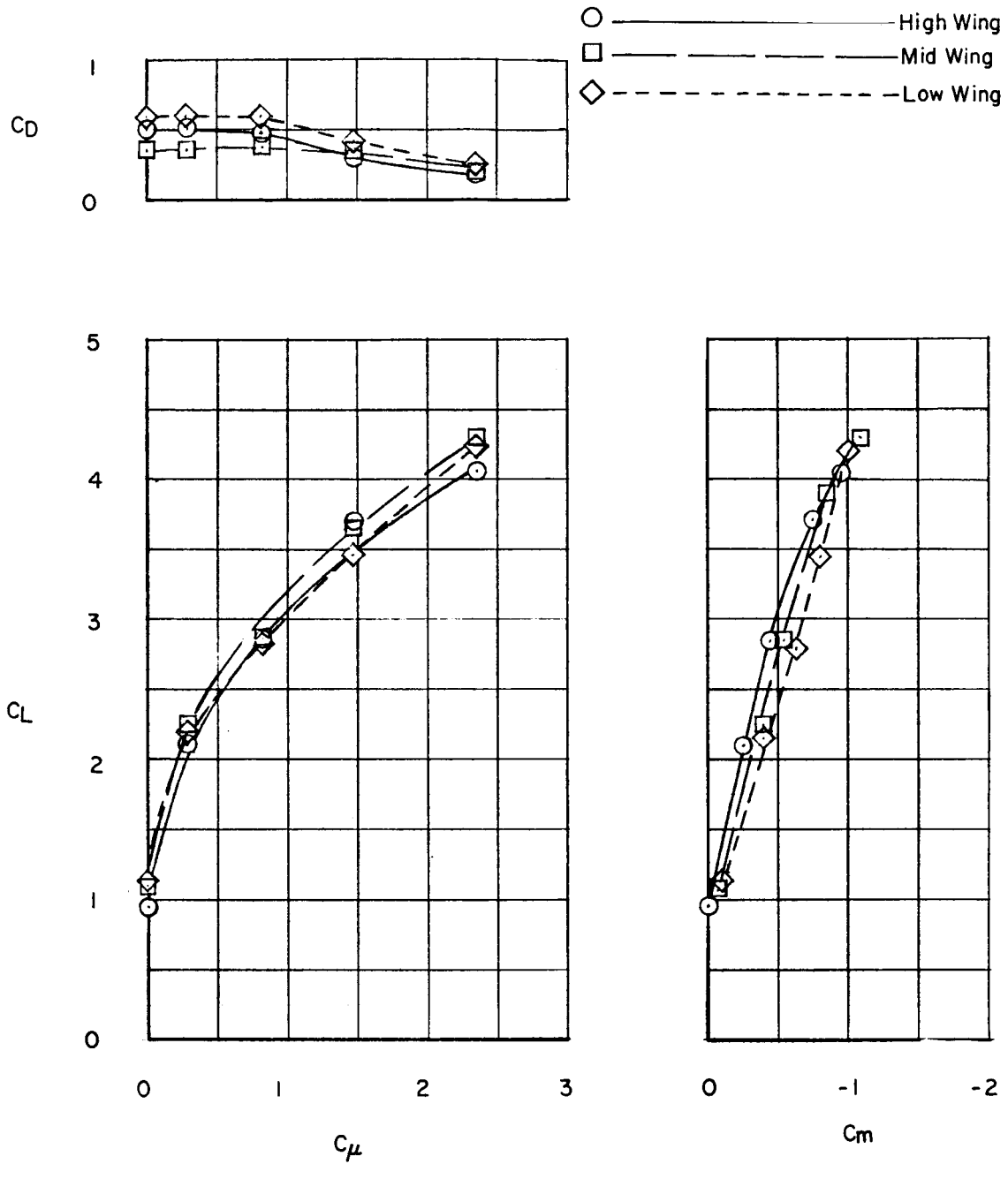

Figure 13.- Effect of wing position on the aerodynamic characteristics of the model. Horizontal tail off; $\alpha = 0^\circ$; $\delta_f = 55^\circ$.

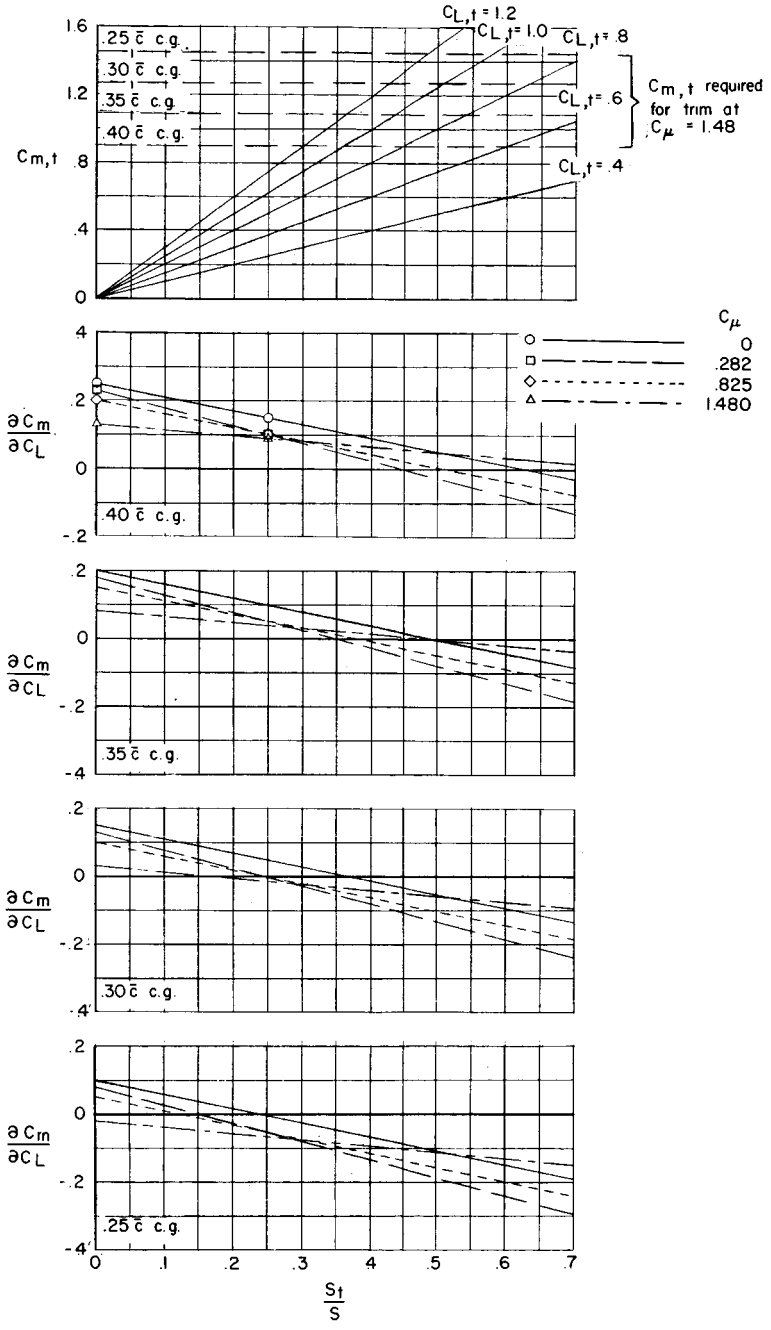

(a) Mid wing; $\frac{h}{\bar{c}} = 0$.

Figure 14.- Variation of longitudinal stability and trim parameters with horizontal-tail area for several center-of-gravity locations.

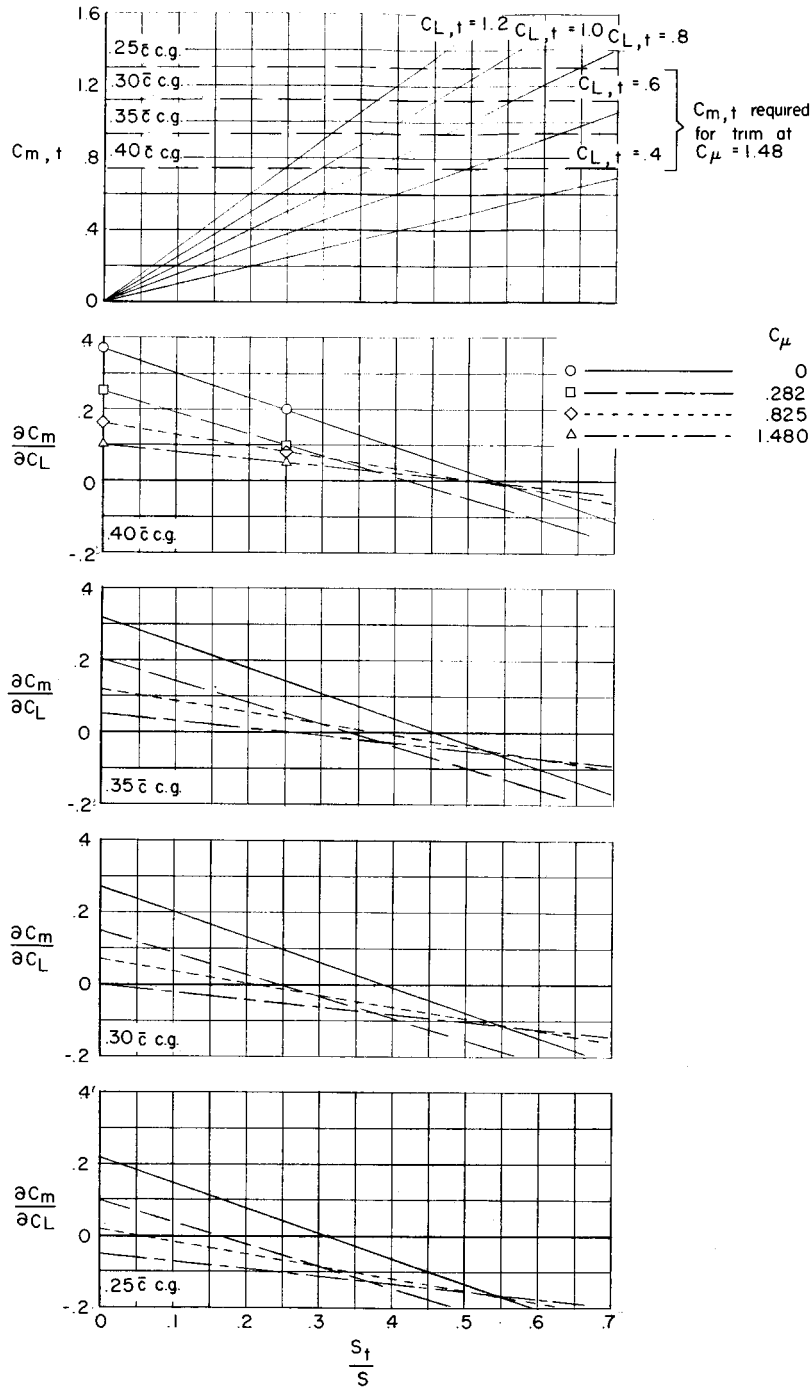

(b) High wing; $\frac{h}{\bar{c}} = 0$.

Figure 14.- Concluded.

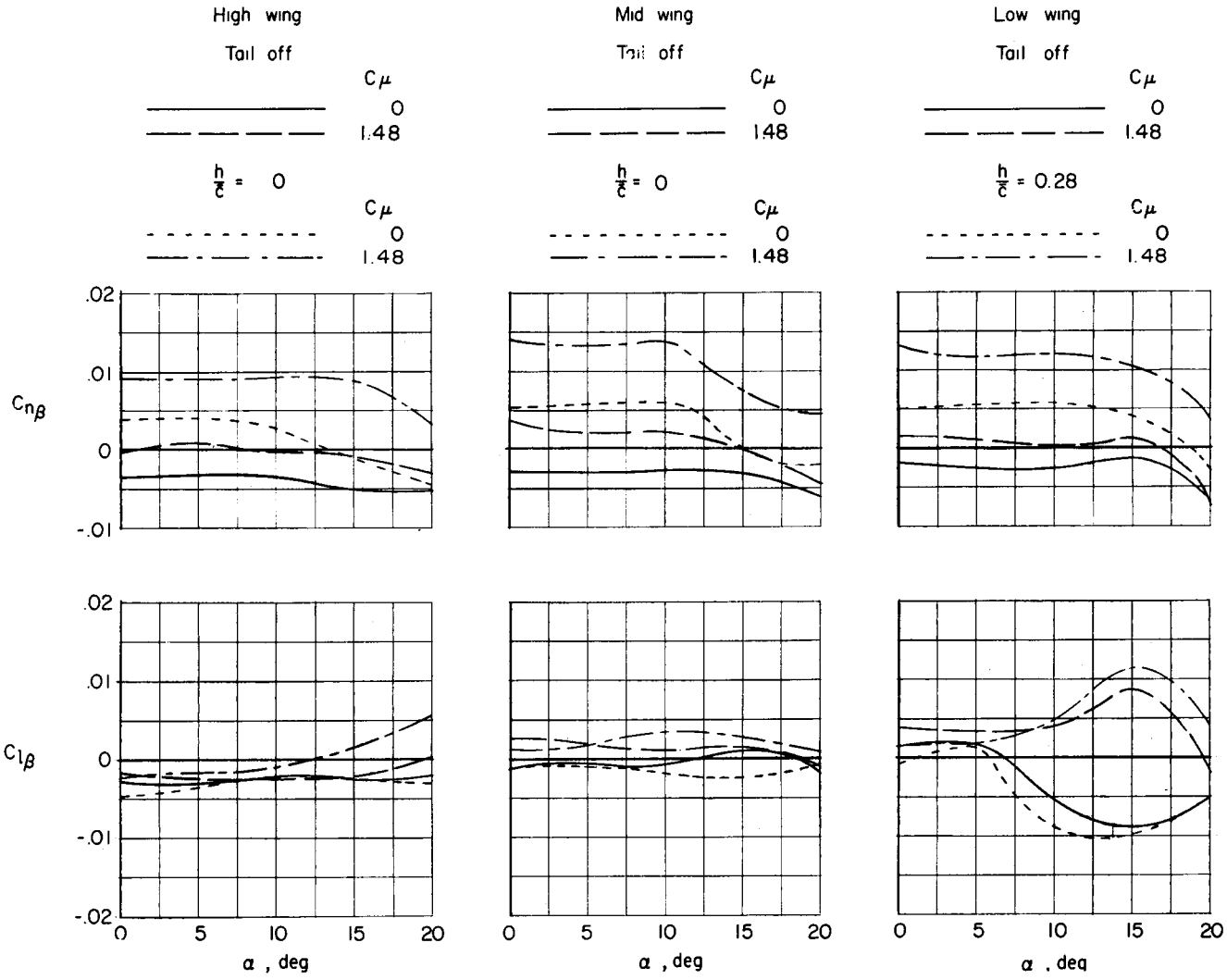

Figure 15.- Variation of directional stability and effective dihedral with angle of attack for two values of momentum coefficient.

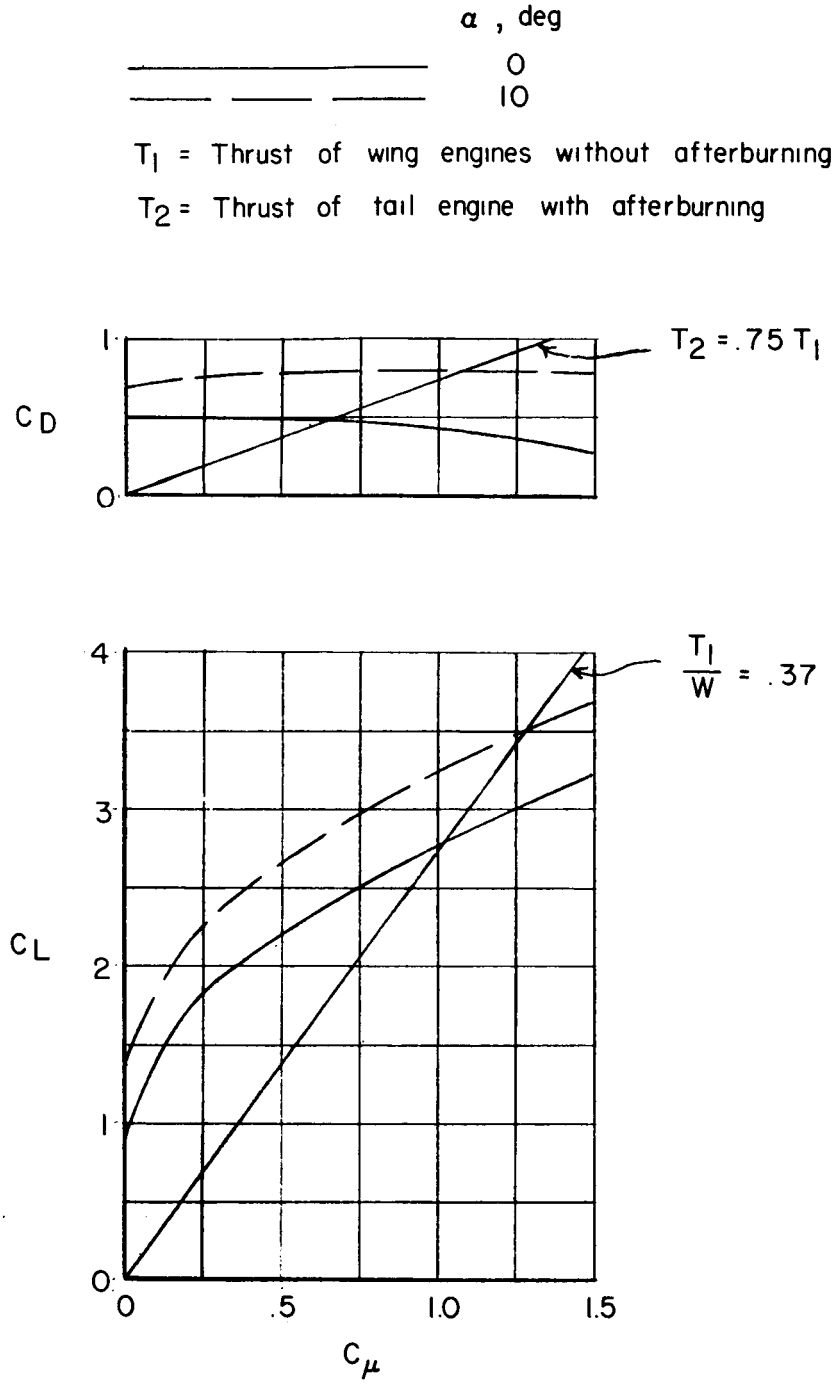

Figure 16.- Variation of lift coefficient and drag coefficient with momentum coefficient at trim pitching moment (C_m = 0) for the high-wing—chord-plane-tail configuration.